Transient Heat Flow Simulations for Assessing the Performance of Radiant Panel Installations Under Concrete Building Floors

by

Eric Labrecque

Bachelor of Engineering, Carleton University, 2015

A THESIS SUBMITTED IN PARTIAL FULFILLMENT OF THE REQUIREMENTS FOR THE DEGREE OF

Master of Science in Engineering

In the Graduate Academic Unit of Mechanical Engineering

Supervisor(s):	Andrew Gerber, Ph.D., Mechanical Engineering
Examining Board:	Tiger Jeans, Ph.D., Mechanical Engineering (Chair)
	Clodualdo Aranas, Ph.D., Mechanical Engineering
	Muhammad Afzal, Ph.D., Mechanical Engineering
	Kush Bubbar, Ph.D. J. Herbert Smith Centre for Technology Management and Entrepreneurship

This thesis is accepted
by the
Dean of Graduate Studies

THE UNIVERSITY OF NEW BRUNSWICK

January, 2020

Abstract

Three models are developed to study the long-term thermal performance of a radiant heat floor system with sub-grade thermal storage. An existing steady-state 1D model of the system is verified using a quasi-1D CFD-CHT model. A full-scale parametric study is performed using a Simulink-based model representing a central vertical section of a typical industrial installation, including conjugate heat transfer at the floor surface. The transient conjugate heat transfer modelling capability of the EXN/Aero CFD suite is verified. A prescribed set of CFD-CHT simulations using EXN/Aero is developed, tested, and proposed to further study the systems performance. These simulations include conjugate heat transfer at solid-fluid interfaces, radiation field and natural convection modelling coupled with the energy equation in the heated space, and an embedded temperature-controlled heating element, all of which have been tested and verified. Results confirmed the hypothesis that insulation installed between the heating panel and the concrete slab is severely detrimental to the system's performance, while insulation installed below the heating panel is somewhat beneficial. Recommendations regarding sub-grade insulation for the system and further studies are provided based on Simulink and EXN/Aero simulation results.

Acknowledgements

I would like to begin by thanking Dr. Andrew Gerber for his support and guidance through my journey at UNB. His continued dedication to my growth as a researcher and to the success of the project were instrumental in the academic and professional growth that I have experienced under his supervision. I would also like to thank Dr. Jeans, Dr. Aranas, Dr. Afzal, and Dr. Bubbar for being on my examining board and for their guidance in the completion of my graduate research and of this thesis. Your feedback brought my work to a calibre that would have never been achieved otherwise. To my colleagues, especially Ben and Farhad, thank you for all the inspiration and laughs that your friendships have brought me. Shout out to Joline, my better half and 'editor-in-chief'. Finally, I am eternally grateful to my friends and family for their unwavering support through my graduate studies, which have spanned four research topics, three years, and two universities.

Eric Labrecque

University of New Brunswick

December 2019

Table of Contents

List of Tables

List of Figures

Nomenclature

Vectors are identified in bold.
Variables denoted with a unit of "—" are unitless.

Symbol	**Units**	**Description**
α	$\mathrm{m}^2\ \mathrm{s}^{-1}$	Thermal Diffusivity
κ, κ_a	m^{-1}	Radiative Absorption Coefficient
η_i	—	Performance of System (i)
μ	Pa s	Dynamic Viscosity
ω	sr	Solid Angle (ω' for Propagation Term) (Spatial Domain)
$\Psi(s', s)$	—	Phase Function for Scattering from s' to s (Spatial Domain)
$\boldsymbol{\phi}$	—	**Conservative Variable**
ρ	$\mathrm{kg\ m}^{-3}$	Density
σ_S	m^{-1}	Scattering Coefficient
θ	rad	Azimuthal Angle (Spatial Domain)
ϕ	rad	Polar Angle (Spatial Domain)
Γ	—	Diffusion Coefficient of $\boldsymbol{\phi}$
ζ	—	Panel Area to Concrete Slab Surface Area Ratio

Symbol	Units	Description
A	m^2	Area
c_p	J kg^{-1} K^{-1}	Specific Heat Capacity
d	m	Diameter or Width
D	$m^2\ s^{-1}$	Binary or Thermal diffusion coefficient
e	J kg^{-1}	Specific Internal Energy
$\boldsymbol{G}$	**—**	**General Conservative Species Variable**
H	m	Ceiling Height
h	W K^{-1} m^{-2}	Heat Transfer Coefficient
h_c	W K^{-1} m^{-2}	Convective Heat Transfer Coefficient
h_r	W K^{-1} m^{-2}	Radiative Heat Transfer Coefficient
h_{tot}	W K^{-1} m^{-2}	Total Heat Transfer Coefficient
i		Index for Cartesian Coordinates (Directional Domain)
$\boldsymbol{I}$	**W sr^{-1} m^{-2}**	**Intensity of Radiation**
$\boldsymbol{I_b}$	**W sr^{-1} m^{-2}**	**Blackbody Radiation Intensity**
k	W K^{-1} m^{-1}	Thermal Conductivity
k_{eff}	W K^{-1} m^{-1}	Effective Thermal Conductivity
L	m	Thickness or Characteristic Length
L_C	m	Hydraulic Diameter ($\frac{A_{Floor}}{P_{Floor}}$)
L_s	**—**	Number of Solid Angles (Spatial Domain)
L_{ins}	cm	Insulation Thickness
p	**—**	Index for Polar & Azimuthal Angles (Spatial Domain)
P	Pa	Pressure
P_{Floor}	m	Floor Perimeter
q_c	Wm^{-2}	Convection Heat Flux
q_{floor}	W m^{-2}	Total Heat Flux from a Radiant Floor (Upwards)
q_{heater}	W m^{-3}	Current ETS Panel Volumetric Heat Generation
$\boldsymbol{q_i}$	**W $\mathbf{m}^{-2}$**	**Heat Flux**
$\boldsymbol{q_{rad}}$	**W $\mathbf{m}^{-2}$**	**Radiation Heat Flux**
q^*_{rad}	**—**	Normalized Radiation Heat Flux
q_{max}	W m^{-3}	Maximum Volumetric Heat Generation
$\boldsymbol{q_{wall}}$	**W $\mathbf{m}^{-2}$**	**Multi-Mode Heat Transfer from a Wall**
Q_{air}	m^3 s^{-1}	Air Flow Rate

Symbol	Units	Description
R_{cond}	m^2 K W^{-1}	Conductive Thermal Resistance
R_{conv}	m^2 K W^{-1}	Convective Thermal Resistance
R_n	m^2 K W^{-1}	Thermal Resistance of Layer 'n'
s_i	m	Position Vector in i Direction (Directional Domain)
s_p	–	Position Vector in p Direction (Spatial Domain)
s'	–	Propagation Direction (Spatial Domain)
$\boldsymbol{S}$	–	**Source Term**
t	s	Time
t_{cycle}	s	Length of a complete cycle
t_{sim}	s	Length of a simulation
T	°C	Temperature
T_A	°C	Farfield Temperature in the Heated Space
$T_{ceiling}$	°C	Interior Temperature of Ceiling Surface
T_E	°C	Exterior Air Temperature
T_{floor}	°C	Surface Temperature of Concrete Slab
T_G	°C	Temperature at Full Depth
$T_{op,1.1}$	°C	Operative Temperature at 1.1 m above floor surface
T_{ref}	K	Reference Temperature
$T_{SlabAir}$	°C	Temperature of air in heated space immediately above the concrete slab
T_U	°C	Upper ETS Panel Temperature Setpoint
ΔT_a	°C	Temperature difference between the average of the inlet and outlet temperatures of a radiant hydronic system and the set point air temperature of the heated space ($T_{op,1.1}$)
ΔT_w	°C	Temperature difference between the average heat source temperature and the non-heating surface weighted average temperature
ΔT_{ETS}	°C	T_C - T_A
$\boldsymbol{u_i}$	$\boldsymbol{m\ s^{-1}}$	**Velocity in direction i**

Abbreviations

BC	Boundary Condition
CFD	Computational Fluid Dynamics
CHT	Conjugate Heat Transfer
CV	Control Volume
DOM	Discrete Ordinate Method
ESR	Energy Storage Ratio
ESS	Earth Storage System
ETS	Earth Thermal Storage
FVM	Finite Volume Method
GSADE	General Scalar Advection-Diffusion Equation
MPS	Modified Parametric Study
NRC	National Research Council
NBC	National Building Code
NSCC	Nova Scotia Community College
PD%	Percentage of Dissatisfied Occupants
SIMPLE	Semi-Implicit Method for Pressure-Linked Equations
SPS	Standard Parametric Study
SST	Shear Stress Transport
TE-RCP	Thermoelectric Radiant Ceiling Panel
TES	Thermal Energy Storage
TOU	Time of Use
XPS	Extruded Polystrene

Chapter 1

Introduction

1.1 Background

ThermaRay, Inc. ("ThermaRay") is a manufacturer of radiant heating products based in Fredericton, New Brunswick whose earth storage radiant heat system has been gaining popularity in the United States and internationally in recent years [1]. Their Earth Storage System (ESS), a type of electric thermal storage (ETS) system, generally consists of six distinct thermal energy storage (TES) layers, from the exposed concrete slab down to the undisturbed soil below. A cross-sectional view of the ESS is shown in Figure 1.1. Table 1.1 outlines the order and thickness of the TES layers (see Table A.1 in Appendix A for additional TES layer specifications). The thickness of the "Heated Space" layer represents the ceiling height and therefore varies between applications, but a height of 10 m is used in the full-scale models [2]. The thickness of the "Undisturbed Soil" layer is set to 6.644 m based on the isothermal soil depth in Ottawa, ON [3], while the thicknesses of all other layers are based on ThermaRay's installation guide

for the ESS [4]. These other layers, from the concrete slab through to the layer of compressed sand, are represented to scale in Figure 1.1.

ThermaRay's ESS has been designed to be a cost-effective radiant heating system with sub-grade TES layers comprised of natural, locally-sourced materials. Electric heating panels are entombed in the sand layer, as shown in Figure 1.1. Heat from these panels warms the surrounding TES layers, which then provide consistent, uniform heat to the occupied space above. With a combined specific heat capacity of nearly 7 MJ per square meter for every degree Celcius increase in the TES region's temperature (6.8 MJ/m^2K, assuming even temperature distribution [3–9]), the thermal mass of the ETS layers allows for the electric heating panels to only operate periodically, essentially "topping-up" the thermal energy in the system.

ThermaRay, Inc. believes that the majority of heat "lost" to the soil beneath a building with an ESS will eventually pass upwards into the heated space. This would mean that, for a central region of an ESS-heated building, the system's efficiency could approach 100%. The limited computational domain of the simulations performed in this research limits the ability to study this phenomenon using their results. However, if the system's performance appears to improve over time, this may speak to the accuracy of ThermaRay, Inc.'s claim.

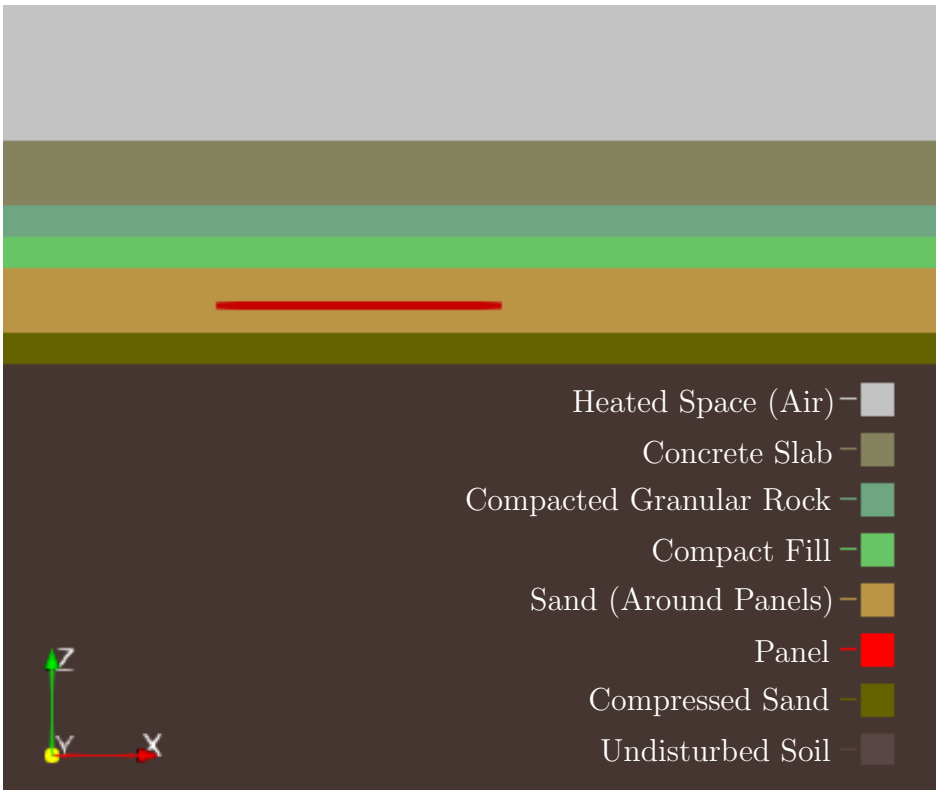

Figure 1.1: Cross-sectional View of ThermaRay's ESS [4]

Table 1.1: TES Layer Thickness

Layer	**Thickness [m]**
Heated Space	-
Concrete Slab	0.1016
Compacted Granular Rock	0.0508
Compacted Fill	0.0508
Sand (Around Panels)	0.1016
Heating Panels	0.0127
Compacted Sand	0.0508
Undisturbed Soil	6.6444

The ability of the system to reliably maintain occupant comfort (by ensuring the floor surface and air temperatures remain within a comfortable range) while only activating the heating panels periodically allows building operators to take advantage of time-of-use (TOU) rates, where available, and to reduce the building's peak electrical demand. As a radiant heat system, utility costs are further decreased because the occupants and surfaces in the heated space receive the majority of the heat rather than the air around them. In contrast, forced-air-based heating systems primarily heat the air in a space. This increases the amount of heat lost to the exterior environment through exfiltration (such as when exterior doors are open) or ventilation. This is of particular concern in industrial spaces, where it is common for large loading doors to be open for extended periods of time.

Industrial buildings that rely on forced air heating systems lose a vast amount of heat each time loading doors are opened during winter months. A significant loss of heated air leads to a spike in heating demand, which can push heating systems beyond their design point, impacting their efficiency. It also causes a drop in occupant comfort both for those closest to the open door, who would be too cold, and those closest to the heat vents, who would be too hot. In contrast, buildings with radiant heat systems are better suited for maintaining occupant comfort when loading doors are open as occupants continue to receive heat from the surrounding warmed surfaces, which are radiating heat to them. The lack of a sudden peak in demand or drastic decrease in occupant comfort is one of the primary principles supporting the

use of radiant heat systems over forced air systems in industrial spaces.

The benefits of radiant heat systems compared to traditional forced air systems have been thoroughly studied in recent decades, as summarized in a 2010 report by Alban [10]. Rather than comparing radiant and forced air systems in general, as has been done several times, this research seeks to specifically study the long-term transient performance of ThermaRay's ESS. In this work, the term "long-term transient performance" is used to describe the system's performance in a quasi-steady state in which the system's temperature field is fluctuating about a constant state due to daily and seasonal heat load cycles. The project's specific objectives are outlined in Section 2.7, based on the problem statement provided in the following section and gaps in the existing research presented in Section 2.6.

1.2 Problem Statement

The Canadian National Building Code (NBC), overseen by Codes Canada at the National Research Council (NRC), requires that insulation with a minimum RSI of 1.32 be installed between a building's concrete slab and the undisturbed soil beneath when the slab is heated (either with hydronics or an electric system like ThermaRay's ETS) [11, 12]. This regulation was developed with traditional hydronic radiant heating systems in mind. The performance of hydronic systems is not particularly reliant on thermal

storage, due to the proximity of hydronic piping to the surface of the concrete slab (as shown in Figure 2.1. As such, insulation below the concrete slab can improve the systems' efficiency by reducing the amount of heat that is transferred into the ground below the concrete slab. This hydronic system-based understanding of heated slab efficiency is the basis of the NBC-mandated insulation.

ThermaRay's ESS, on the other hand, typically does not include this insulation so as to facilitate thermal energy storage beneath the building. This also facilitates heat transfer to the heated space from the heating panels, which are situated below where the NBC-required insulation is typically installed for hydronic systems [12]. Based on discussions with representatives from ThermaRay and literature [13], installing ESS's without this insulation reduces installation cost, improves thermal mass and therefore occupant comfort, and can reduce operational costs by allowing the majority of electricity use for heating to occur during off-peak power rate periods. Inclusion of this insulation between the ETS heating panel and the concrete slab would cut the TES region to a fraction of its original size while increasing the system's cost. It is also theorized that this would reduce the ETS' efficiency, further impacting its economical viability. This NBC-required insulation requirement has thereby limited the growth of ThermaRay's market for its ESS in Canada.

Studying the thermal performance of their ESS, with a focus on the

importance of the insulation currently required by the NBC, would seek to address Code Canada's concerns regarding the impact of sub-grade insulation on the thermal efficiency of buildings with radiant heat systems like the ETS. This improved understanding would allow a more informed decision regarding whether Codes Canada should grant ThermaRay's ESS an exemption to the regulation. Such an exemption would encourage the growth of ThermaRay's ETS market into Canada and that of the radiant heat system industry in Canada overall. Therefore, the primary objective of this research was to examine the long-term transient performance of ThermaRay's ESS both with and without the currently required insulation between the concrete slab and unaltered soil below to support Code Canada's decision as to whether such an exemption should be granted.

Chapter 2

Literature Review

In recent years, there has been a significant rise in the use of low temperature energy sources for space heating, often serving as the heat source for radiant thermal systems [14–17]. These systems are typically more efficient than traditional fossil-fuel furnaces [10, 16]. They also encourage the use of renewable energy sources such as geothermal and solar thermal and provide an improved thermal comfort to occupants [10, 18, 19]. To further improve system performance and occupant comfort, and to address the intermittent nature of some renewable energy sources, thermal energy storage has become increasingly popular in energy efficient buildings [10, 20–22]. This rise in popularity has sparked a growth in academic research in the fields of thermal energy storage (TES), radiant heat transfer, and predictive control for radiant thermal systems.

2.1 TES System Performance

A plethora of research has been performed in the study of conductive heat transfer within and between TES materials and the effect thereof on the performance of TES systems.

Wang et al. [23] and Zhou & He [24] found that conductive heat transfer in thermal energy storage materials in areas not adjacent to a building's perimeter could be considered one-dimensional after two hours of TES system discharge. This finding supports the simplification of numerical analyses and encourages the use of the 1D analyses that form the first phase of the research presented herein.

The paper by Zhou & He [24] published in 2015 is among the only literature available that provides a comparison of the thermal performance of thermal storage hydronic heating systems with different heat storage materials and heating pipe designs. It was found that phase change materials release heat for twice as long as sand and that radiant heating with capillary mats (with small diameter hydronic tubing in a tighter, serpentine spacing) achieved the set room temperature in nearly half the time required by traditional polyethylene coils [24]. This emphasizes the sensitivity of ETS performance to panel spacing and TES material selection, the latter of which is often based on what is locally available. Zhou & He [24] also refer to the "energy storage ratio" (ESR) first defined in a paper published by Zeng et al. in 2010

[25]. The ESR, as defined in Equation 2.1, is the ratio of heat transferred while a radiant heat system is active on a given day to the heat transferred over the entire day, both passively and actively. A low ESR signifies the heat provided to the system is being transferred into the heated space evenly and consistently throughout a given day. This ratio, as a potentially useful metric for quantifying the performance of ThermaRay's ESS, was calculated for some of the simulations performed in this research. Please refer to page 144 (Section 5.4) for the results.

$$\text{ESR} = \frac{\text{Heat Transferred during Active Heating}}{\text{Total Heat Transferred (Passive \& Active)}} \tag{2.1}$$

Heat loss through the foundation from a heated concrete slab, a key aspect of the research presented here, was studied by Chuangchid & Krarti [22]. A mathematical approach was used to study heat transfer through and from an on-grade heated concrete slab into the surrounding soil, with the water table serving as an isothermal heat sink 5.25 meters below grade. It was shown that the inclusion of insulation between the on-grade cement slab and the undisturbed soil beneath could reduce heat transfer downward by over 40%. Regardless of the presence of sub-grade insulation, the majority of heat passed into the heated space. This suggests that what while the inclusion of sub-slab insulation discourages TES, the heat that was presumed to be lost to the environment as it passes from the slab into the soil below in the

development of the NBC does eventually contribute to the heating of the above-grade space, as presumed in the design of ThermaRay's ESS.

The same paper by Chuangchid & Krarti [22] showed that the majority of heat loss through the foundation was along the perimeter. This suggests that increasing the thickness of insulation that is installed along the perimeter of a foundation while excluding insulation throughout the building's footprint would significantly reduce heat loss beyond the footprint of the building, addressing the NRC's energy efficiency concerns. This calls for additional research into the affect of the thickness of insulation along the building's perimeter on the system's thermal performance without insulation across the entire foundation, though this is outside of the present research's scope. Additionally, installing insulation solely along a building's perimeter rather than throughout the footprint would be much less expensive than footprint-wide insulation while allowing for the expansion of the thermal energy storage region beyond the concrete slab, as ThermaRay is seeking to implement in Canadian installations of its ESS. This finding from literature put a spotlight on the results of simulations performed without insulation installed across the entirety of the building's footprint.

A recent paper by Tahersima et al. [13] studied the performance of a heated concrete slab radiant heating system paired with two geothermal heat pumps for the heating of a 3000 m^2 industrial facility. Two 650 m^2 floor sections were constructed for the purposes of studying two approaches to radiant heat

storage. Both sections were based on a concrete slab made of limestone and fly ash through which hydronic heating tubes were serpentined. One section's slab was 1.22 m thick with hydronic heating tubes running 0.15 m below the surface. A 0.075 m thick layer of lean concrete was situated between the slab and the undisturbed soil beneath to serve as a mud slab. The other section's slab was just 0.18 m thick with hydronic heating tubes embedded along the bottom of the slab. Insulation 0.025 m thick was placed between the slab and undisturbed soil below. In relation to the research presented here, the thicker slab is akin to ThermaRay's ESS, as it has a larger TES region, while the thinner slab with a layer of insulation below is akin to the NBC's required insulation arrangement.

The thicker section, with a TES region overly 1 m deep, provided a more uniform slab surface temperature throughout the day than the thin section, which had a depth of just 0.205 m including insulation. The primary downside of the thicker slab design was the high economic and environmental cost of the thick concrete slab. This issue is addressed through ThermaRay's use of primarily local, natural materials for the majority of their system's TES region. The thermal mass of the thick concrete slab facilitated the maintenance of occupant comfort while reducing utility costs by allowing the geothermal heat pumps to operate almost exclusively during the overnight hours. This reduced operational costs as electricity rates overnight were as low as a quarter of daytime hour rates due to the time-of-use (TOU) rates in the facility's jurisdiction. The reduction in utility costs combined with the

system's improved efficiency compared to traditional forced air systems on a square footage basis provided a 77% reduction in the operating cost of the facility's heating system [13]. The full-scale study's results were validated by a 3D finite-volume model, as described in a paper by the same authors [26]. The advantageous performance of the section without insulation and with a thicker TES region supports the theory that an absence of insulation beneath ThermaRay's ETS panels does not have a significant negative impact on the efficiency of the system. An in-depth study will be necessary to study the hypothesis that a lack of insulation across the footprint of a building's foundation will not be significantly detrimental to the system's long-term transient performance.

Heated Slab Radiant System Modelling

Through research conducted at the National Research Council in Ottawa, Laouadi [27] led the development of a 1D numerical energy model of a hydronic heated slab radiant system. This expanded upon previous numerical model research performed by Ritter & Kilkis [28] in 1998. While the work by these researchers was invaluable to the development of the radiant heating industry, their work focused solely on hydronic systems. Other models, developed primarily for the validation of experimental studies, were hydronic-based as well [29, 30]. Research-based development of models studying the performance of radiant heat systems based on electric thermal storage, rather

than hydronic systems, have been rather sparse to date. This gap in the field of heated slab radiant system modelling is what this research sought to address, as discussed in Section 2.6.

2.2 Radiative Heat Transfer & Radiant Temperature Fields

A second area of study that has been of particular interest since the rise in popularity of radiant heat systems is that of radiative heat transfer and temperature field analysis. The topic at hand, specifically, is the study of radiant heat transfer from either floor- or ceiling-based radiant panels and the relationship thereof with the temperature field within the room. The impact of the room's non-heating surfaces (such as walls and furniture) on the performance of a radiant heat system has also been studied.

A paper by Cholewa et al. [31] from 2013 may be the most relevant piece of literature in this field. It presents a study of heat transfer from and to radiant floors for heating and cooling, respectively. While other papers on the topic calculated heat transfer from radiant floors based on the enthalpic flux supplied to hydronic panels [30,32,33], Cholewa et al. [31] used a more direct method. Their experimental setup used heat flux density sensors placed directly on the floors and at different elevations above the floor surface for the calculation of heat transfer from radiant floors and occupants perception

thereof at different elevations. Using this method, the total heat transfer coefficient from radiant floor panels were up to 30% lower than values found from empirically derived equations commonly used in literature and industry [31]. This led to the development of a modified equation for total heat transfer from radiant floors based on the temperature difference between the radiant floor temperature and the room's operative temperature at 1.1 meters above the ground (Equation 2.2). Recommended values for radiative and convective heat transfer, h_r and h_c, respectively, are also provided based on experimental results. In a later paper focused instead on radiant ceilings, Cholewa et al. [34] found that 30-40% of heat produced by a hydronic ceiling radiant panel was lost to the plenum, a range that was in agreeance with an earlier paper by Li et al. [35]. Determining the equivalent of this percentage for ThermaRay's ESS was one of this study's objectives.

$$h_{tot} = 7.67 \cdot (T_{Concrete} - T_{op,1.1})^{0.1} \tag{2.2}$$

Seyam et al. [29] published a paper in 2014 covering many of the same topics but with a different approach. Their research focused on the use of a scale room model built solely from insulation-backed electric heating panels supported by a steel frame. A series of simulations were run with various sections of heaters on, demonstrating the effects of wall-based versus floor-based radiant heating, for example. To validate experimental results, a computational model that included radiation through a discrete

ordinate model (DOM) was also developed. The computational model also extended the scope of the study through the addition of a full-scale model to determine whether thermal behaviour observed in the scale model room would be replicated in a full-scale simulation. The experimental and computational results were in agreement, with any discrepancies attributed to the significantly higher volume-weighted average velocity in the full-scale computational model. The two methods produced the same radiative heat flux, 46.9 W/m^2, with the full-scale computational model producing an average heating surface total heat transfer coefficient of 4.47 W/m^2K to the scaled experimental model's 5.38 W/m^2K. The inclusion of a radiation model makes these results particularly useful for comparison with those from the research presented in this paper.

The contents and thermal behaviour of the room being heated must be considered when designing radiant heat flooring systems. Fontana [33] has been adopted by researchers as the foundational piece of literature on this topic. The paper describes an experimental study with parameters including thermal insulation of the enclosed space's walls, floor coverings, and outside temperature. The number and typology of furniture pieces varied for each arrangement of the study's parameters. Fontana's study sought to experimentally validate previous numerical analyses of the same scenarios [36, 37]. These earlier numerical analyses indicated a notable negative correlation between radiant heat transfer from radiant floors (and therefore room air temperature) and the density of furniture arrangements, with low-

lying furniture having a more significant impact than higher furniture. An experimental study showed similar trends, finding that the heat flux from radiant floors had a slightly negative linear correlation with the ratio of furniture surface area to floor area. A nearly linear negative correlation was observed at low ratios, becoming increasingly negative and non-linear as the furniture surface area to floor area ratio increased beyond 25%. The impact of the wall's insulation thickness in the enclosed space was more notable when high furniture was in place than with low furniture. Rooms dominated by low-lying furniture have a smaller portion of the exterior walls exposed to radiant heat transfer directly from the floor, reducing their impact on radiant heat system performance. This suggests that furniture arrangement has a significant effect on radiant heat systems in small spaces, such as offices and residential buildings, while wall insulation plays a larger role in large open spaces, such as industrial warehouses.

Papers by Luo et al. and Zheng et al. [30, 38–40] have contributed to the understanding of the temperature field of radiant floor systems and the effect of non-heating surface temperatures on the heat output thereof. In their research published in 2016 and 2017, Luo et al. [38–40] explored the three dimensional temperature field of a thermoelectric radiant heating panel using analytical models and experimentation. Zheng et al. [30] went a step further, developing an equation for heat flux from a radiant heat floor based on (1) the temperature difference between the average of the inlet and outlet water temperature and the set point air temperature of the

occupied space (ΔT_a), and (2) the difference between the average radiant panel temperature and the non-heating surface weighted average temperature (ΔT_w), as shown in Equation 2.3. The accuracy of the equation was tested against a numerical simulation of the test standards from four different countries and experimentally validated based on a test standard from the researchers' home country, with relative deviations of the heat output ranging from 2% to 7%.

$$q_{floor} = 29.166 \cdot \Delta T_a^{1.079} \cdot \Delta T_w^{0.023} \tag{2.3}$$

2.3 System Control

Several publications in recent years have highlighted the potential benefits of radiant heating regarding energy savings and occupancy comfort, particularly when paired with modern controls [24, 41–47]. Model predictive control (MPC) stands out as the most effective control approach for optimizing the benefits of radiant heating systems. MPC optimizes current system operation based on user and environmental inputs paired with set schedules and learned occupant behaviour. It has been shown to provide energy savings of up to 42%, without sacrificing occupant comfort [41,44,46]. The benefits of MPC appear to be compounded by the use of pulse-based heating, wherein the heating supply is provided in short pulses of

several minutes with off periods of intermittent length [45, 47]. Based on these findings, pulse-based MPC was included in the recommendations for ThermaRay to further improve system performance and occupant comfort, though it was not studied in this research. Similarly, the potential benefits and challenges associated with integrating proportional-integral (PI), proportional-integral-derivative (PID), and other continuous control approaches into the ESS should be studied [48].

2.4 Hydronic Heating Systems

The source of NRCan's concerns regarding ThermaRay's intentions to install their ESS in Canada is that they will be less efficient than traditional hydronic systems without the currently required insulation. This research focuses on the impact of the requried insulation on the thermal performance of ThermaRay's ESS rather than a direct comparison between it and traditional on-slab hydronic heating systems, shown in Figure 2.1 (refer to Figure 1.1 for a visual comparison with ThermaRay's ESS, which does not typically include insulation across the entirety of the building's footprint). Future studies could focus more directly on the comparison between the two systems though, given the variety of hydronic systems and applications available on the market, this would likely necessitate the parallel development of a whole-building, full-scale model of both types of systems to allow for an accurate and direct comparison. As shown in the figure, insulation is usually

installed immediately below the hydronic piping. Compared to ThermaRay's ESS, the design hydronic systems is typically less focused on the inclusion of thermal mass. As such, placing insulation immediately below the heat source (piping, in the case of hydronic systems) redirects heat upwards directly at its point of delivery to the system. The inclusion and location of this sub-grade insulation is the focus of this research.

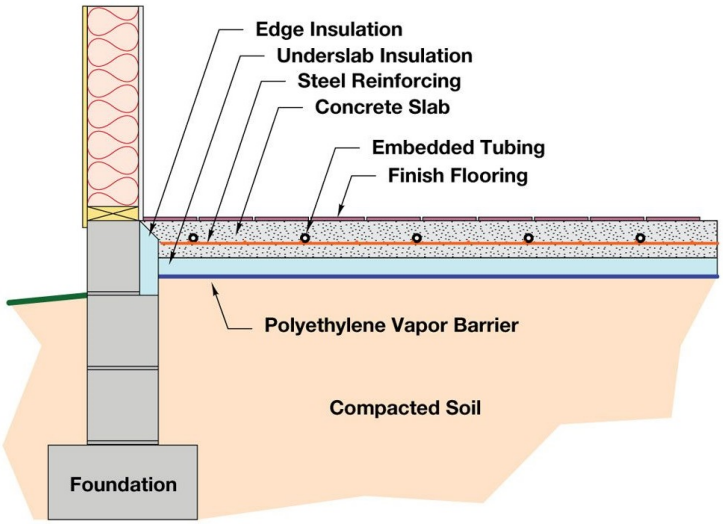

Figure 2.1: Traditional On-Slab Hydronic System with Insulation

2.5 NSCC 1D Study

ThermaRay commissioned a team from the Nova Scotia Community College (NSCC) led by Dr. Alain Joseph in 2017 to produce a report that studied the performance of their ESS in one dimension (depth) measured by the fraction of heat produced by the panel that passed from the panel into the

heated space [49]. The geometry of the model was essentially a $1\,m^2$ slice of a standard ETS installation. Variables whose effects on system performance were studied included: the thickness of insulation between the TES layer containing ThermaRay's heating panels and the layer below, the setpoint temperatures of the panel and of the heated space, and the moisture content and therefore thermal conductivity of the sub-slab TES region's layers. Note that only insulation below the heating panel was included in this study; insulation above the panel was not considered.

The relatively simple Excel-based model assumed one directional, steady state heat flow through materials of constant thermal properties with constant boundary conditions to provide a preliminary thermal evaluation of ThermaRay's ESS. Figure 2.2 displays the model with settings based on the reference case, which is described further in Section 4.1.

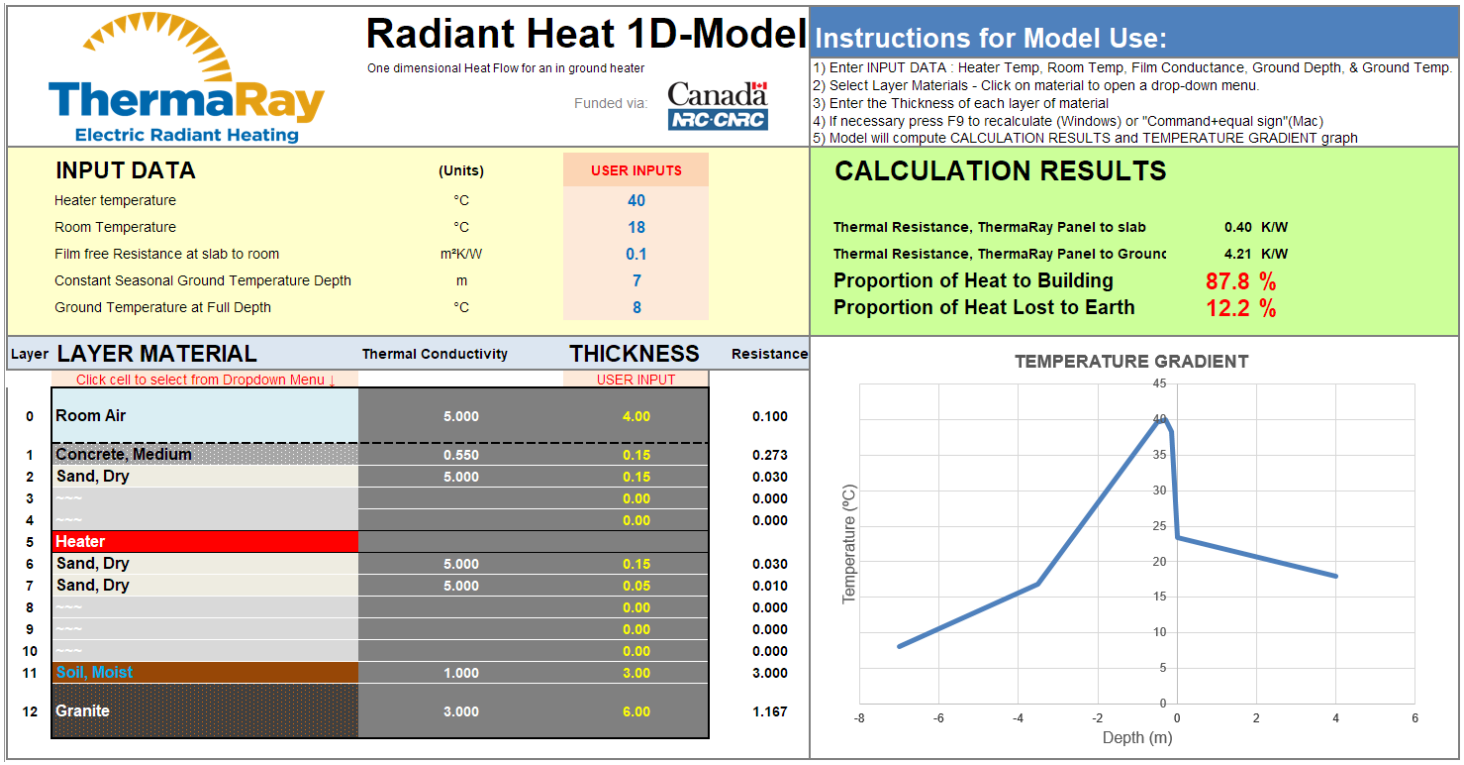

Figure 2.2: Excel-Based Model - Reference Case

Table 2.1: Literature Review Summary - Part 1

Study	**Approach**	**Key Findings**
Chuangchid & Krarti [22] Build. Environ. 2001	Numerical analysis of seasonal thermal losses for a radiant slab-on-grade with and without insulation	- Majority of heat loss occurs along perimeter - Heat source temp. more critical than insulation - Insulation effects soil temperature field far more than the radiant floor output to the room
Fontana [33] Appl. Therm. Eng. 2011	Parametric scaled experiment: studied effect of high and low furniture, wall insulation, and exterior temperature on radiant heat floor performance	- Radiant floor output decreases with increase in furniture floor cover ration, especially beyond 40% - Low-lying furniture has a significant negative effect on radiant floor output; it also decreases the impact of wall insulation on floor performance
Cholewa et al. [31] Energy Build. 2013	Parametric scaled experiment: studied effect of radiant heat supply temp. & air flow rate on h values of radiant floors	- h_c, h_r, and h_{tot} for similar supply temperature and air flow rate range from 2.2 to 3.7, 5.7 to 6.1, and 9.2 to 10.8, respectively (W/m^2K) - h_c values in literature overestimated by 24%
Seyam et al. [29] Energy Build. 2014	Experimental study w/ num. validation incl. radiation model of a scaled room made from electrical heat panels	- Used a discrete-ordinate radiation model (DOM) - Radiation accounted for 75% of total heat flux - h_{tot} ranged from 4.47 to 5.38 W/m^2K - Scaled room shown to be representative of full-scale
Wang et al.[23] Appl. Therm. Eng. 2014	Num. simulation with exp. validation: studied effect of various parameters on hydronic radiant floor system	- Preheat period most sensitive to panel spacing - Conduction effectively 1D after 2 hours (as in [24]) - TES layer thickness critical for heat release time - Numerical results within 7% of experimental results
Li et al. [35] Energy Build. 2015	Full-scale study based on the performance of radiant heat & cool ceilings in a Tokyo building under normal conditions	- h_{tot} = 3.7 & 4.8 for heating & cooling (W/m^2K) - 30 to 40% of heating or cooling 'lost' to plenum - Recommends insulation between panels and plenum - Thermal comfort monitored (PD% < 10%)

Table 2.2: Literature Review Summary - Part 2

Study	**Approach**	**Key Findings**
Zhou & He [24] Appl. Energy 2015	Parametric scaled experiment: studied effect of TES materials and hydronic pipe material on radiant system performance	- PCM releases heat for twice as long as sand - Defines the ESR: active vs. passive heating - Capillary mats provided most uniform, steady heat - Conduction effectively 1D after 2 hours (as in [23])
Cholewa et al. [34] Appl. Therm. Eng. 2017	Parametric scaled experiment: studies effect of radiant heat supply temp. & air flow rate on h values of radiant ceilings	- Expands work done in [31] to ceilings - Measured h_c values as low as 0, well below literature values of up to 0.23 (W/m^2K) - Measured h_{tot} 9 – 24% lower than in literature
Luo et al. [39] Int. J. Heat Mass Transfer 2017	Numerical analysis of the 3D temperature field of a TE-RCP with methods similar to [38]	- Experimental results more stable over time than numerical simulation values - Studies factors effecting temperature field
Zheng et al. [30] Energy Build. 2017	Numerical study to determine effect of non-heating surfaces on radiant floors. Test standards from four countries compared.	- Proposes an equation for q_{floor} that considers non-heating surfaces temperature - q_{floor} inversely proportional to non-heating surface temperature
Tahersima et al. [13] Build. Environ. 2018	Full-scale experiment: studies performance of two designs of radiant heat flooring in an instrumented 3000 m^2 building	- System with less insulation and a thicker TES region performs best, reducing operation costs by 77%, taking advantage of local TOU rates - Majority of heat loss occurs along perimeter

2.6 Knowledge Gaps

ThermaRay's assessments of their ESS's thermal performance to date have been limited to the 1D, steady state, spreadsheet-based model described in Section 2.5 [49]. However, the ETS operates in an environment that is constantly changing, requiring a transient assessment approach. Transient, unsteady computational fluid dynamics and computational heat transfer (CFD-CHT) simulations can be used to study temporal changes in the floor, room, wall, and outdoor air temperatures and their affect on system performance. Developing simulations that consider the effects of these transient factors including all three forms of heat transfer in three dimensions allows for an in-depth analysis of the long-term thermal behaviour of ThermaRay's ESS.

In reviewing the available literature it became clear that the vast majority of relevant studies have focused on one of two topics. The effect of non-heating surfaces, air flow rates, and building insulation on the performance of radiant systems has been studied thoroughly [30, 31, 33–35, 38, 39], as has the transient performance of sub-grade TES systems [13, 22–25]. These studies addressed either the thermal behaviour above or below the slab surface. However, research studying the relationship between the thermal energy storage region below grade and the heated space above grade have been sparse. The vast majority of models developed to date, such as those

presented in research by Laouadi [27], Ritter [28], Seyam et al. [29], and Zheng et al. [30] have focused solely on hydronic systems and/or were numerical in nature. Studying the relationship between above and below grade thermal behaviour through the development of the models presented in this research provides a valuable contribution to the understanding of radiant heat systems while facilitating the development of ThermaRay's ESS.

One of the transient models developed in this research was the first full-scale, three-dimensional representation of an ETS system in a CFD-CHT model which includes a complete vertical section of such a system, from an isothermal point below grade up through the heated space, wherein all forms of heat transfer are modelled, to the ceiling surface and beyond. While the heat source in this research was below the concrete slab, the model could be adapted to study other electricity-based radiant floor or ceiling systems. The creation of this model represents a signficant step forward in the studying and development of these systems, addressing a long-standing gap in the existing knowledge base.

Sections 2.1 through 2.5 provided an overview of the current knowledge base in the fields of thermal energy storage, radiative heat transfer, radiant temperature field modelling, and system control, particularly in recent years. However, this research seeks to address a number of gaps or barriers that are not yet covered in the literature. The roles of each of the key variables in the long-term transient performance of ThermaRay's ESS was unknown.

These include the inclusion, location, and thickness of sub-slab insulation, the size of the heated floor space relative to the number of panels used, the materials selected for the TES region, the significance of contact resistance between those materials, the response of the system as a whole to transient operation, and the exterior temperature.

2.7 Project Components & Objectives

As stated in Section 1.2, the primary objective of this research was *to examine the long-term transient performance of ThermaRay's ESS both with and without the currently required insulation between the concrete slab and unaltered soil below.* This objective was addressed through the development and testing of two models built in two modelling environments.

To achieve the primary objective and to advance the field of radiant heat system research, this project has been divided into two complementary major components based on two simulation environments:

1. The first was focused on the development of the capability of a computational fluid dynamic (CFD) suite called "EXN/Aero". The desired outcome of this portion of the research project was a fully functional model developed for EXN/Aero and an accompanying proposed set of simulations that could be used for in-depth transient studies of ThermaRay's ESS. This included all settings and procedures

required to model ThermaRay's ESS transiently with all modes of heat transfer and buoyancy modelled. Significant effort has gone into the testing and validation of EXN/Aero's modelling capabilities in the development of the proposed set of simulations. The research presented here expands the research community's ability to model the transient thermal behaviour of a variety of radiant floor systems, from an isothermal point well below the concrete slab up through the ceiling above.

2. The second was the development of a model in a second software suite, MATLAB, including its visual modelling environment Simulink. The Simulink model was built to perform a parametric study that would indicate the relationships between various system parameters and the performance of the ESS. Furthermore, the model was developed in such a manner so as to allow for someone who is not well-versed in MATLAB and Simulink to use it as a tool to study the system's performance further. The results of the parametric studies performed with the Simulink-based model allows for the research's primary objective to be addressed directly. Additional results provides ThermaRay and other radiant heating companies and researchers with guidance as to how various parameters effect the thermal performance of radiant systems.

The development of the Simulink model began following the completion of the majority of the formation and testing of the proposed set of EXN/Aero

simulations. As such, its development benefited from lessons learned during the testing the EXN/Aero's simulations. It was the testing and validation of EXN/Aero's contact resistance capabilities which indicated that contact resistance should be included as an optional capability, for example. Furthermore, the design of the Simulink model was based directly on that of the EXN/Aero model, with many of the same properties and dimensions used; the Simulink model was built to be akin to the EXN/Aero model but capable of performing simulations with a duration orders of magnitude shorter than the proposed EXN/Aero simulations. These two complementary models are described in Section 4.2, for the Simulink model, and 4.3 for the EXN/Aero-based simulations.

Based on these two major components, the research was conducted through a sequence of secondary objectives:

- Reproduce the cases presented in the 2017 report by Joseph et al. [49] at NSCC as a quasi-1D simulation in EXN/Aero to fine-tune the CFD solver's conjugate heat transfer capabilities and verify the results of the NSCC study.
- Validate EXN/Aero's contact resistance capabilities through a series of simulations with contact resistance at a variety of interfaces using the quasi-1D EXN/Aero model.
- Test EXN/Aero's transient control algorithm for the ETS heating panels based on the local surface temperature of the concrete slab by

reproducing a selection of the cases from the NSCC report.

- Test EXN/Aero's radiation transport simulation capabilities, first with a 2D steady state analytical validation case [50] then an experimental, transient case from literature [31].
- Produce a three-dimensional full-scale mesh with one of ThermaRay's ETS panels embedded within the TES region of a representative section of a standard ETS installation in an industrial building.
- Produce a set of EXN/Aero simulations using the software's recently developed computational heat transfer capabilities to study the long-term, transient behaviour of ThermaRay's ESS.
- Demonstrate EXN/Aero's modelling capabilities by performing simulations based on the proposed set of EXN/Aero simulations.
- Create a transient model of a full-scale, $1\,\mathrm{m}^2$ slice of ThermaRay's ETS model in the Simulink visual modelling environment.
- Perform parametric studies with this model that includes parameters listed in Section 4.2.2.
- Utilize the results from the parametric studies to address the project's primary objective and to contribute to the existing knowledge base in the field of radiant heat systems research.

Chapter 3

Theory & Methodology

3.1 MATLAB & Simulink

MATLAB is a matrix-based technical computing language and software produced by MathWorks. Its main purposes are data analysis, algorithm development, as well as model creation and testing [51]. MATLAB code is written in either functions, which are defined by their inputs and outputs, or scripts, which do not have defined inputs and outputs. MathWorks also has a model-based design software called Simulink, which can be used for graphical programming and which works seamlessly with code-based MATLAB programming [52]. The Simulink model used in this research, and the MATLAB script written to set it up, run it, and analyze its results, is presented in Section 4.2.

3.2 EXN/Aero CFD Solver

The CFD solver used in this research was EXN/Aero, which has been developed at the University of New Brunswick by Envenio, Inc [53]. Originally created for ocean engineering applications, EXN/Aero is based on a time-implicit SIMPLE approach for pressure-velocity coupling [54]. Its ability to simulate models with hybrid meshes (comprised of both structured and unstructured blocks) and both single and double precision cells while using both CPUs and GPUs efficiently has made EXN/Aero an attractive CFD solver for a wide variety of applications [53]. This was the first industry-partnered project that necessitates the use of EXN/Aero's radiation modelling capabilities. Simulations run in EXN/Aero are set up in the solver's graphic user interface, called EXN/View.

3.2.1 BC Connectivity

EXN/Aero's ability to import multi-block meshes with interfacing heterogeneous blocks is of particular importance to the research presented here. During the simulation setup process, homogeneous blocks such as those comprising the sand layer surrounding the panel in the full-scale EXN/Aero model, are sorted into groups that are referred to as cell families. These cell families are then assigned the various properties and boundary conditions, as necessary. Adjacent cell families with interfacing heterogeneous domains

are treated with EXN/Aero's "BC Connectivity" boundary condition ('BC' being short for boundary condition). This functionality allows the two interfacing domains of adjacent blocks to have different resolutions. This facilitates localized mesh refinement at layer interfaces and in the regions immediately surrounding the ESS's panels, where heat transfer is most transient and intense. Coarser meshing can then be used in regions further from the heating panel to improve computational efficiency.

EXN/Aero's "BC Connectivity" settings also allow for the heat transfer properties at each solid-solid interface within the TES region to be specified based on the thermal properties of the interfacing materials and of the interface itself. This includes contact resistance, discussed in Section 3.3.7. Interface treatment options may also be accessed for the interface of two adjacent layers of the same dimensions if each side of the interfacing domain is assigned to a separate boundary condition group in the meshing software. In this case, the blocks consisting of either side of the interfacing domain must still be assigned to a different cell family.

3.2.2 Governing Equations

Simulations using CFD are based on a series of governing equations. These equations are generally derived from the laws of conservation of mass, energy, momentum, and continuity. In CFD solvers which are based on a finite control volume approach, the General Scalar Advection-Diffusion Equation

(GSADE), shown in Equation 3.1, is the general form of the governing equation for any conservative variable (ϕ) that experiences advection and diffusion.

$$\frac{\partial(\rho\phi)}{\partial t} + \frac{\partial(\rho\phi u_i)}{\partial t} = \frac{\partial}{\partial s_i}\left(\Gamma\frac{\partial\phi}{\partial s_j}\right) + S_\phi \tag{3.1}$$

The GSADE can also be represented as follows:

$$\begin{array}{c}\text{Rate of increase}\\ \text{of } \phi \text{ in CV}\end{array} + \begin{array}{c}\text{Net rate of flow}\\ \text{of } \phi \text{ out of CV}\end{array} = \begin{array}{c}\text{Rate of increase}\\ \text{of } \phi \text{ due to diffusion}\end{array} + \begin{array}{c}\text{Rate of increase}\\ \text{of } \phi \text{ due to sources}\end{array}$$

A 2018 paper by Motasemi and Gerber [55] highlighted the benefits of the GSADE. Each conservative variable, ϕ, has a diffusion term Γ, and a source term, S_ϕ. The most common diffusion and source terms for mass, momentum, and energy are provided in Table 3.1, demonstrating the versatility of the GSADE.

Table 3.1: GSADE Table from Motasemi & Gerber [55]

Conservative Variable	ϕ	Γ	S_ϕ
Mass	1	0	0
Momentum	u_i	μ	$-\frac{\partial P}{\partial s_i} + S_u$
Energy	h	$\frac{k}{c_p}$	S_h
General Species (G)	f_G	ρD_G	S_G

As this study is primarily interested in the transfer of energy between and within solids and fluids, the most important governing equation for this research was derived from the conservation of energy. The governing equation for energy within a solid, based on the GSADE, the conservation of energy (1st Law of Thermodynamics), and conductive heat transfer (Fourier's Law),

is shown in Equation 3.2.

$$\rho \frac{\partial(\rho h)}{\partial t} + \frac{\partial q_i}{\partial s_i} = S_E \tag{3.2}$$

Where h is enthalpy and the heat flux, q_i, is found using Fourier's Law, Equation 3.5. Note that the temperature in a given solid or air space is related to enthalpy through Equation 3.3.

It should be noted that in EXN/Aero, each cell family has its own properties. Therefore to solve Equation 3.1 EXN/Aero must couple all cell family domains together at each iteration to arrive at an end of time step energy distribution, from which a temperature difference was determined using Equation 3.3.

$$dh = c_p dT \tag{3.3}$$

The GSADE equation for energy, paired with Fourier's Law of conduction, is sufficient for solving the energy field within the TES region. Between the TES region and the heated space, and within the heated space, additional equations are required to solve for radiation and convection. Solving the temperature field for the heated space and the boundaries thereof is particularly complex. This is due to the two-way coupling between the energy and radiation equations, based on Equations 3.2 and 3.21, respectively.

This two-way coupling at the concrete-air interface is called multi-mode heat transfer, with the total heat transfer defined in Equation 3.4. Solving for

the radiation field within the heated space is typically based on the predicted temperature field of the space's boundaries, which is based partially on the radiation field within the heated space, as well as conduction and convection from the heated slab surface and any non-heated surfaces. This requires an iterative solution approach, as is common in CFD simulations. The governing equations for mass and momentum, which are included in Table 3.1, are necessary for the modelling of buoyancy within the heated space. Buoyancy modelling is discussed in Section 3.3.3.

$$q_{wall} = q_{rad} + q_{conv} + q_{cond} \tag{3.4}$$

3.3 Modes of Heat Transfer in the ThermaRay ESS

Despite being the only form of heat transfer mentioned in the title of this thesis, radiation is not the only mode of heat transfer that has an important role to play in ThermaRay's ESS. Conduction was paramount within each of the various layers of the TES region, as discussed in Section 3.3.1. According to the results of the 2013 study by Cholewa et al. [31], convection represents roughly 40% of the total heat transfer from the TES region into the heated space at the upper surface of the concrete slab. This convective heat transfer was discussed in Section 3.3.2. The remaining 60% of the heat transfer at

the concrete slab surface occurs via radiative heat transfer, the modelling of which was delved into in Section 3.3.5. The expected values for radiative, convective, and total heat transfer from the concrete surface, based on literature, are provided in Table 5.2 (Section 5.2).

3.3.1 Conductive Heat Transfer

The study of conduction is typically based on Fourier's Law, provided in Equation 3.5. In many applications, both conductive and convective heat transfer play important roles. Understanding the strength of these two modes of heat transfer relative to one another can lead to some simplifications. The Biot number, defined in Equation 3.6, is a non-dimensional comparison between the significance of each of these two forms of heat transfer in a given situation. This non-dimensional number is the basis of the "lumped capacitance" approach to scenarios wherein the significance of conductive and convective heat transfer, individually, are unknown. This method uses the Biot Number to assess whether conduction within a solid is negligible compared to convection occurring at the surface [56]. As the name implies, it is a lump parameter assumption which lumps the thermal capacitance of the solid into one thermally homogeneous solid to simplify calculations.

$$q_i = -k\frac{\partial T}{\partial s_i} \tag{3.5}$$

$$Bi = \frac{R_{cond}}{R_{conv}} = \frac{h_c L}{k} \tag{3.6}$$

In order for the lumped capacitance method to be valid, the Biot number of a solid must be below 0.1. Otherwise, conduction within the material is not negligible and must be considered. The layer of Joseph et al.'s 1D model [49] with the lowest Biot number was the 15 cm thick layer of sand immediately below the concrete slab, with a Biot number of 1.57, based on a contact resistance of 52.48 W/m^{2}K as discussed in Section 3.3.7. In the full-scale model used in both the Simulink model, described in Section 4.2, and the proposed set of EXN/Aero simulations, detailed in Section 4.3, the lowest Biot number was 1.33. This was the Biot number for the 2 inch thick layer of compacted granular rock immediately beneath the concrete slab. Using the thickness-weighted average thermal conductivity of the entire TES region and the expected coefficient of convective heat transfer from the concrete slab surface ($\sim$3 W/m^{2}K) led to a Biot Number of nearly 30. These values confirmed that conduction was the dominant form of heat transfer within the thermal storage region, as expected from other studies [23, 24].

In cases where the Biot number is greater than 0.1, spatial effects within the solid must be considered. This increases the number of variables involved, which then requires that initial spatial and boundary conditions be set to solve the system of equations. Exact and approximate analytical solutions for various simple geometries with set initial and boundary conditions have

been derived. Conduction in transient, three-dimensional cases, such as those studied here, can be simulated using computational fluid dynamics (CFD) applied to solid regions, commonly referred to as computational heat transfer (CHT or CFD-CHT). In this case, simulations will have a governing equation developed based on the conservation of energy and Fourier's Law, as discussed in Section 3.2.2.

Thermal Diffusivity Time Constant

The thickness and thermal properties of each TES layer will dictate how long it takes for them to experience a change in temperature over time, given a non-zero heat flux from their surfaces. To indicate the relationship of this period for each TES region, the "thermal diffusivity time constant" can be used. The equation for this variable is derived below. Equation 3.7 represents one-dimensional conduction, from [56]. The second equation (Equation 3.8) defines the thermal diffusivity constant (D). The third equation (Equation 3.9) demonstrates the simplification used to isolate the time variable, t, which was achieved in Equation 3.11. The thermal diffusivity time constant for each TES layer was provided in Table 3.2, calculated using this final equation. As indicated in the table, the undisturbed soil layer has a thermal diffusivity time constant over 1000x the next highest time constant of the other TES layers. This indicates that the undisturbed soil temperature will take order of magnitude more time to reach a quasi-steady state temperature than the

other TES layers.

$$k\frac{\partial^2 T}{\partial x^2} = \rho c_p \frac{\partial T}{\partial t} \tag{3.7}$$

$$D = \frac{k}{\rho c_p}[m^2/s] \tag{3.8}$$

$$\frac{\partial^2 T}{\partial x^2} \simeq \frac{\frac{\Delta T}{\Delta x}}{\Delta x} = \frac{\Delta T}{(\Delta x)^2} \& \frac{\partial T}{\partial t} \simeq \frac{\Delta T}{\Delta t} \tag{3.9}$$

$$D\frac{\Delta T}{(\Delta x)^2} \simeq \frac{\Delta T}{\Delta t} \tag{3.10}$$

$$\Delta t \simeq \frac{(\Delta x)^2}{D} \tag{3.11}$$

Table 3.2: Thermal Diffusivity Time Constant of TES Layers

TES Layer	**Thickness [m]**	**Thermal Diffusivity [m^2/s]**	**Thermal Diffusivity Time Constant [s]**
Concrete	0.1016	7.14E-07	14450
Compacted Granular Rock	0.0508	1.02E-06	2538
Compacted Fill	0.0508	5.77E-07	4471
Sand	0.1016	1.98E-07	52000
Compressed Sand	0.0508	2.54E-07	10170
Undisturbed Soil	6.644	7.48E-07	58980000
XPS Insulation	0.05	7.57322E-07	3301.107488

3.3.2 Convective Heat Transfer

Convection accounts for roughly 40% of the heat transfer occurring at the surface of the concrete slab [31]. Equation 3.12 was used to calculate

convective heat transfer into the heated space:

$$q_c = h_c \cdot A \cdot (T_C - T_A) \tag{3.12}$$

The value of h_c can be assumed to be constant in simple, theoretical cases. At the concrete-air interface in ThermaRay's ESS, h_c is primarily a function of both of temperature and air flow rate. To simplify calculations the maximum velocity of the air in the heated room (outside the velocity boundary layer along the floor) was assumed to be constant and less than 0.2 m/s. This assumption, which relies on a relatively low variation in air flow within the heated space, reduces h_c to a function of temperature. Values can then be obtained from the 2013 paper by Cholewa et al. [31]. This air flow rate was reasonable based on the required ventilation rates from the ASHRAE Handbook 62.1, Table 6.2.2.1, which states a ventilation rate of 0.06 cfm/ft^2 is required for warehouses [57]. Based on this ventilation rate, the average air velocity in a 60' x 100' warehouse (a common application for ThermaRay's ESS) would be in the range of 0.0005 m/s, well below the assumed 0.2 m/s. Seyam et al. [29] further supports this assumption, having found a maximum air velocity of 0.02 m/s based on the analysis of an electric radiant heating panel. However, this assumption [EXTEND]

In the 2013 report by Cholewa et al. [31], the heat transfer coefficient from a heated radiant floor to the room was studied with parametric variables including the water flow rate and supply temperature for the hydronic

radiant heat floor system, and elevation of the measurement point above the heated floor. Values of h_c ranged from 2.2 to 3.5 W/m^{2}K [31] for various temperature and measurement height arrangements. The paper also suggested that h_c obtained from commonly used equations derived from the traditional enthalpy-based approach (specifically, those developed by Awbi and Hatton [58] and by Min et al. [59]) should be reduced by 24% prior to use.

The values from Cholewa et al. [31] were corroborated by a more recent study performed by Koca et al. [60], which found h_c values between 2.59 and 2.73 W/m^{2}K for water supply temperatures between 31 and 42°C using a wall-based hydronic radiant heat system. A 2012 paper by De Carli et al. [61] suggests a slightly lower value of 2.1 – 2.4 W/m^{2}K for the scenario being studied here, as calculated using Equation 3.13 (from [61]).

$$h_c = \left(\frac{2.175}{L_C^{0.076}}\right) \times (\Delta T_{ETS})^{0.308} \tag{3.13}$$

Using h_c values from literature allows for ΔT_{ETS} to be the sole transient variable in the calculation of convective heat flux (q_c) from the slab surface with this equation. While the accurate approximation of this variable is challenging and error-prone, including it in the parametric studies performed in this research allowed for the sensitivity of the simulations' results to the selected values of h_c to be estimated and supported the independence of the research's conclusions from the potential inaccuracy of the values obtained

from Cholewa et al. ([31]).

Free Convective Heat Transfer

Convective heat transfer within the heated space, from immediately above the concrete floor to the ceiling above, cannot be estimated in the same manner as that from the concrete slab into the heated space. Also known as natural convection, free convection within the heated space is driven by buoyancy.

EXN/Aero's buoyancy and turbulence models with velocity-pressure coupling can be used to model the buoyancy-driven natural convection within the heated space. While necessary for accurate modelling of flow within the heated space, the use of these models should be limited as they require a significant reduction in the simulations' time step and a substantial increase in their computational demand. A combination of using these models with a reduced time step and a less computationally intense alternative, based on an effective thermal conductivity value (k_{eff}), with a larger time step has been proposed and tested. Effective thermal conductivity is discussed in Section 3.3.4. The combination of modelling approaches for within the heated space is detailed in Section 4.3, which covers the proposed set of full-scale, transient, three-dimensional simulations of ThermaRay's ESS using EXN/Aero.

3.3.3 Buoyancy Modelling

The modelling of buoyant flow within the heated space in the proposed set of EXN/Aero simulations was based on the Boussinesq assumption. This assumption is based on the premise that when the spatial variation of density is low enough, such as in flow driven solely by natural convection, the variation in density can be assumed to only impact the affect of gravity on the flow and no other aspect of the flow field [56]. The validity of this assumption was explored by Gray & Giorgini [62], which has since been established as the standard test thereof. Their work established firm bounds on the validity of the Boussinesq assumption. Given the average air temperature in simulations of EXN/Aero's ESS of approximately 20 °C and a ceiling height well under 10^2 m, the Boussinesq assumption is valid for the simulations performed in this research. The graph from Gray & Giorgini [62] is provided in Figure 3.1.

This reduces the full Navier-Stokes Equation for compressible flow (Equation 3.14) to a much simpler equation, Equation 3.15). Treating the air in the heated space as an ideal gas allows for further simplification by permitting the local difference in fluid density to be directly correlated to the local variation in temperature. The result of the Boussinesq and ideal gas assumptions is displayed in Equation 3.16. This assumption significantly reduces the computational demand of EXN/Aero's buoyancy model. However, due to the complexity of turbulence, the buoyancy-driven flow still requires a much smaller time step to capture the formation of the

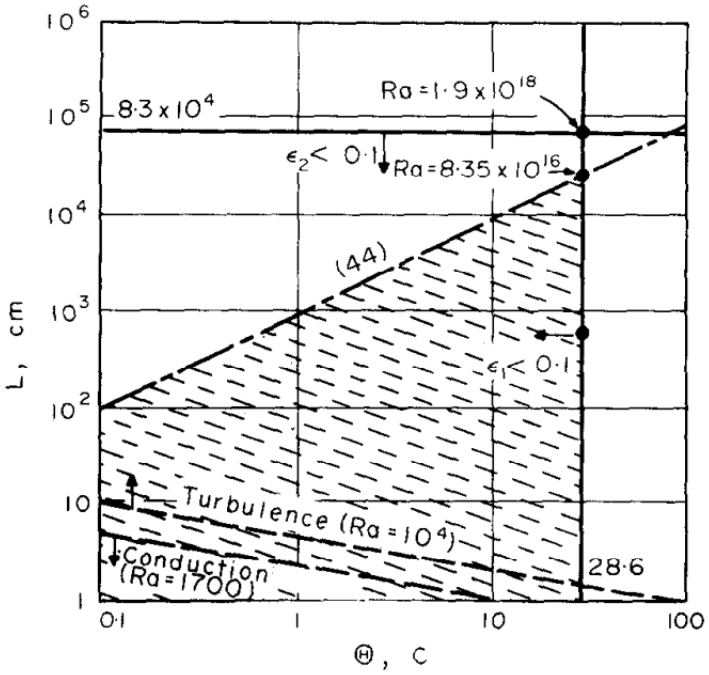

Figure 3.1: Boussinesq Assumption Validity Test
(Shaded Area Indicates Validity)

buoyant flow field.

$$\rho\left(\frac{\partial \mathbf{u}}{\partial t} + u \cdot \nabla \mathbf{u}\right) = -\nabla p + \nabla \cdot \left[\mu\big(\nabla \mathbf{u} + (\nabla \mathbf{u})^T\big) - \frac{2}{3}\mu(\nabla \mathbf{u})\mathbf{I}\right] + \rho \mathbf{g} \quad (3.14)$$

$$\rho_0\left(\frac{\partial \mathbf{u}}{\partial t} + u \cdot \nabla \mathbf{u}\right) = -\nabla p + \mu \nabla^2 \mathbf{u} + (\rho_0 + \Delta\rho)\mathbf{g} \quad (3.15)$$

$$\rho_0\left(\frac{\partial \mathbf{u}}{\partial t} + u \cdot \nabla \mathbf{u}\right) = -\nabla P + \mu \nabla^2 \mathbf{u} - \rho_0 \frac{T - T_0}{T_0}\mathbf{g} \quad (3.16)$$

Where ρ_0 is the reference density, based on the fluid's reference temperature T_0, $\mathbf{u}$ is the fluid's local velocity, μ is the dynamic viscosity of the fluid, and P is the elevation-adjusted pressure, equal to $p + \rho_0 g z$ where z is the local elevation [56, 63].

EXN/Aero's buoyancy model has been rigorously tested and demonstrated in multiple publications [64–67]. As such, it was used in this research without additional prior validation. The settings in EXN/Aero used for buoyancy modelling and an example of a buoyancy-driven flow field are provided in Section 4.3.

3.3.4 Effective Thermal Conductivity

Accurately modelling buoyancy-driven natural convection was imperative as it represents 40% of the heat transfer occurring between the heated concrete slab and the ceiling 10 m above. Despite the computationally intense nature of buoyancy and turbulence modelling, not including natural convection would be detrimental to the accuracy of the EXN/Aero model of ThermaRay's ESS. A set of simulations was sought that would include buoyancy and turbulence models within the heated space while mitigating their impact on the computational resources required to perform the simulations.

The first in the proposed set of EXN/Aero simulations, described in Section

4.3, includes an inflated value of air's thermal conductivity to reflect the contribution of convection to heat transfer through the heated space with the buoyancy model deactivated. This inflated value is called the effective thermal conductivity (k_{eff}).

Using effective values in CFD is not a novel concept. For example, the use of effective viscosity, μ_{eff}, is a well established approach for buoyant flows with both laminar and turbulent characteristics [68, 69]. In the case of μ_{eff}, it is approximated as the sum of the flow's laminar and turbulent viscosities. Substituting it into the previously provided equation for buoyant flow based on the Boussinesq assumption, Equation 3.16, the equation becomes Equation 3.17:

$$\rho_0\left(\frac{\partial \mathbf{u}}{\partial t} + u \cdot \nabla \mathbf{u}\right) = -\nabla P + \mu_{eff}\nabla^2\mathbf{u} - \rho_0\frac{T - T_0}{T_0}\mathbf{g} \tag{3.17}$$

The premise behind k_{eff} is similar to that for μ_{eff}. The value of μ_{eff} is the sum of viscosity from laminar and turbulent flow. Likewise, k_{eff} is the sum of heat transfer from heat transfer via conduction (akin to laminar flow) and natural convection (due to buoyancy, akin to turbulent flow). While the use of μ_{eff} is more common than k_{eff}, k_{eff} has previously been used to study natural convection and buoyancy in recently published papers [70, 71]. Despite its established nature as a tried-and-true manner of approximating heat flow within buoyant flow, k_{eff} is only recommended for use in establishing a priminary estimate of the temperature field within the

heated space. The use of k_{eff} in the proposed set of EXN/Aero simulations is further discussed in Section 4.3. The two methods for calculating k_{eff} considered in this research are presented below.

The first and primary method used to calculate k_{eff} is based on a 2005 paper by Brucker & Majdalani [72] entitled "Effective Thermal Conductivity of Common Geometric Shapes". It provides a detailed description of how to calculate the effective thermal conductivity from a variety of heated surfaces. The closest approximation to the heated floor of a warehouse is a "horizontal plate, hot side up". To calculate the effective thermal conductivity, several air properties must be first determined. These properties and values used in the calculations are provided in Table 3.3. The equation for k_{eff} was based on the geometry and the Rayleigh Number (Ra), which is analogous of Reynold's Number (Re) for free convection. Based on the model's Rayleigh Number of 1.5 x 10^7 (see Table 3.3 for calculations), the free convection within a warehouse heated by ThermaRay's ETS would be at the critical point between laminar and turbulent flow. A Rayleigh Number of 10^7 is an order of magnitude less than that proposed by De Carli et al. [61], and so equations for turbulent and laminar flow were considered. Using the equation provided in [72] for turbulent free convection led to an effective thermal conductivity of less than the standard thermal conductivity of air, while the equation for laminar flow (Equation 3.20) provided a value of 0.806 W/mK (k_{eff}, k_{eff} (1) in Table 3.3. As the effective thermal conductivity was expected to be much higher than the standard thermal conductivity due to

the inclusion of convection, the result based on assuming the flow is laminar was selected.

There is a second, more straightforward approach to calculating the effective thermal conductivity. Based on the definition of the Nusselt Number (defined in Equation 3.18), it can be used to find k_{eff} directly. Two methods for calculating the Nuesselt Number are presented in Table 3.3, labelled as methods (a) and (b). These methods, despite the significant differences between them, lead to similar results for k_{eff} in the range of 0.962 to 1.10. Values of k_{eff} using Nusselt Numbers are labelled as values (a) and (b) for k_{eff} (2) in Table 3.3. Further modelling with these k_{eff} is recommended in the future development of the proposed EXN/Aero simulations.

$$Nu_L \equiv \frac{k_{eff}}{k_{air}} \simeq \frac{h_c L_c}{k} \tag{3.18}$$

This simplified approach to modelling convection through the heated space requires several assumptions and treats buoyancy-based free convection as diffusion-based conduction. While this significantly reduces the computational demand of the simulations, it may also significantly reduce the accuracy of the simulation results. This concern is supported by a recent paper by Li & Tu [75], which determined that turbulence modelling is critical for the accurate prediction of near-wall flow and heat distribution patterns. The much higher Nusselt Number values in Zheng et al. and Acikgoz et al. [30, 74], over five times that which was found in the calculation of k_{eff}, was

Table 3.3: k_{eff} Calculation Variables

Property	**Value**	**Unit**	**Equation / Source**
T_{Air}	293.15	K	—
$T_{Concrete}$	291.15	K	—
ν	1.506 x 10^{-5}	$m^2\ s^{-1}$	[73]
α	2.17 x 10^{-5}	$m^2\ s^{-1}$	[73]
μ	1.817 x 10^{-5}	Pa s	[73]
g	9.81	$N\ g^{-1}$	[73]
c_p	1006	$J\ kg^{-1}\ K^{-1}$	[73]
β	3.4 x 10^{-3}	K^{-1}	$\frac{1}{T_{Air}}$
k_{air}	0.026	$W\ m^{-1}\ K^{-1}$	[56]
Pr	0.7	—	$\frac{\mu c_p}{k_{air}}$ [56]
L_c	0.3673	m	$\frac{A_{Floor}}{P_{Floor}}$
Nu_L (a)	42.4	—	$\frac{h_c L_c}{k_{air}}$
Nu_L (b)	36.99	—	$0.15 \cdot Ra_L^{1/3}$ [56]
Ra_{L_c}	1.5 x 10^7	—	$Gr_{L_c}Pr = g\beta(T_{Concrete} - T_{Air})L_c^3(\nu\alpha)^{-1}$ (3.19)
Gr_{L_c}	2.17 x 10^{-5}	$m^2\ s^{-1}$	$g\beta(T_{Concrete}–T_{Air})L_c^3\ \nu^{-2}$
h_{tot}	9.6	$W\ K^{-1}\ m^{-2}$	[31] ($h_{tot,0.6}$) & [74]
k_{eff} (1)	0.1895	$W\ m^{-1}\ K^{-1}$	$2.274\sqrt[3]{\frac{(h_{tot}L_c)^4}{Gr_{L_c}\mu c_p}}$ (3.20)
k_{eff} (2)	1.10 (a) 0.962 (b)	$W\ m^{-1}\ K^{-1}$	$Nu_L \cdot k_{air}$ (4.2)

also cause for concern. To determine the impact of these assumptions and simplifications, simulations were run based on k_{eff} (1), k_{eff} (2a), and k_{eff} (2b). The value of effective thermal conductivity had no significant impact on heat transfer through the heated spaced. The results of these simulations made it clear that buoyancy modelling would be necessary to accurately represent the contribution from convection to the total heat transfer between the heated concrete slab surface and the ceiling, 10 m above. This is further supported by the results of the full-scale EXN/Aero simulations provided in Section 4.3. Effective thermal conductivity nonetheless has a part to play in the proposed set of EXN/Aero simulations, described in Section 4.3.

3.3.5 Radiative Heat Transfer

Raithby [50], Kim & Huh [76], Hassanzadeh & Raithby [77], and Murthy & Mathur [78] have studied how the discrete ordinate method (DOM) and finite-volume method (FVM) have allowed for the seamless integration of computational fluid dynamics and computational heat transfer (CFD-CHT). Both DOM and FVM are based on the radiation transfer equation (RTE), defined in Equation 3.21. The RTE was derived from the premise that as a ray of radiation passes through a medium it will gain and lose energy via absorption, emission, and scattering. Each of these phenomena are included

in the RTE.

$$\frac{dI}{ds} = -(\kappa_a + \sigma_S) \cdot I(s_i, s_p) + \kappa_a \cdot I_b(R) + \frac{\sigma_S}{4\pi} \int_{4\pi} \Psi(s', s) \cdot I(R, s') d\omega' \quad (3.21)$$

As identified in the aforementioned papers ([50, 76–78]), FVM is more apt for use with traditional CFD meshes and solvers, primarily because it treats directional and spatial discretization in the same manner as existing CFD solvers. This allows for radiative heat transfer to be treated much like the fluid properties traditionally solved through CFD. The FVM-based radiation model is also more computationally efficient at the same level of accuracy when compared to other approaches, such as the proton-based Monte-Carlo method, based on the findings of Li et al. [79]. EXN/Aero's FVM-based radiation modelling capabilities were developed for this study and will be the focus of this section.

To solve for radiative heat transfer between two surfaces or bodies, FVM calls for the division of the space between the two surfaces or bodies into a number of control volumes (CVs) as in traditional CFD meshes, referred to as the directional domain. The space is also divided into a number of azimuthal and polar subdivisions ($N_\phi \times N_\theta$), referred to as the solid angles, representing the directions in which radiation is being calculated. A sample solid angle discretization is shown in Figure 3.2. These solid angles comprise the spatial domain; together, the directional and spatial domains allow for radiation to be modelled in a manner similar to that used for convective

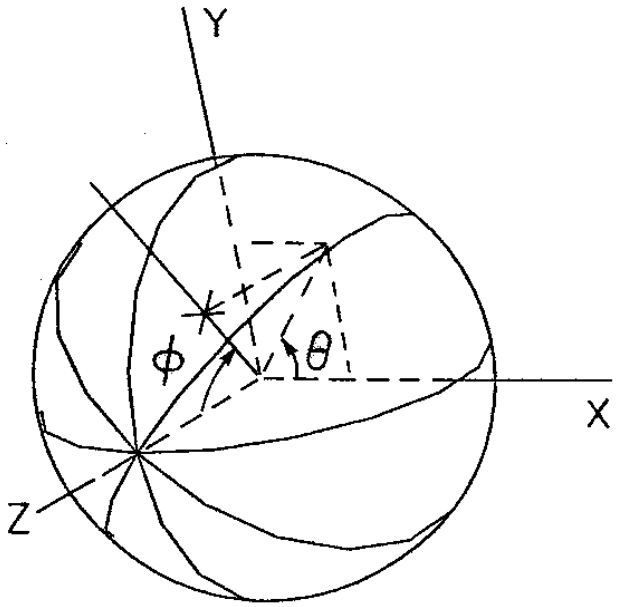

Figure 3.2: Sample Solid Angle Discretization [50]

and conductive heat transfer in CFD-CHT. While radiative heat transfer generally occurs in all directions, this is a systematic approach to reducing the number of directions considered in calculation to optimize the accuracy and computational demand of radiation modelling.

To begin the process of modelling radiation between two surfaces, an initial estimate of the radiative heat flux (q_r) emitted from the fluid-solid interface to the central nodes of adjacent CVs in the fluid must be made. The initial estimate of q_r for the nodes of each of these adjacent CVs is then calculated, a process which continues propagating throughout the computational domain until a preliminary estimate of the radiative heat flux has been calculated for all CVs. As in traditional CFD, this process is iterated until the difference in

radiative heat flux from one cycle to the next has fallen to a predetermined value or until a preset number of iterations has occurred.

3.3.6 Preliminary Radiation Model Validation

EXN/Aero's radiation model was validated prior to proceeding with the development of the parametric study. The initial phase of the validation process was focused on a 1995 paper by Cheong & Song [80]. Cheong & Song provided an analytical solution for a 2D enclosure shown schematically in Figure 3.3. The schematic consists of a unitless square comprised of four diffuse blackbody walls. The lower wall radiates heat via radiation to the other three walls. The paper provided an equation for the intensity of radiation along the upper wall (opposite the radiating wall), F(s), provided in Equation 3.22.

$$F(s) = I_{bw}^{+} exp(-\kappa s^{+}) + I_{bw}^{-} exp(-\kappa s^{-}) + I_b[2 - exp(-\kappa s^{+}) - exp(-\kappa s^{-})] \tag{3.22}$$

In this equation, s^+ is the distance from the leftmost end of the wall and is therefore equal to s. s^- is the distance from the rightmost end of the wall, and is therefore equal to $D - s$, with $D = 1$ in a non-dimensional square domain. Cheong & Song provide a plot of the analytical results, shown as a solid line in Figure 3.5.

The validation efforts in Raithby [50] were based on the 20 x 20 mesh shown

in Figure 3.4 [50]. Their results, represented as the normalized radiative heat flux (q^*_{rad}) along the wall opposite that was set at temperature T_1, are plotted alongside the analytical solution in Figure 3.5. This normalized radiative heat flux was defined in Equation 3.23. Also plotted in Figure 3.5 are the results of DOM- and FVM-based models, with FVM results labelled as 'Present' along with the number of solid angles used for each simulation. The closest result to the analytical solution is the 'Present, L = 16' simulation, indicating the benefit of using an FVM-based model with an adequate number of solid angles.

Raithby's 20 x 20 mesh was the basis of the preliminary validation simulations. The aim of these simulations was to validate EXN/Aero's radiation model based on the analytical solution from Cheong & Song [80] while developing a better understanding of the radiation model's behaviour through a parametric study.

$$q^*_{rad} = \frac{q_{rad}}{\sigma(T_1^4 - T_2^4)} \tag{3.23}$$

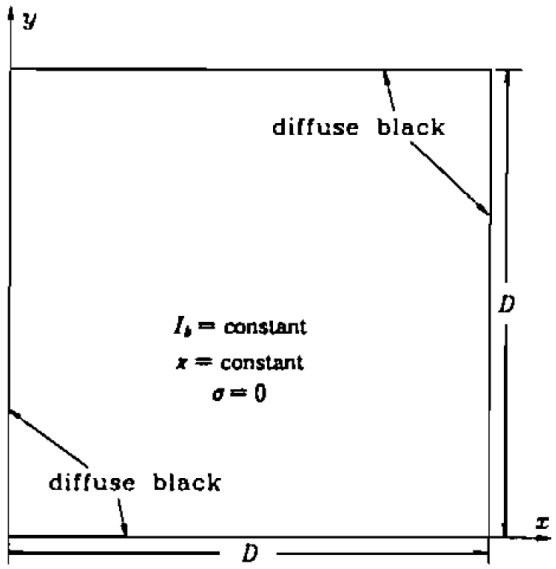

Figure 3.3: Schematic for Cheong & Song's Analytical Solution [80]

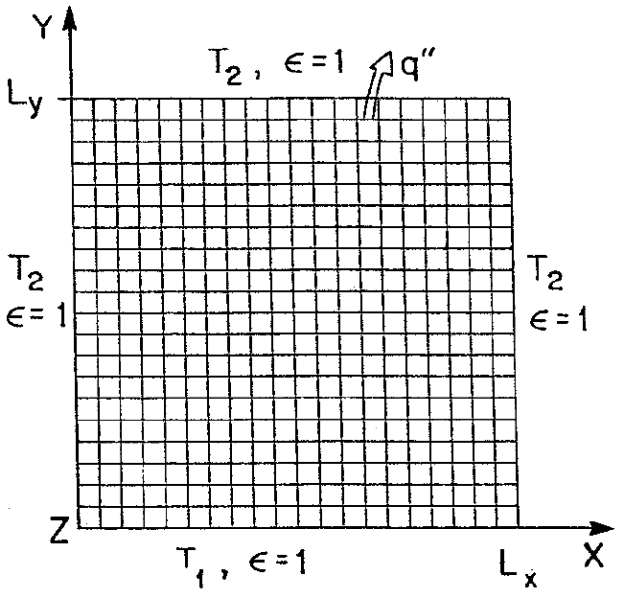

Figure 3.4: Computational Mesh Used in Raithby [50]

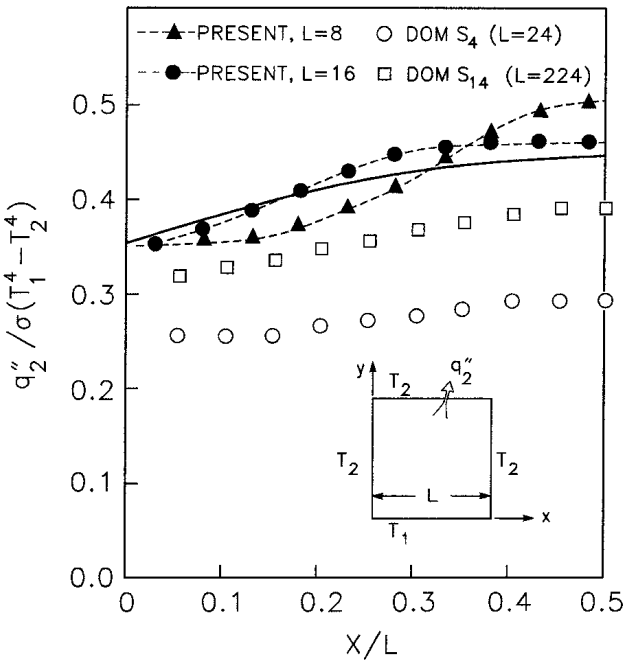

Figure 3.5: Plot of Analytical Solution from [80]

The papers by Cheong & Song [80] and Raithby [50] did little to describe the methodology of their validation case. The effect of the key variables on the normalized radiative heat flux (q^*_{rad}), found through a parametric study, was summarized in Table 3.4 and detailed in Appendix D. The only variable that affects q^*_{rad} in a non-uniform manner across the length of the T_2 wall opposite the T_1 wall (hereto referred to as the T_2 wall) is κ. Scattered radiation comprises a significant portion of the radiative flux encountered by the center of the T_2 wall. Radiation between two opaque walls is reduced by absorption [50, 81], and so an increase in absorption disproportionately affects the center of the T_2 wall. All other variables affect the entire length of the T_2 wall evenly.

Table 3.4: Affect of Key Variables on q^*_{rad}

Parameter	**Variable Affected**	**Relation**	**Reason for Affect**
κ	q^*_{rad}	$\propto^{-1}$	Absorption decreases radiative flux on opposite wall
T_{ref}	q^*_{rad}	$\propto^{-1}$	Increases in q_{rad} due to a higher T_{ref}
T_1-T_2	q^*_{rad}	$\propto^{-1}$	or T_1-T_2 are reduced by absorption, but that on $\sigma(T_1^4 - T_2^4)$ is not
L_s	Smoothness of q^*_{rad}	$\propto$	Increasing the number of solid angles used improves accuracy but increases the computational demand of the simulation

The medium's aborption coefficient was not specified in the Cheong & Song paper [80]. A trial-and-error process found that a κd value (the non-dimensional product of the absorption coefficient and the width of the computational domain) of 0.23 provided a response within 0.6% of the analytical solution. This value of κd was used in all subsequent simulations. The paper also did not provide values for T_1, T_2, and T_{ref}. The radiative intensity of the T_1 wall (I_b, defined in Equation 3.24) was stated to be "Unity" and that the other walls were "cold black". From this, temperatures of 64.8 K for T_1 and 0 K for T_2 were obtained with a T_{ref} of 0 K as these values yielded accurate results based on the analytical solution. Setting T_1 and T_2 to 100°C and 0°C, led to identical results with a T_{ref} of 273.15 K (0°C). These two sets of results overlap in Figure 3.6.

$$I_b(T) = \frac{q_{rad}}{\sigma T^4} \tag{3.24}$$

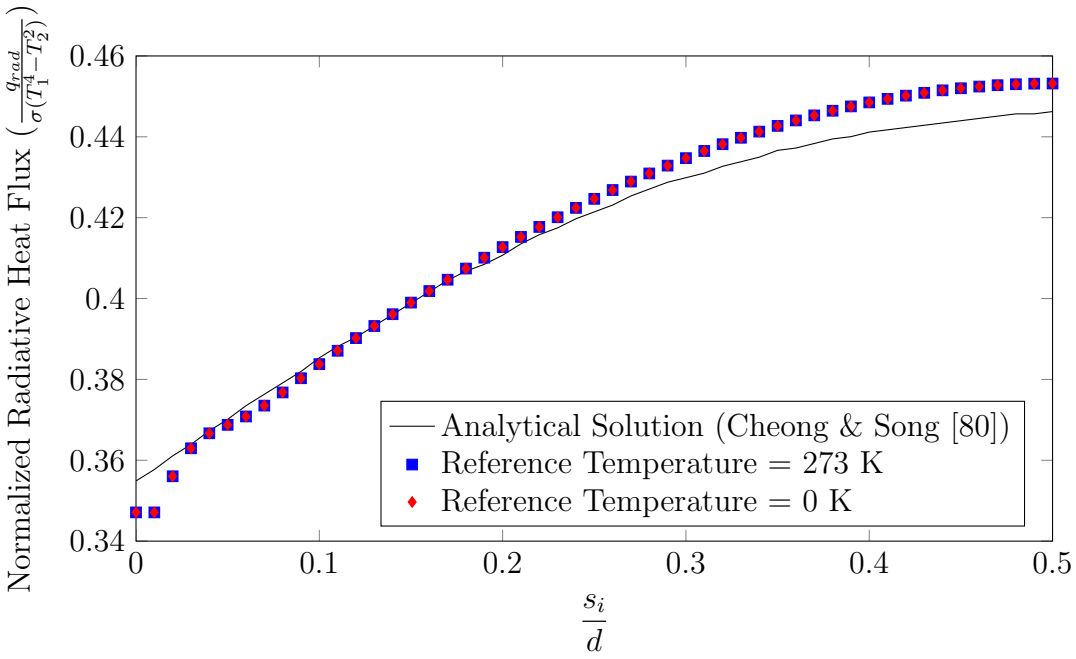

Figure 3.6: Validation of EXN/Aero's Radiation Model - 2D Assessment

A demonstration of EXN/Aero's recently added ability to output the radiation intensity within a medium is provided in Figure 3.7. This figure shows the 2D radiation field from one of the validation cases described by Raithby [50]. A series of plots is provided in Appendix D outlining the results of the parametric study that was performed as a part of the validation process.

This figure indicates a radial decrease in radiation intensity due to absorption by the air within the computational domain. This phenomena was expected based on the RTE equation (Equation 3.21, validating the

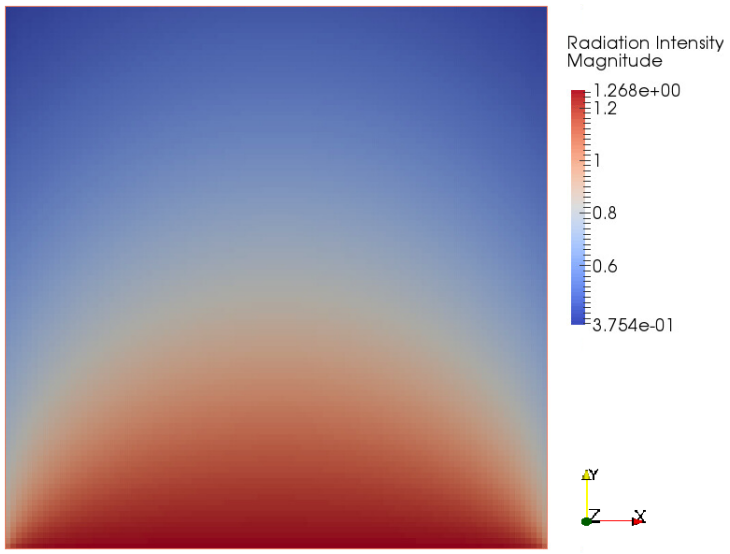

Figure 3.7: Radiation Intensity - Validation Case

functionality of EXN/Aero's radiation model in two-dimensional simulations. Despite this validation of the full functionality of the radiation modelling, including absorption and scattering, the air within the heated space was treated as a non-participating medium in the models utilized in this research. In radiation modelling, a non-participating medium is one that does not absorb or scatter radiative heat transfer that passes through it. Treating the air within the heated space as a non-participating medium requires one to assume that scattering and absorption within the heated space are negligible. The validity of this assumption is discussed in Section 5.3.1.

A second stage of validation was performed for the radiation model as part of the demonstration of EXN/Aero's capability of modelling ThermaRay's ESS. This is presented alongside the proposed set of EXN/Aero simulations

in Section 4.3.3.

3.3.7 Contact Resistance

Contact resistance is defined here as thermal resistance between two interfacing surfaces or materials due to the imperfect nature of the interface. For example, if a coarse material, such as sand paper, is interfaced with a smooth surface, such as a piece of paper, there will be small air gaps anywhere that the grains of the sandpaper are not in contact with the paper. The approach used to determine the effect of contact resistance on results of this research was to estimate the average size of the air gaps at solid-solid interfaces within the TES region. An air gap thickness of 0.5 mm, roughly the diameter of a grain of sand [82], between two solid regions was assumed in the full-scale simulations performed for this research. This allowed for the influence of contact resistance on the overall heat transfer to be examined. An example calculation of this contact resistance is shown in Equation 3.25. While the results were heavily dependent on the assumed air gap thickness, the magnitude of contact resistance was varied in this research to determine the sensitivity of the system's performance to contact resistance and minimize the potentially negative impact of this assumption on the accuracy of the conclusions drawn from the results of this research.

$$\text{Surface Conductance Coefficient} = \frac{k_{air}}{\Delta s_{gap}} = \frac{0.02624\ W/mK}{0.0005\ m} = 52.48\ \text{W/m}^2\text{K} \quad (3.25)$$

Contact resistance was not included in the Excel-based model developed by Joseph et al. [49], and so it was not included in the 1D simulations presented in Sections 4.1 and 5.1. However, as per Figure 1.1, there are more solid-solid interfaces present above the heating panel than below, indicating it could impact the system performance values obtained from the models used in this research. Contact resistance was studied accordingly using the 1D model to determine whether it should be included in the full-scale models that followed. Default settings for the 1D model was used for this study (for default data, refer to Table 4.1). To simplify verification of whether the energy balance was maintained in each simulation, the volumetric heating panel output was reduced to 10 kW m^{-3} from the 12.7 kW m^{-3} that would otherwise be used for Case 5 simulations, as per Table B.5. The case was first run with no contact resistance, assuming pure conduction at all solid-solid interfaces. It was then run with contact resistance equivalent to a 0.5 mm air gap, as described above, at two locations of interest. The interface between the heating panel and the sand layer immediately above was selected as an area of interest due to the intense and critical nature of the heat transfer occurring there. Secondly, the interface between the moist soil layer and the granite below was selected to examine the performance of EXN/Aero's

contact resistance modelling in a region of less intense heat transfer. A final verification simulation was run with contact resistance present at every solid-solid interface.

The results of these simulations are shown in Figure 3.8. Solid-solid interfaces are denoted with vertical lines in the inset plots, with the two interfaces of interest shown as solid black lines while other solid-solid interfaces are represented with grey lines. The upper heating panel-sand interface is referred to as Interface 1 while the moist soil-granite layer interface is referred to as Interface 2. The plotted results indicate that contact resistance at interfaces nearest the heat source have the most significant impact on the vertical temperature gradient throughout the system. This is most evident in comparison of the first three runs; introducing contact resistance at the moist soil / granite interface does not affect the performance of the system, while contact resistance at the heating panel-sand interface decreases system performance by 0.3%. It is also apparent that uniformity in the application of contact resistance throughout the TES region is ideal for maintenance of the energy balance.

The affect of adding contact resistance is further visualized in Figure 3.9. The percentage difference between the temperature gradients of each simulation with contact resistance modelled at one or more interface compared to a simulation without contact resistance ('pure conduction') is plotted. The figure demonstrates that it is the interface closest to the

heating panel, interface # 1, which has the greatest impact on the results. Simulations with contact resistance included at this interface, which is in the immediate vicinity of the heating panel, have a maximum percentage difference of at least 2%, while that with contact resistance only included at interface #2, further from the heating panel, has a maximum percentage difference of just 1%. This finding indicates that, should contact resistance be found to have a significant impact on system performance, efforts to enhance or mitigate it should focus on the area immediately surrounding the heating panels.

Contact resistance – specifically, the presence and magnitude thereof – has been considered in the parametric study described in Section 4.2. However, it was not included in the proposed set of EXN/Aero simulations described in Section 4.3 due to the significant computational resources required for each set of EXN/Aero simulations compared to the simulations used for the parametric study. This thoroughly tested functionality could easily be added to any future simulations of ThermaRay's ESS in EXN/Aero.

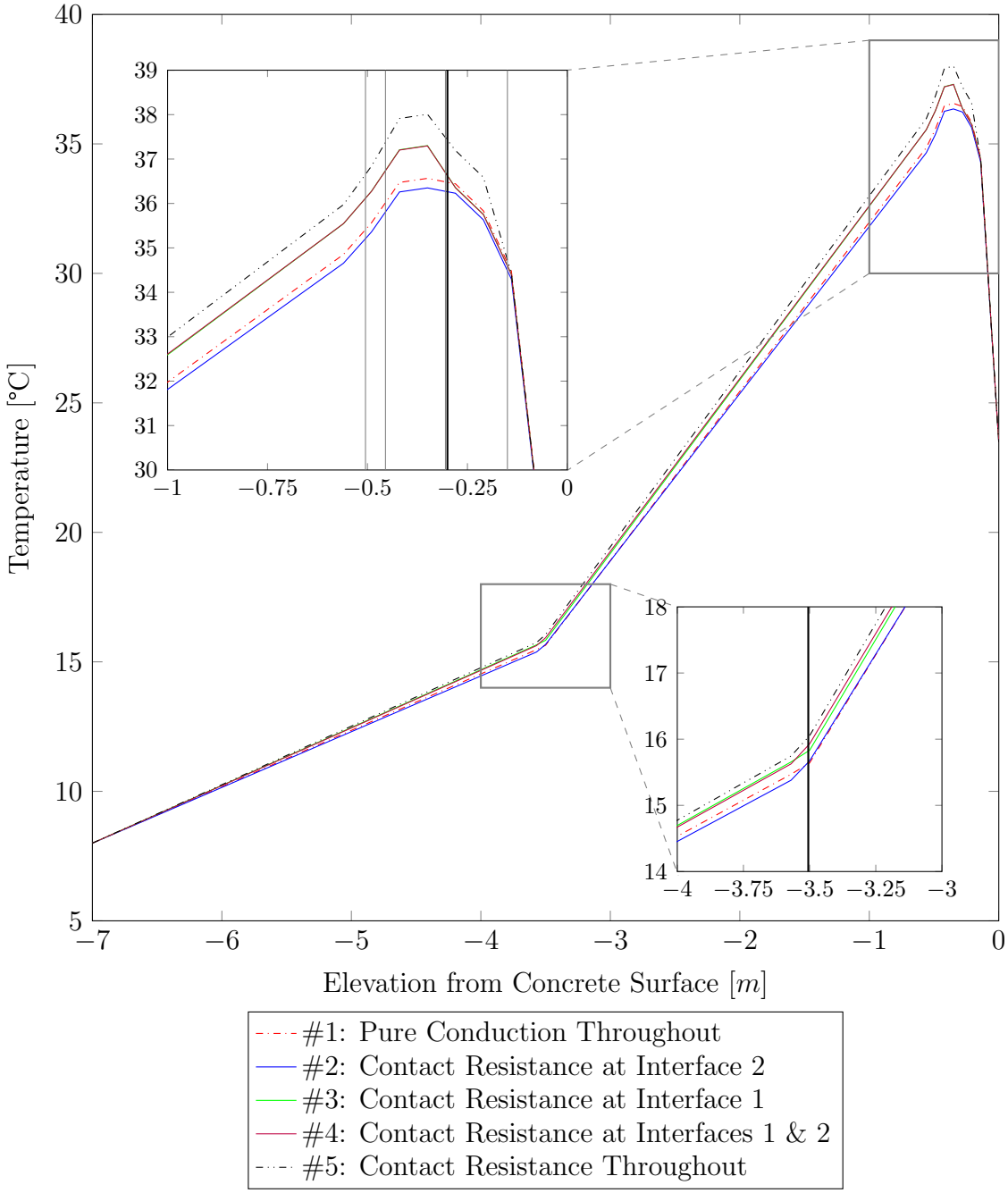

Figure 3.8: Validation of EXN/Aero's Contact Resistance Capabilities

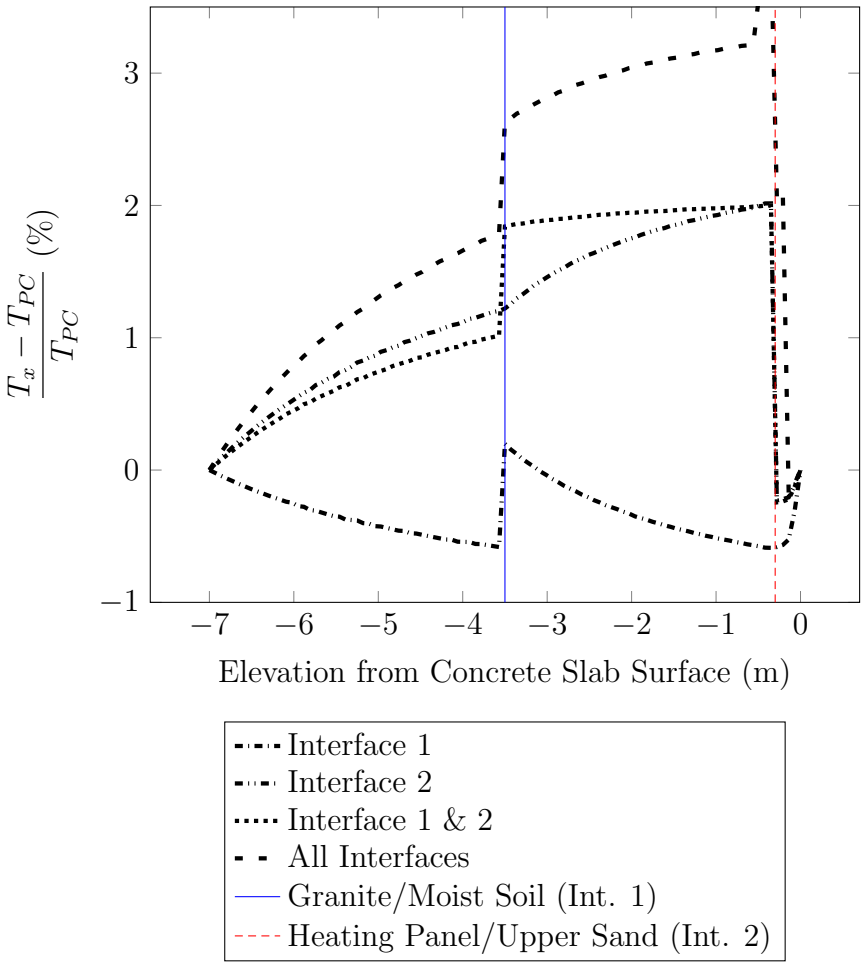

Figure 3.9: Contact Resistance Validation - Difference Percentages

Table 3.5: Verification Cases for 1D Contact Resistance Validation

Run #	% Heat Upwards	Energy Imbalance (% Difference)	Max. Temp. (°C)	Location of Contact Resistance
1	86.9%	0.0008	36.565	N/A
2	86.9%	1.5950	36.35	Granite / Moist Soil (Int. 1)
3	86.6%	0.2370	37.302	Heating Panel Upper Surface / Sand Layer Above (Int. 2)
4	86.6%	0.3258	37.296	Granite / Moist Soil & Heating Panel / Sand (Int. 1 & 2)
5	86.4%	0.0000	38.008	All Solid-Solid Interfaces

3.4 ThermaRay ESS Panel

3.4.1 Panel Specifications

The sources of energy in this research are ThermaRay's ETS heating panels. The model of ETS heating panels currently in production consists of a half inch (0.0127 m) sheet of gyprock that is grooved lengthwise. The heating element wires are placed in these grooves, which are then filled with drywall compound to produce a flush surface. The next generation of ETS panel will be comprised solely of a mesh-like structure of heating element wires to improve panel flexibility and versatility. The current and upcoming designs of the ETS panels are shown on the left and right of Figure 3.10, respectively. Specifications from the ThermaRay's ES7C460-240 heating panel were used in this research as it is commonly used in ETS installations [4]. The heating panel's specifications are provided in Table 3.6.

Table 3.6: ES7C460-240 Heating Panel Specifications [4]

Variable	**Value**	**Unit(s)**
Voltage	240	V
Max. Heat Output	460	W
Width	18 [0.46]	Inches [m]
Length	7 [2.13]	Feet [m]
Thickness	0.5 [0.0127]	Inches [m]
Weight	17.5 [7.94]	lb [kg]

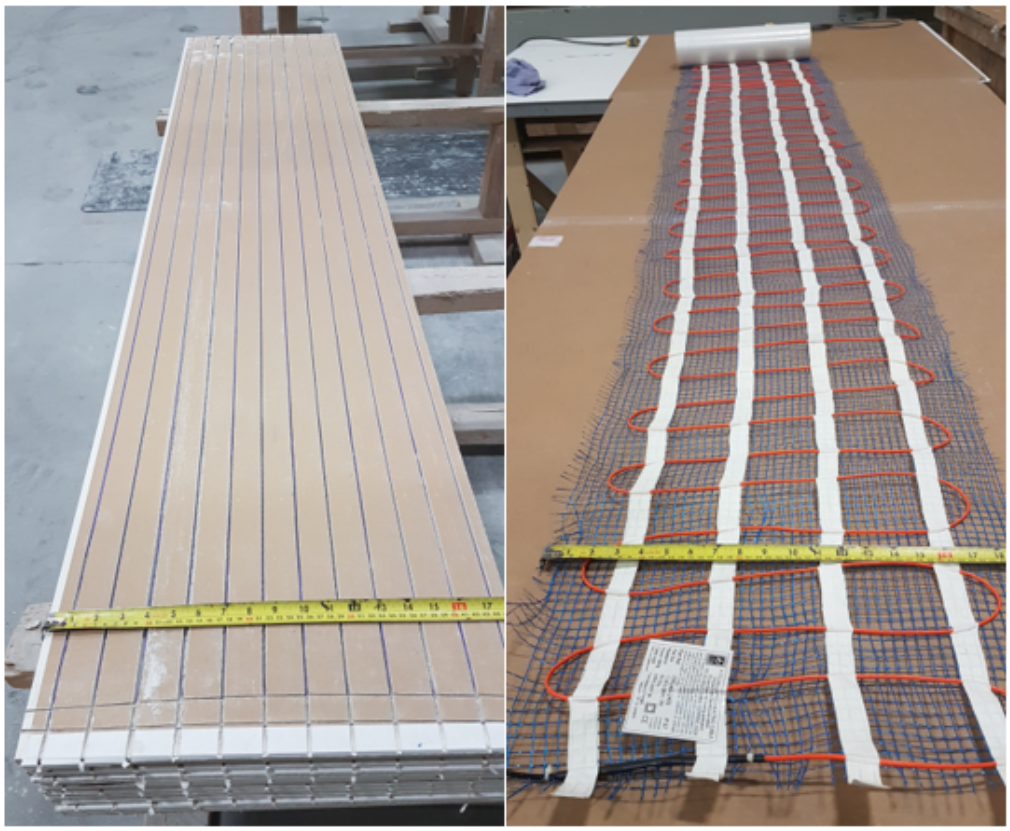

Figure 3.10: Current (Left) and Next (Right) Generations of the ETS Panel

3.4.2 Maximum Heating Panel Output

The three stages of this research (the 1D simulations, the MATLAB-based parametric study, and the development and testing of a proposed set of EXN/Aero simulations) have differing approaches to the representation of the ETS heating panels and their heat output at any given point of a simulation.

For the 1D simulations, the value of the volumetric heat output of the

heating panel was calculated based on a series resistance circuit similar to the one shown in Figure 3.11 with resistances and boundary values based on the thermal properties and boundary conditions of each study case. Details on each study case are provided in Table 4.1 (page 88. Figure 3.11 represents Case 5, hence the lack of insulation. Contact resistance between each solid layer was also omitted both in this figure and the equations that follow. It would have otherwise been included as an additional $\frac{L_n}{k_n}$ term in Equation 3.26. R_{Air} represents the total heat transfer coefficient from the heated concrete slab surface into the heated space, including radiative, convective, and conductive heat transfer, with a far-field temperature of T_A. In the Excel-based and quasi-1D EXN/Aero simulations, a value of 0.1 m^2K/W was used (this value is also supported by Cholewa et al. [31]). The thermal inertia of the system, discussed in Section 3.3.1, is not included in this figure. While it was not included in the Excel-based model (which is a steady-state model), the thermal mass of each TES layer was included in the quasi-1D EXN/Aero model.

Figure 3.11: 1D Model Series Resistance Circuit

The total resistance (R_{tot}) between and two points, A and B, can be found using Equation 3.26. Equation 3.27, based on Fourier's Law (Equation 3.5), demonstrates how the heat flux between two given points is a function of the temperature difference and thermal resistance between them.

$$R_{tot} = \sum_{n=1}^{N} \frac{L_n}{k_n} + \frac{1}{h_n} \tag{3.26}$$

$$q_{A \to B} = \frac{\Delta T_{A \to B}}{R_{tot,A \to B}} \tag{3.27}$$

The $\frac{L_n}{k_n}$ terms represent the thermal resistance from each layer's thermal conductivity and thickness. The $\frac{1}{h_n}$ term represents the convective heat resistance at the upper surface of the concrete slab, which is discussed in Section 3.3.2. For the 1D simulations, this heat flux was calculated from the heating panel to the top of the Room Air layer, and from the heating panel to the bottom of the Granite layer. These two heat fluxes are summed to determine the heating panel's output, q_{1D} (Equation 3.28). The heat output for each 1D case is provided in Table B.5.

$$q_{1D} = q_{HeatingPanel \to RoomAir} + q_{HeatingPanel \to Granite} \tag{3.28}$$

While q_{1D} was calculated prior to the initialization of each simulation, in cases where a transient heating panel control method was used the actual output of each heating panel at any given simulation time step was based on whichever control approach was being used. Transient heating panel control is discussed in Sections 3.4.3.

Studying conduction heat transfer within a 3D transient system is more complex, but the same kind of resistance circuit as that provided in Figure

3.11 could theoretically be produced between any two points in the system.

For the MATLAB-based parametric study, which was conducted using a model developed in Simulink (MATLAB's visual modelling environment), the heating panel was treated as an point heat source with a 1 m^2 footprint and a maximum heat output of 124 W, based on Equation 3.29 and Table 3.6. A 1 m footprint was used to simplify calculations, as was done in the Excel-based model [49]. For further discussion on heating panel control in the Simulink model, refer to Sections 3.4.3 and 4.2.1.

$$q_{max_{Simulink}} = q_{max_{real}} \times \frac{A_{Simulink}}{A_{Real}} = 460 \text{ W} \times \frac{1 \text{ m}^2}{3.7 \text{ m}^2} = 124 \text{ W}. \qquad (3.29)$$

Where $q_{max_{MATLAB}}$ is the maximum heating panel output in the Simulink model, $q_{max_{real}}$ is the ETS panel's maximum output based on the panel's specifications [4], A_{MATLAB} is the footprint of the MATLAB model, and A_{Real} is the average building footprint per ETS panel, based on a 60' x 100' industrial building (from discussions with representatives from ThermaRay, Inc.).

In the full-scale EXN/Aero model, the heating panel was included as a structured block in the simulation mesh, as described in 4.3. This block was selected as energy sources in EXN/View and assigned a maximum volumetric heat output (q_{max}) based on the panel's specifications in ThermaRay's ETS installation guide [4]. It is then controlled during simulations based on the algorithm described in the following section.

3.4.3 Transient Heating Panel Control

Studying the long-term, transient performance of ThermaRay's ESS necessitates the integration of a transient heating panel control algorithm based on the control method used by ThermaRay. Most of ThermaRay's ETS installations are based on the division of the heated space into a number of zones, each controlled individually through a relay box. The typical control approach for each zone's relay is based on a setpoint temperature of the surface of the concrete slab at the center of each zone. In most applications this setpoint temperature is set at 18 °C, hence the use of that value as the default for all models presented in this research. In each zone, once the heating panels have raised the concrete slab's surface temperature to the setpoint temperature the relay switches the heating panel off. The heating panels remain off until the surface temperature has fallen to 1.1 °C below the setpoint temperature (i.e. 16.9 °C if the setpoint temperature is 18 °C), at which point they turn back on until the setpoint temperature is once again achieved. ThermaRay also sets a maximum panel temperature of 60 °C to ensure the panels do not exceed their design specifications. The Simulink model and the proposed set of EXN/Aero simulations each have their own approaches to heating panel controls, described below.

Heating Panel Control in Simulink

The most complex aspect of the Simulink model, described in Section 4.2, is the heating panel control. Multiple heating panel control approaches have been built into the Simulink model including a concrete setpoint temperature, a maximum heating panel temperature, and a time-of-use (TOU) based control algorithm. The option to turn off the concrete setpoint temperature control was included to allow for more direct comparison with results from the proposed EXN/Aero simulations, which do not include a concrete setpoint temperature. The MATLAB model also includes an option to implement a ramp-down temperature range for the heating panel, as defined in Equation 3.30, to further facilitate comparison. Under default conditions, three conditions must be met in order for the heating panel to be on at any given moment:

- Heating panel temperature is less than the maximum heating panel temperature.
- Current time of day corresponds to an 'on' period, based on a 12 hour 'on' - 12 hour 'off' cycle.
  - This control approach is similar to that defined by Equation 3.31 for the EXN/Aero simulation design, with "CycleStart" set to 0 time steps and "CycleLength" set to the number of time steps equivalent to twelve hours.

- Concrete surface temperature has recently reached the setpoint temperature minus the "ConcreteSetpoint_Diff" value and therefore needs additional heat to meet the heating load.
  - As the proposed EXN/Aero simulations do not include a concrete surface setpoint temperature, the Simulink-based parametric study included a variable called "ConcreteSetpoint_Activate", which determines whether the concrete surface temperature is to be considered in the heating panel output control logic.
  - Note that while it was not considered in this research, an override setting could be added to the model to allow for the heating panel to be turned on if the concrete surface decreases below a specified temperature regardless of the time of day.

If all three of these conditions are met, the next step is to determine whether the heating panel is set to have variable output according to the parametric study's simulation matrix. As previously mentioned, ThermaRay's ESSs are usually relay-controlled based on the concrete slab's surface temperature. In this arrangement, heating panels are either off or on at their maximum rated output. However, it is worth noting if allowing variable output would be beneficial or detrimental to the system's performance, so that has been included in the study. When variable heating panel output is permitted and the three aforementioned conditions are met, the heating panel output is based on Equation 3.30, with the value of the "HeaterRampDownTemp_Diff"

variable serving as the value of $T_{upper} - T_{lower}$ from the piecewise equation. When variable output is not permitted, the heating panel output is either zero or the maximum rated output of the panel. This maximum heating panel is 124 W, based on Equation 3.29.

Heating Panel Control in EXN/Aero

The control approach based on the concrete slab's surface temperature described above was not utilized in EXN/Aero as doing so would produce a computationally intensive feedback loop. A heating panel control based on the floor surface temperature was tested and verified, however, and could be implemented if additional compuational resources were made available. In the proposed set of EXN/Aero simulations presented here, the energy source was controlled based on the temperature of the heating panel itself. There are two setpoint temperatures, a lower bound at which the heating panel begins to decrease its output, and an upper bound at which the heating panel is turned off. The heating panel output decreases linearly between the lower and upper setpoint temperatures. The code for this heating panel-centric control method was based on the piecewise function described in Equation 3.30. Refer to Section 4.3 for a full description of the EXN/Aero simulations have been developed, tested, and proposed in this research.

$$q_{heatingpanel} = \begin{cases} q_{max} & T_{heatingpanel} \leq T_{lower} \\ q_{max} \times \left(\dfrac{T_{heatingpanel} - T_{low}}{T_{upper} - T_{lower}} \right) & T_{lower} < T_{heatingpanel} < T_{upper} \\ 0 & T_{heatingpanel} \geq T_{upper} \end{cases} \tag{3.30}$$

Additionally, EXN/Aero has the capability of controlling the output of the heating panel transiently based on the current simulation time. A user function was created for EXN/Aero to call during simulations for this purpose. The function is based on the logic equation defined in Equation 3.31.

$$IF(currentstep < CycleStart)\, OR \tag{3.31}$$
$$MOD((FLOOR(currentstep/CycleLength)), 2) \neq 0$$

Where 'currentstep' is the current time step of the simulation, 'CycleStart' is a user variable which determines when the heating cycle begins, and 'CycleLength' is a user variable which sets the cycle length. For a demonstration of how these variables would be set for a typical simulation, please refer to Section 4.3. Images of the transient heating panel control working are provided in Section 5.8.

Building Heat Load & Losses

In all simulations performed for this research, the heat load (which draws heat upwards from the heat panel(s)) is varied by the exterior air temperature. In the EXN/Aero simulations (quasi-1D and full scale), this value is a constant. In the Simulink model, this value is varied based on a daily sinusoidal function and included in the parametric studies. In reality, the system's heat load would be dictated primarily by an occupant-controlled temperature setpoint and the system's thermal losses are a function of external air temperature, forming a less direct relationship between the exterior air temperature and the system's heat load. Heating panel control, however, is based on the occupant-controlled setpoint when the concrete surface temperature based control approach is active. On the topic of thermal losses, it should be clarified that infiltration and exfiltration are assumed negligible in all simulations presented in this research.

3.5 Evaluation of Performance

The primary objective of this research was to determine the transient performance of ThermaRay's ESS under realistic conditions for comparison with traditional forced air systems in order to support the integration of the system into the NBC. Therefore, clearly defining the performance metrics that are used in this research was of utmost importance.

Evaluation of performance for the quasi-1D, steady-state simulations performed with EXN/Aero was based on that used in the study by Joseph et al. [49]. As the vertical walls of the domain are treated as adiabatic surfaces, the only heat leaving the system was through the upper and lower bounds of the domain. The performance of the system (η_{1D}) was then based on the fraction of the total heat provided to the system from the heating panel (q_{max}) that was passing upwards into the heated space above the concrete slab (q_{floor}), as defined in Equation 3.32.

$$\eta_{1D} = \frac{q_{floor}}{q_{max}} \tag{3.32}$$

The instantaneous performance evaluation used for a quasi-steady-state, one-dimensional system would not be representative of a transient three-dimensional system Furthermore, including the system's performance during the start-up period may produce results that are not indicative of the system's long-term performance. The period over which the system's performance was evaluated for each model must be carefully considered accordingly.

The Simulink model defines system performance as the integral of the heat transfer upwards from the model's concrete floor over the sum of the total heat transfer through the concrete floor and the bottom model's "undisturbed soil" layer. To mitigate any of the aforementioned bias due to start-up behaviour, the Simulink model's simulations are run for a longer period of time, up to 16 months with a default duration of one year. Additionally, the

Simulink model's code, written in MATLAB, only uses data from the second half of the simulation. This is reflected in Equation 3.33.

$$\eta_{MATLAB} = \int_{t_{sim/2}}^{t_{sim}} \frac{q_{floor}(t)}{q_{floor}(t) + q_{soil}(t)} dt \tag{3.33}$$

The proposed set of EXN/Aero simulations, on the other hand, focuses on the system's performance over a narrower period of time as a simulation time of a full year was not feasible within our computational restraints. The focus of the system performance evaluation for the EXN/Aero model was during the third and final simulation of the set of three described in Section 4.3. During this simulation, the buoyant flow field and temperature field within the heated space has reached a quasi-steady state and the heating panels were cycling based on the time of day.

The most critical moment for the system's performance was identified through discussions with ThermaRay as when the heating panels are turning on, having recently been off for several hours. The real world equivalent of this is when the panels coming on at the end of the day to heat the thermal storage region overnight sufficiently to provide the next day's heat demand. At this moment the thermal storage region is at its lowest energy content level for a given day; this is when the heating process is most dynamic. It is therefore at this moment that significant losses are most likely to occur. While the system's performance was monitored over the entirety of the third simulation of each set, it was these specific moments that are the focus of

the system evaluation effort.

The transient performance of ThermaRay's ESS was determined by monitoring the amount of heat passing from the surface of the concrete slab into the heated space compared to the total heat provided to the system over a particular period of time. The equation for this approach is provided in Equation 3.34. Note that this method, directly comparing the heat into the heated space (the desired output) with the heat provided into the system (the input), is more exact than that used in the Simulink model. This more direct approach was originally used in the Simulink model. However, the significant fluctuations in the heating panel input introduced error into the calculation. As the sum of heat leaving the TES region through the concrete slab and undisturbed soil over a sufficiently long period of time beginning after the establishment of a quasi-steady state is equal to the amount of heat provided into the system over the same period, this sum was used as it provided a smoother and therefore less error-prone value.

$$\eta_{3D} = \int_{t_1}^{t_2} \frac{q_{floor}(t)}{q_{heatingpanel}(t)} dt \tag{3.34}$$

It is noteworthy that none of the performance evaluation equations provided above consider occupant comfort or setpoints. Rather, the responsibility of maintaining is left with the heating panel control approaches, described in Section 3.4.3. The results from these approaches to assessing the thermal performance of ThermaRay's ESS using the 1D EXN/Aero model

and the Simulink model are presented in Sections 5.1 and 5.4, respectively.

Chapter 4

Simulation Setup & Design

4.1 1D Simulations

The Excel-based model developed by Joseph et al. [49] at NSCC were used as the basis for the series of quasi-1D simulations performed at the outset of this research. The purpose of these 1D simulations was to verify the model produced by Joseph et al. [49] in preparation for the 3D, transient studies to follow. The five 1D cases that will be studied are discussed below and summarized in Table 4.1. The depth and thermal conductivity of each layer in the 1D simulations was obtained from the Excel-based model, with the exception of the heating panel. A thickness of 5 mm was chosen for the heat source as a small, non-zero value that was low enough that the thickness would not have a significant effect on energy calculations but not so small as to adversely effect the quality of the computational mesh ('the mesh'). Examination of the equations used to develop the Excel-based model revealed that the quasi-1D model was based on a 1 m^2 footprint meant to represent a vertical section of a ThermaRay ETS installation. To further simplify the

mesh and therefore reduce the computational demand of the 1D simulations, this footprint was further reduced to just 25 mm^2. This dimension was based on a width equal to the chosen thickness of the heating panel, 5 mm, to improve mesh uniformity. This thickness was selected somewhat arbitrarily as a small value and tested to ensure it was sufficiently large to support simulation stability.

BC Connectivity settings, first discussed on page 32 (Section 3.2.1), were used to specify that the layer interfaces were treated as having negligible contact resistance, limiting the heat transfer to pure conduction in an attempt to reproduce the results of the Excel-based model, as discussed in Section 3.3.7.

Boundary conditions of these simulations are discussed in Section 4.1.2 and summarized in Table B.4.

4.1.1 Quasi-1D Mesh Optimization

This mesh design was chosen following the culmination of an optimization process based on the percentage difference between the steady state results of simulations using the mesh with constants from the Excel-based model. The mesh was considered final once this percentage fell below 1%, which was selected as the maximum allowable error. Coincidentally, this value also appeared to be approximately equal to the asymptotic error as shown in

Figure 4.1.1. The labels on Figure 4.1.1 indicate the order of the optimization simulations, demonstrating how hap-hazard the optimization process was due to the level of uncertainty as to how each aspect of the mesh affected the results. The optimization process was based on a parametric study with parameters including the lengthwise, width-wise, and depth-wise dimensions, as well as the distribution of points along the perimeter of each block. Details for the final quasi-1D computational mesh used in these 1D simulations are provided in Appendix B.2.1.

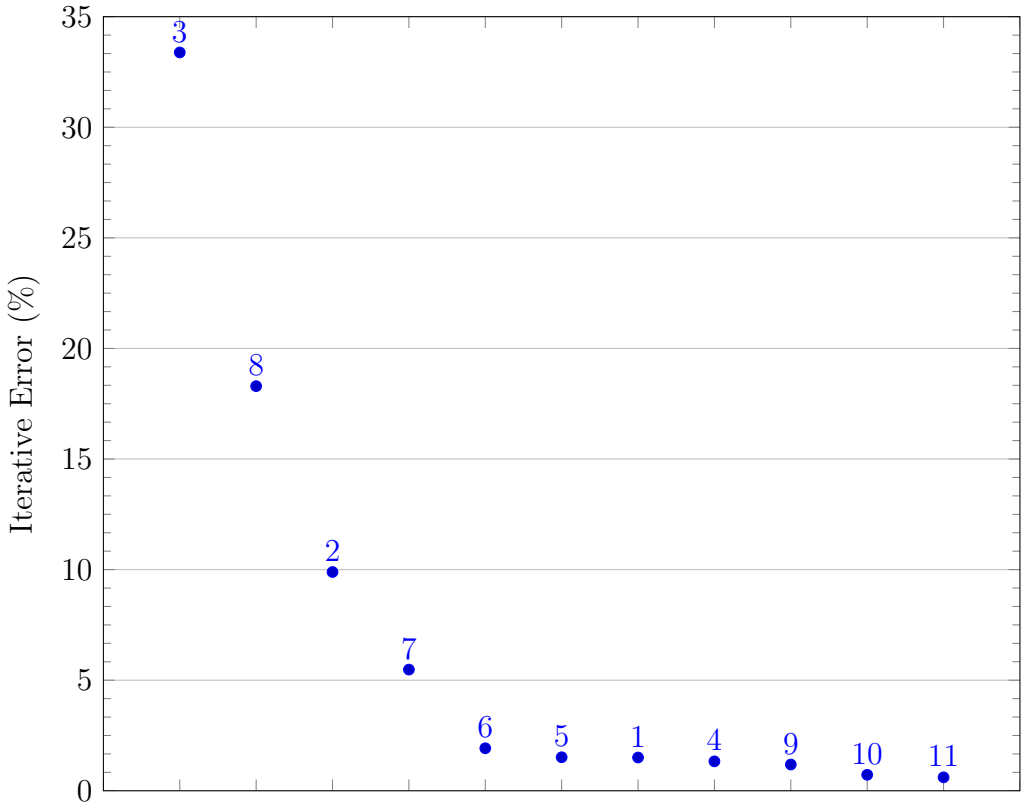

Figure 4.1: Iterative Error in 1D Mesh Optimization

4.1.2 Boundary Conditions

The boundary conditions for the 1D simulations were based primarily on the model developed by the team from NSCC [49], with a few additional considerations to better represent the heat transfer that would be present in a real installation. The surface heat transfer coefficient value of 10 W/m^2K at the room-concrete slab interface is the inverse of the value of the "free film resistance at slab to room" from the Excel-based model, 0.1 m^2K/W [49]. This value was also corroborated by the 2013 paper by Cholewa et al. [31]. This value is the total heat transfer coefficient at the concrete slab's surface, encompassing radiation, conduction, and convection.

Heat transfer along a 2D horizontal slice of a full-scale installation is negligible after the initial system warm-up period, particularly in regions distant from the perimeter [23, 24, 32]. As such, the vertical boundaries of the Excel-based model and the quasi-1D EXN/Aero domain were treated as adiabatic surfaces. With this approach, the 1D model represents a vertical section taken from a standard full-scale ThermaRay ETS installation, at a point distant from any exterior walls and under steady state conditions.

The boundary conditions and other constants used in the 1D simulations are provided in Tables B.3 and B.4. These values are based on the 2013 paper by Cholewa et al. [31], the Excel-based model by Joseph et al. [49], and a NRC publication by Williams and Gold [3] on soil temperatures in

Ottawa, Ontario (the sole Canadian location for which soil temperature data was available).

4.1.3 Simulation Matrix

The description of the five 1D cases is shown in Table 4.1. Additional details, including the thermal conductivity and thickness of each layer from the reference case, are provided in Table B.1, within Appendix B. The dependent variable in each case is that specified in the case description column. The values of all other variables are fixed and equal to those specified in the reference case, which is included in bold text in the simulation list provided in Table 4.1. The rightmost column, "R_{tot} Below Panel", provides the total thermal resistance from the bottom surface of the heating panel to the lower extremity of the computational domain. It indicates the effect of insulation on the overall thermal resistance impeding the downward flow of heat from the heating panel. The heating panel output for each case is provided in Table B.5, using data from the Excel-based model [49].

Table 4.1: 1D Model Simulation List (Default Bolded)

Case #	Thermal Conductivity (k, W/mK)	Case Description	% of Heat into Room (from [49])	R_{tot} Below Panel (m^2K/W)
1	0.029	20 cm XPS	95.0%	16.48
2	0.029	10 cm XPS	92.9%	13.03
3	0.029	5 cm XPS	91.0%	11.31
4	0.029	2.5 cm XPS	89.6%	10.45
5	**0.27**	**None (5 cm sand)**	**87.8%**	9.771

4.2 MATLAB/Simulink Model

The creation of the MATLAB model used in this research came about when a need was identified for a model that was more accurate, detailed, and flexible than the 1D model, described in the Section 4.1. It also had to be less time consuming and computationally intensive than the proposed set of EXN/Aero simulations, described in Section 4.3. A model was needed that could be used to perform a wide-ranging parametric of the study. Such a parametric study provided a more informed understanding of how variables like floor setpoint temperature affect the system's performance. This system dynamics model would also allow for the project's objective to be addressed more thoroughly by providing system performance information from a wide range of scenarios.

The MATLAB model was created based primarily on the full-scale EXN/Aero model and documentation from ThermaRay [4]. The model was

designed to be an elemental 1 m^2 slice of a 60' x 100' industrial building with 10 m ceiling. The following section will work through each section of the model, "from the ground up".

4.2.1 Model Components

In Simulink, model components are referred to as blocks; the same block type, such as a 'Temperature Source', can be used multiple times in a model. Each usage of a block type, referred to as an individual block, has its own independent settings. Images of the Simulink model are provided in Appendix C.1.

Bottom Boundary

The bottom boundary of the MATLAB model was built around the premise that, at a depth of 7 m, the soil temperature is constant throughout the year. A report from Natural Resources Canada [3] provided the isothermal temperature of 8 °C at a depth of 7 m in Ottawa. The affect of the value of this temperature on the system's performance was studied in the parametric study. For each simulation, soil temperature at 7 m was set using Simulink's 'Temperature Source' component. Heat transfer through this block was monitored using a 'Heat Flow Rate Sensor'.

TES Region

All thermal energy storage (TES) layers are represented with the same block types in the Simulink model, a 'Thermal Mass' block and a 'Conductive Heat Transfer' block. The 'Thermal Mass" block's parameters include the mass and specific heat capacity of a given TES layer. Together, these parameters define the thermal storage capacity of the TES layer. The 'Conductive Heat Transfer' block's parameters are area, thickness, and thermal conductivity. The area for all blocks was equal to the model's footprint, $1\,m^2$. TES layer thicknesses and thermal conductivity are provided in Table A.1 of Appendix A. Each layer of the TES region has two 'Conductive Heat Transfer' blocks, each with a thickness equal to half of the total layer thickness. The layer's 'Thermal Mass' block was connected between the two heat transfer blocks to provide the conductive heat transfer blocks with a midpoint temperature for the block.

TES Region Interfaces

All TES layer interfaces share the same two thermal blocks, a 'Variable Thermal Resistance' block and a 'Temperature Sensor' block. The interface's thermal resistance, which represents the contact resistance between the two neighbouring TES layers in W/m^2K, was controlled based on the 'ContactResistanceOn' and "ContactResistanceValue' parameters. These

parameters are set for each simulation by the SimSet.m MATLAB code, described in Section 4.2.3.

One interface between the heating panel and the concrete slab has additional components, as do all interfaces between the heating panel and the lowest point in the model's domain. At the interface between the concrete slab and the compacted granular rock layer beneath it, there are three additional "Variable Thermal Resistance" blocks that are used to study the affect of the insulation currently required by the Canadian National Building Code [11] (this is of utmost importance to the research's primary objective). Two are used for modelling contact resistance between the insulation (if present) and the surrounding layers and one was used to model the thermal resistance of the XPS insulation itself (if present). A similar setup was used for each internal interface below the heating panel (Heating Panel-Sand, Sand-Compressed Sand, Compressed Sand-Undisturbed Soil). Additional logic-based controls are necessary for these sub-heating panel interfaces in order to vary the location or presence of XPS insulation below the heating panel. The location, in the case of the insulation below the heating panel, and thickness of this insulation was varied in the parametric study described in Section 4.2.3 and controlled by the 'SimSet.m' MATLAB code.

Heat Transfer Through Heated Space

While heat transfer through the TES region is solely conduction, heat transfer from the surface of the concrete slab is comprised of all three forms of heat transfer. Of the three, convective and radiative heat transfer are expected to play the largest part in the total heat transfer through the heated space [31, 34].

Radiation was modelled using Simulink's 'Radiative Heat Transfer' block type, whose variables include area ($1\,\mathrm{m}^2$) and radiation coefficient (h_{rad}, $\mathrm{W/m^2K^4}$), which is defined in Equation 4.1. The emissivity of the concrete floor, ϵ, was set to be 0.94 [83]. Despite appearing to be similar to h_c, the convective heat transfer coefficient, it should be noted that the relationship between dT and q_{rad} is not linear as it is with convection:

$$h_{rad} = \epsilon\sigma = \frac{q_{rad}}{(T^4_{ceiling} - T^4_{floor}) \cdot A} \tag{4.1}$$

Where $T_{ceiling}$ is the temperature of the interior surface of the ceiling and T_C is the temperature of the upper surface of the concrete slab. To provide the block with $T_{ceiling}$, the model's radiative heat transfer block is connected directly to the ceiling's 'Conductive Heat Transfer' block, bypassing the air's 'Thermal Mass' block.

Convection was modelled using Simulink's 'Convective Heat Transfer' block

type, whose variables are area ($1\,m^2$) and convection coefficient (h_c, W/m^2K). For the parametric study the convection coefficient was varied from 2 to 3 W/m^2K with a default value of 3, based on literature [29, 31, 34, 35].

$$h_c = \frac{q_c}{(T_A - T_{floor})A} \tag{4.2}$$

Where T_A is the farfield air temperature in the heated space and T_C is the temperature of the upper surface of the concrete slab. To provide T_A for the calculation of convective heat flux from the concrete slab, the convective heat transfer block is connected to the heated air's thermal mass block.

Conduction was modelled using a 'Conductive Heat Transfer' block. Unlike for each of the TES layers, only one such block was used. Early in the development of the model, the heated air's 'Thermal Mass' block was connected to both the 'Convective Heat Transfer' and a point between two 'Conductive Heat Transfer' blocks (each representing half of the heated space) to provide both with the farfield air temperature. However, this approach led to the heat flow diverting around the second 'Conductive Heat Transfer' block through the air's 'Thermal Mass' block, decreasing the already low amount of heat passing through the heated space via conduction. As such, only one 'Conductive Heat Transfer' block was used in the final edition of the model. The block has three variables, including area ($1\,m^2$), thickness

(m), and thermal conductivity (k, W/mK)

$$k = \frac{q_{conduction}}{(T_{ceiling} - T_C) \cdot \Delta s} \tag{4.3}$$

Where $T_{ceiling}$ is the temperature of the interior surface of the ceiling and T_C is the temperature of the upper surface of the concrete slab. See note above on why $T_{ceiling}$ is used in place of T_A.

Heat Transfer Through Ceiling

The sole mode of heat transfer (heat loss) considered for the ceiling was conduction, as infiltration and exfiltration were assumed to be negligible. This assumption was made as any infiltration or exfiltration through a $1\,m^2$ of the ceiling would be insignficant regarding heat transfer into or out of the heated space, respectively, compared to conduction through the same area. To model conduction through the ceiling, a 'Conductive Heat Transfer' block was used with its settings specified based on the ceiling's R-value. The values selected for this variable, 'Ceiling_R_Value', and the reasoning for them are provided on page 97. [EXTEND] (include radiation)

Heat Transfer from Roof

Heat will be lost from the model's roof to the surrounding air using a 'Convective Heat Transfer' block with a convective heat transfer coefficient

based on data from ASHRAE [84]. Based on an average wind speed in Ottawa of 10 mph (4.5 m/s) for the months of January through March [85], a default convective heat transfer rate for the roof into the exterior air of 30 W/m^2K was selected. Rather than assuming the roofing material, an average of the values provided in the 'Surface Conductance as Affected by Air Movement' figure in [84] was used, as shown in Figure 4.2.

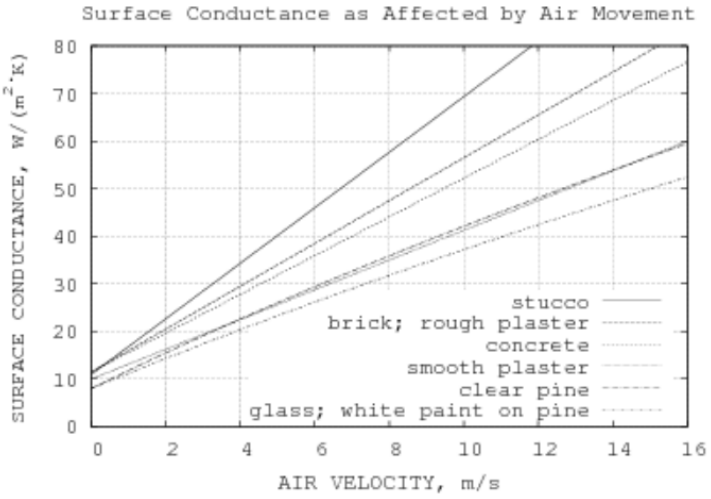

Figure 4.2: Surface Conductance as Affected by Air Movement

Performance Data

All heat transfer sensors, shown as 'Heat Flow Rate Sensor' in Table 4.2, are identical. The two variables used by these components are the heat flow into and out of the block sets the heat flow out equal to that entering the block and produces a physical signal output equal in magnitude to the heat flow through the sensor.

A set of three 'Heat Flow Rate Sensors' were used to measure heat flux through the three forms of heat transfer described above from the concrete slab's surface upwards to the ceiling at each time step. Their sum was used as $q_{floor}(t)$ in Equation 3.33, with the heat flux measured from the constant temperature source at the bottom of the model used as $q_{ground}(t)$. The average system performance value from the second half of the simulation, as per Equation 3.33, was saved in the data table for analysis following the completion of the parametric study.

Table 4.2: Simulink Components

Block Name	**Block Variables**	**Image**
Temperature Source	Temperature (K)	
Temperature Sensor	Inlet Temperature (K) Outlet Temperature (K)	
Heat Flow Rate Sensor	Inlet Heat Flow (W) Outlet Heat Flow (W)	
Thermal Mass	Mass (kg) Specific Heat (J/kgK)	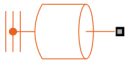
Conductive Heat Transfer	Area (m^2) Thermal Conductivity (W/mK) Thickness (m)	
Radiative Heat Transfer	Area (m^2) Radiation Coeff. (W/m^2K^4)	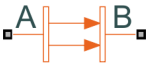
Convective Heat Transfer	Area (m^2) Convective Coeff. (W/m^2K)	
Variable Thermal Resistance	Thermal Resistance (K/W)	

4.2.2 Parametric Study - Parameter Selection

This section provides a description of each variable included in the parametric study and an explanation of the range selected for each.

Air_Convection

This variable represented the *convection coefficient from the surface of the concrete slab into the heated space above*, in W/m^2K. The range of 2 to 4 W/m^2K with a default value of 3 W/m^2K was selected based on literature [29, 31, 35, 74, 86].

Ceiling_R_Value

This set the *total R-value of the modelled building's ceiling*, with a range of 20 to 60 and a default of R-30. As radiant heat systems generally perform best in well insulated buildings [33, 87], ThermaRay suggested the R-value of a typical industrial building should be used rather than a modern, well-insulated building. The default value of R-30 corresponds to the minimal requirement for the overall ceiling R-value of a building in Ottawa, based on the National Energy Code of Canada for Buildings 2015 [12]. If ThermaRay's ESS was found to perform well in a building with a mediocre R-value, it would be reasonable based on the findings of Fontana et al. and Cvetkovic & Bojic [33, 87] that they would expect it to perform even better in a building with

a higher R-value. R-20 was chosen as a minimum value so as to include a poorly insulated building in the study, with R-60 representing a well insulated building.

ConcreteSetpoint_Activate

As described on page 74 (Section 3.4.3), this variable set *whether the heating panel control considers the concrete setpoint temperature* ('ConcreteSurfaceSetpoint'), as described below. It was added to facilitate comparison between results from this parametric study and the proposed set of EXN/Aero simulatons that are described in Section 4.3. The aforementioned EXN/Aero simulations did not consider the concrete setpoint temperature due to the significant computational resources that would have been required to do so, as mentioned in Section 3.4.3. This variable's default value was set to 1 to ensure that the majority of the Simulink model simulations were run with the concrete setpoint temperature active.

- 0: Concrete setpoint temperature **is not** included in the heating panel control algorithm.
- 1: Concrete setpoint temeprature **is** included in the heating panel control algorithm.

ConcreteSurfaceSetpoint

The *concrete surface setpoint temperature* was varied from 16 °C to 25 °C, while a default value of 18 °C was set as requested by ThermaRay to align with the value commonly used in their ETS installations. The upper bound was established based on the ideal floor temperature range for occupant comfort from an ASHRAE report [88]. The lower bound was established to study the system's performance if the concrete surface temperature was to be set below that range, such as for a low-occupancy storage facility.

ContactResistanceOn

This variable acted as a boolean value that dictates *whether the model considers the effect of contact resistance between each layer of the TES region is considered*, as desribed below. Understanding the impact of contact resistance on the system's performance could be used to inform ESS installation techniques for ThermaRay. If contact resistance is detrimental to the system's performance, then ThermaRay could alter its installation technique to encourage compacting of the layers, reducing contact resistance. While the ETS layers are not solid blocks, as this model treats them, this compaction could still alter the system's performance. When contact resistance is being considered, its value is set by the 'ContactResistanceValue' variable.

- 0: Contact resistance between each TES layer **is not** included in the simulation.
- 1: Contact resistance between each TES layer **is** included in the simulation.

ContactResistanceValue

As mentioned above, this variable set the *magnitude of contact resistance* present between each layer of the TES region when the 'ContactResistanceOn' variable is set to "1". Accurately calculating the magnitude of contact resistance between layers comprised of sand particles and gravel of non-homogeneous size would be quite difficult. As such, an approximation was made based on the predicted average air gap thickness between particles or gravel pieces at each interface. For the default value, an air gap thickness of 0.5 mm was used. The tested range was from 0.25 to 1.25 mm. The gravel and sand grain size distribution for a typical ETS installation was unknown and therefore as was the accuracy of this range. However, the results obtained for the selected range will provide an indication of the relationship between the magnitude of contact resistance and system performance. This could then inform ThermaRay's installation technique, as contact resistance between TES layers could be reduced through various means such as additional compaction of each layer. Furthermore, there are more TES material interfaces above the heating panel than below. It was

then hypothesized that an increase in the magnitude of contact resistance, which was applied equally to all TES material interfaces, will have a similar yet lower magnitude impact on the ESS's performance as increasing the value of the 'UpperInsulationThickness' variable.

Exterior_Air_Conv

This variable set the *magnitude of natural convection at the exterior surface of the model's roof*, which was exposed to the outdoor ambient temperature, in W/m^2K. Please refer to Section 4.2.1's subsection on 'Heat Transfer from Roof' for an explanation of the default value of 30 W/m^2K. A range of 20 to 60 W/m^2K was selected, corresponding to wind speeds of 2 to 12 m/s [84, 85].

HeaterFraction_Activate

This variable determined whether the heating panel was permitted to have a variable output. As mentioned in Section 3.4.3, ThermaRay's ETS heating panels are usually controlled with relays, restricting their output to 0 or 100% of the panel's rated output. However, a concrete surface setpoint temperature was excluded from the proposed set of EXN/Aero simulations due to the computational resources it would require. The heating panel control in EXN/Aero is instead based on the temperature of the heating panel itself. As such, this variable was included in the parametric study to

allow for the study of the system both (a) without variable heating panel output, as in most ETS installations, and (b) with variable heating panel output, as in the proposed set of EXN/Aero simulations. Results from this variable will indicate the impact of not including a concrete surface setpoint in the EXN/Aero simulation design on the accuracy of its results and the importance of ThermaRay incorporating variable heating panel output in their system control.

- 0: The heating panel **is not** permitted to have a variable output (on or off only).
- 1: The heating panel **is** permitted to have a variable output.

HeaterRampDownTemp_Diff

This variable dictated the *temperature difference between the heating panel's ramp-down temperature and the heating panel's maximum temperature*, in degrees Celcius (°C). When this variable was active, heating panel control was based in part on Equation 3.30. This variable was varied from 2.5 to 10 °C with a default value of 5 °C, arbitrarily, to study its effect on the system's performance.

LowerIns_Layer

This variable dictated the location of insulation at an interface within the TES region below the heating panel. This variable helps determine whether situating the currently required insulation below the heating panels would be a suitable alternative to immediately below the concrete slab, potentially meeting the building code requirement without severely impacting the system's thermal performance. The values and their corresponding insulation values are as follows:

- 0: No insulation below the concrete slab.
- 1: Insulation between the heating panel and the 'sand' layer beneath it.
- 2: Insulation between the 'sand' and 'compressed sand' layers.
- 3: Insulation between the 'compressed sand' and 'undisturbed soil' layers.

LowerInsulationThickness

This variable corresponds to the *thickness of insulation at an interface within the ETS region below the heating panel*, in meters (m). The particular interface that this insulation is situated at is dictated by the 'LowerIns_Layer' variable. A range of 0 to 0.1 m was selected. The lower bound and default

value was chosen to study the system performance without the insulation (0 m), which is typical for ThermaRay's ETS installations to date. The maximum value of 0.1 m was set to make the NBC-mandated insulation thickness near the mid-point of the selected range of tested values. Sentence 3.2.3.3 of the Canadian National Building Code requires a below slab RSI value of 1.32 for heated slabs in Ottawa, which corresponds to 1.5 inches (3.81 cm, 0.0381 m) [12]. This value is near the middle of the selected range, which is ideal for addressing the research's primary objective.

MaxHeaterTemp

For the *maximum heating panel temperature*, a range of 20 to 60 °C was selected with a default value of 55 °C. This minimum value was chosen as it is just two degrees warmer than the default concrete floor setpoint temperature. This was done on the basis that it would be beneficial for studying whether a maximum heating panel temperature only slightly greater than the concrete setpoint would be beneficial or detrimental for the system's performance. During discussions with representatives from ThermaRay, the maximum temperature that they would usually operate the ETS heating panels at was identified to be 60 °C, with 55 °C being the typical value. While higher temperatures could have been included, it was expected that a 40 °C range would be sufficient for revealing the effect of this variable on the system's performance.

SimLengthMonths

This variable set the *length of each simulation*, in months. It was used to assess the impact of the simulation length on the simulation's outputted values. A default value of one year was chosen to mitigate the potential impact of start-up fluctuations on simulation results. A minimum of four months was selected, which could represent a situation where the ESS was installed shortly before a heating season began, with a maximum of 16 months to provide sufficient data points to approximate any effects of the variable. This variable will indicate the impact of each layer's thermal time scale, defined on page 39 (Section 3.3.1), on the system's performance. Results from this variable may also inform ThermaRay as to whether their hypothesis that much of the heat "lost" to the soil beneath a building is eventually recovered.

SimTimeStepMinutes

This variable set the *length of the simulation's time step*, in minutes. Early simulations suggested the time step had little to no impact on the resulting overall performance value. This was confirmed by the results of the parametric studies, wherein the time step was varied from 5 to 20 minutes with a default value of 10 minutes, as portrayed in Section 5.4.2 and discussed in Section 5.7.

Soil_Temp_Full_Depth

This set the *temperature of the bottom interface of the 'undisturbed soil' layer*, which is also the bottom boundary of the model's computational domain, in degrees Celcius (°C). A default value of 8 °C was selected based on soil temperature data at a depth of 7 m for Ottawa, Ontario, from NRCan [3]. The range of 5 to 10 °C was selected, providing additional data points indiscriminately to study the impact of this value on the system's performance and behaviour.

UpperInsulationThickness

This variable represents the *thickness of insulation at the interface of the concrete slab and compact granular rock, above the heating panel*, in meters (m). Its range was set to be identical to that of its counterpart below the panel, as discussed above.

4.2.3 Parametric Study - Design & Implementation

Two MATLAB scripts were written to set up, run, and analyze the outputs of the Simulink model. The complete, commented scripts are provided in Appendix C.2. The MATLAB scripts were used to perform both types of parametric studies presented here.

Model Initialization

The initialization portion of the script prepares the model and the MATLAB Workspace, which contains all variables for the current script, for the parametric study. Prior to the outset of the parametric study, a simulation was performed with all parameters set at their default value. The results from that simulation were saved as the first entry in the data table. Tables are also pre-allocated to record temperatures from throughout the computational domain and the values of all parameters for each simulation for temperature-based system analysis and to ensure the MATLAB code was functioning properly, respectively.

Stage 1: Modified Parametric Study

The first stage of the parametric study performed using the Simulink model was focused on the primary objective of this research, centered around the inclusion of insulation below the concrete slab. A modified parametric study was designed for a more thorough assessment of the system's performance for each possible value of variables concerning the thickness or presence of insulation above or below the heating panel. What amounts to a parametric study was performed for each value of each primary variable, as demonstrated in Figure 4.3. This is in contrast with the standard form for a parametric study, wherein all other variables being held at their default values while

the MATLAB code cycled through each value of a particular variable. For example of this 'modified parametric study', a parametric study involving all other variables would be performed with the upper insulation thickness held constant at each value between 0 and 0.1 meters, with a step size of 0.01 m, based on the flowchart in Figure 4.3 and Table 4.3.

Table 4.3: Modified Parametric Study Data

Variable Name	**Min**	**Max**	**Step**	**Default**	**Primary**
Air_Convection	2	4	1	3	No
Ceiling_R_Value	20	60	10	30	No
ConcreteSetpoint_Activate	0	1	1	1	No
ConcreteSurfaceSetpoint	16	25	1	18	No
ContactResistanceOn	0	1	1	1	No
ContactResistanceValue	0.009527	0.047637	0.009527	0.019055	No
Exterior_Air_Conv	10	60	10	30	No
HeaterFraction_Activate	0	1	1	1	No
HeaterRampDownTemp_Diff	2.5	10	2.5	5	No
LowerInsulationThickness	0	0.1	0.01	0	Yes
MaxHeaterTemp	20	60	5	55	No
SimLengthMonths	4	20	4	12	No
SimTimeStepMinutes	5	20	5	10	No
Soil_Temp_Full_Depth	5	10	1	8	No
UpperInsulationThickness	0	0.1	0.01	0	Yes

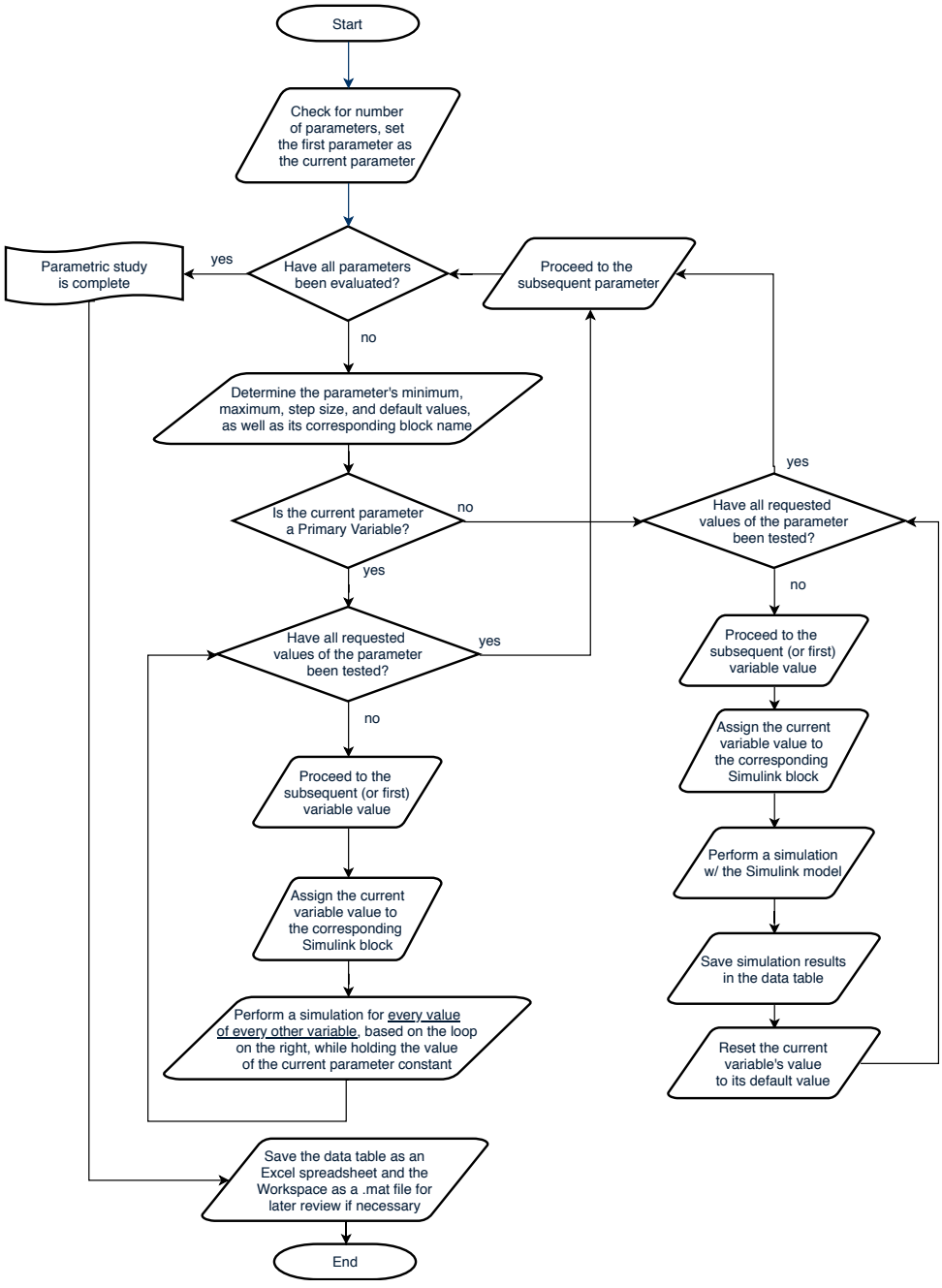

Figure 4.3: MATLAB Model Flowchart

Stage 2: Standard Parametric Study

Initially the results from the modified parametric study were used for all variables, but a standard parametric study was later added with no 'primary' variables to provide a more conventional approach to studying the system's performance. A standard parametric study was performed for all other variables listed in Table 4.3. This standard parametric study was performed using the same code with a slightly different input spreadsheet, provided in Table 4.4. Changed values are in bolded, italic text.

LowerIns_Layer

The 'LowerIns_Layer' variable was excluded from the parametric study input spreadsheet as the default value of 'LowerInsulationThickness' of 0 would negate its effect. As such, a series of Simulink model simulations was performed, with the value of LowerIns_Layer manually set for each simulation. The default values for all other variables were used, with the exception of 'LowerInsulationThickness', whose value was set to the NBC-required 0.0381 m of XPS insulation [12]. The results are summarized and discussed in Section 5.4 and plotted in Appendix C.3.2.

Table 4.4: Standard Parametric Study Data

Variable Name	**Min**	**Max**	**Step**	**Default**	**Primary**
Air_Convection	2	4	***0.5***	3	No
Ceiling_R_Value	20	60	***5***	30	No
ConcreteSetpoint_Activate	0	1	1	1	No
ConcreteSurfaceSetpoint	16	25	1	18	No
ContactResistanceOn	0	1	1	1	No
ContactResistanceValue	0.009527	0.047637	0.009527	0.019055	No
Exterior_Air_Conv	10	60	10	30	No
HeaterFraction_Activate	0	1	1	1	No
HeaterRampDownTemp_Diff	2.5	10	2.5	5	No
LowerInsulationThickness	0	0.1	0.01	0	***No***
MaxHeaterTemp	20	60	5	55	No
SimLengthMonths	4	20	4	12	No
SimTimeStepMinutes	5	20	5	10	No
Soil_Temp_Full_Depth	5	10	1	8	No
UpperInsulationThickness	0	0.1	0.01	0	***No***

4.3 Proposed Set of EXN/Aero Simulations

The culmination of the efforts described in this research to develop and test EXN/Aero's ability to accurately model a typical installation of ThermaRay's ESS was a proposed set of simulations, presented here. Similar to the MATLAB/Simulink model, the computational domain for these simulations consists of an elemental 3D slice of a typical ESS installation in a 60' by 100' industrial space from an isothermal depth up to the ceiling

10 m above the concrete slab floor. The footprint of these simulations is equal to the total building floor space divided by the number of ESS panels required to heat it, as shown in Figure 4.4. This proposed set of simulations consists of three separate simulations which will first establish a smooth temperature gradient throughout the computational domain to decrease the time required for the second simulation to establish a steady buoyant flow field within the heated space. This buoyant flow field was 'frozen' in the third simulation, allowing for all three modes of heat transfer to be modelled within the heated space in a far more computationally efficient manner than if the buoyancy and turbulent models were still running as they do in the second simulation. Each of these simulations is described below, followed by a summary and discussion of settings common to all three.

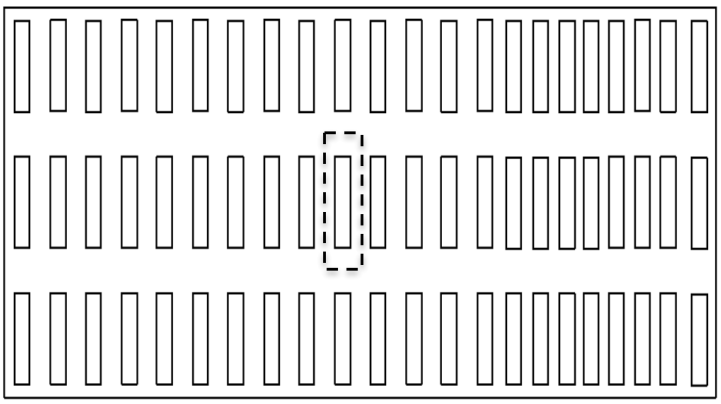

Figure 4.4: Footprint of Proposed EXN/Aero Simulations (Dotted Line)

First Simulation (Initialization)

The purpose of the first simulation was to reduce the duration required for the second simulation to reach a quasi-steady state. The majority of settings for this simulation are provided in the 'Common Settings' section on page 118; specific settings for this simulation are provided below:

- Thermal Conductivity of Air: A value of 0.1895 W/mK was used for this simulation to improve heat transfer through the heated space. This 'effective thermal conductivity' value was calculated in Section 3.3.4.
- Time Step: 450 seconds, based on the optimization process described in Section 4.3.2.
- Simulation Length: Until the temperature field throughout the heated space at one time step is indistinguishable from that of the previous time step, up to 60 days (two months)
- Output Variables: The variables outputted by this simulation are Temperature, Heat Flux, Radiative Flux, and Energy. EXN/Aero's equations relating to velocity, pressure, and turbulence as well as its buoyancy and turbulence models are deactivated for this simulation.
- Inner Loop Equations: Energy, Radiation.
- Deactivated Equations: Velocity, Pressure.

Table 4.5: Proposed EXN/Aero Simulations: #1

Simulation #	**1**
k (W/mK)	0.1895
Time Step (s)	450
Max. Simulation Duration (days)	60
Buoyancy / Turbulence	Deactivated
Inner Loop Equations	Energy, Radiation
Deactivated Equations	Velocity, Pressure
Restart Values	None

Second Simulation (Buoyancy & Turbulence)

The purpose of the second simulation is to establish the buoyant flow field within the heated space. The settings specific to this simulation are provided below:

- Thermal Conductivity of Air: With the buoyancy model active, the thermal conductivity of air within the heated space was reduced back to k_{air}, 0.026 W/mK [56].
- Time Step: As mentioned in Section 3.3.3, buoyancy modelling requires a small time step. While no formal optimization process was performed, a time step of 5 seconds was found to support the stability of simulations with the buoyancy model active.
- Simulation Length: Until the temperature and velocity fields throughout the heated space at one time step is indistinguishable from that of the previous time step, up to one (1) day.

- Output Variables: With buoyancy and turbulence models active, this simulation's outputs include all those from the first simulation plus velocity (in all directions) and turbulent kinetic energy (to monitor the turbulence model).

- Buoyancy Model: EXN/Aero's buoyancy model was activated for this simulation, based on the Boussinesq assumption as described in Section 3.3.3 with a gravity vector of -9.81 in the Y direction (depth) and a reference temperature of 20 °C. This reference temperature was chosen as it was expected to be roughly the average air temperature in the heated space.

- Turbulence Model: EXN/Aero's RANS κ-ω turbulence model was activated for this model. To consider the impact of turbulence model selection on the simulation's outputs, EXN/Aero's κ-ω SST (shear stress transport) model was tested with all other settings held constant. The results of this test supported the selection of the κ-ω model without SST and are provided in Section 5.8.

- Initial Velocity: An initial positive velocity within the heated space of 0.05 m/s was set to provide the turbulence and buoyancy models with a non-zero velocity at the outset of the simulation. This improved simulation stability.

- Inner Loop Equations: Velocity, Pressure, Energy, Radiation, Turbulence.

- Deactivated Equations: None.
- Restart Values: Energy – this provides the second simulation the smoothed-out temperature gradient from the first simulation.

Table 4.6: Proposed EXN/Aero Simulations: #2

Simulation #	**2**
k (W/mK)	0.026
Time Step (s)	5
Max. Simulation Duration (days)	1
Buoyancy / Turbulence	Activated
Inner Loop Equations	Energy, Radiation, Velocity Pressure, Turbulence
Deactivated Equations	None
Restart Values	Energy

Third Simulation (Complete CFD/CHT)

The third simulation is the culmination of all the effort made in this research to develop and test EXN/Aero's capability to studying the long-term transient behaviour of ThermaRay's ESS. With the buoyancy- and turbulence-driven velocity field frozen and the related models deactivated, this simulation can use the same time step as the first (450 seconds) while still modelling buoyancy-driven natural convection in the heated space along with convective and conductive heat transfer. The unique settings for this simulation are provided below:

- Thermal Conductivity of Air: The thermal conductivity of air can

remain at 0.026 W/mK as the buoyancy-driven velocity field is still present within the heated space.

- Time Step: The buoyancy model is no longer active, allowing for the time step to return to the optimized 450 seconds.
- Simulation Length: A duration of 60 days is recommended. Based on discussions with ThermaRay, this is expected to be the point at which their ESS approaches a quasi-steady state. Longer simulations would better represent the long-term behaviour of the system and should be considered if the required computational resources are available.
- Output Variables: Despite the buoyancy and turbulence models being deactivated, the recommended list of output variables for this simulation is the same as that for the second simulation. Outputting the velocity field, for example, allows for analysis of the velocity field on heat flow.
- Buoyancy & Turbulence Models: Deactivated.
- Inner Loop Equations: Energy, Radiation.
- Deactivate Equation: Velocity, Pressure.
- Restart Values: Momentum/Pressure, Energy – This feeds in the velocity-pressure and temperature fields from the second simulation.

Table 4.7: Proposed EXN/Aero Simulations: #3

Simulation #	**3**
k (W/mK)	0.026
Time Step (s)	450
Max. Simulation Duration (days)	60
Buoyancy / Turbulence	Deactivated
Inner Loop Equations	Energy, Radiation
Deactivated Equations	Velocity, Pressure
Restart Values	Energy, Momentum/Pressure

4.3.1 Common EXN/Aero Settings

This section outlines the settings common to all three of the simulations described in the preceding section.

Boundary Conditions & TES Layers

Boundary conditions were set to study the performance of a section of an ETS installation in an industrial building, in a region distant from any exterior walls. Modelling a section near the center of a building, therefore excluding the effect of the building's walls from the study, ensures that the focus of the study remained on the effect of insulation on the system's performance. It also takes advantage of the 1D conduction observed by Wang et al. [23] and Zhou & He [24] in regions distant from any exterior walls under steady state conditions. This simplifies the behaviour of the system, further focusing the study on the primary research objective.

Recreating a section near the center of an industrial space was done by treating the four vertical perimeter walls of the heated space and TES region as symmetry planes. Unlike its walls, the building's ceiling are included in the computational domain. This allows for the exterior temperature, the R-value of the ceiling/roof assembly, and the temperature difference across the ceiling/roof assembly to be included as potential variables for further study.

The thickness and thermal properties of each layer of the TES region (plus the heated space) are provided in Table A.1. Initial TES layer temperatures and boundary temperatures were based in part on ground temperature data from Natural Resources Canada for Ottawa, ON [3].

Contact resistance was thoroughly studied in the Simulink model's parametric study. As such, EXN/Aero's contact resistance settings, validated in Section 3.3.7, were not active for the demonstration of the simulation design presented here. However, incorporating contact resistance in future simulations would simply require an adjustment of the BC Connectivity settings for the interfaces at which contact resistance was sought to be included.

The solid-fluid interface at the upper surface of the concrete slab was treated using EXN/Aero's 'automatic' heat transfer settings, allowing for the solver's CFD-CHT capabilties to model conjugate heat transfer from the TES region into the heated space.

4.3.2 Mesh & Time Step Optimization

As in all CFD research projects with transient simulations, the refinement of the computational mesh and the time step had to be optimized. This was done in two stages. First, the computational mesh (hereto referred to as 'the mesh') was optimized by running a series of simulations with four meshes at different levels of refinement. All mesh and time step optimization simulations were run using settings based on Simulation 1, described on page 113, with the exception of the thermal conductivity of the heated air which was set to 0.026 W/mK (k_{air} rather than k_{eff}). System performance was estimated by dividing the heat flux upwards from the sand layer into the compressed fill layer above by the sum of the same value and the heat flux downwards from the sand layer into the compressed sand layer below. This informal approach to assessing system performance is visualized in Equation 4.4 (which does not account for occupant-set temperature setpoints, as with the other performance evaluation approaches described in Section 3.5).

$$\eta_{opt} = \frac{q_{sand\uparrow comp.fill}}{q_{sand\uparrow comp.fill} + q_{sand\downarrow comp.sand}} \tag{4.4}$$

Each mesh was run three times: once transiently with a time step of 450 seconds and twice as steady state simulations with time steps of 450 and 3600 seconds, respectively. The steady state efficiency of the system found by each simulation was used to select the optimal mesh. Once a computational mesh

was selected, a series of simulations was run with the chosen mesh at six time step lengths: 100, 250, 450, 900, 1800, and 3600 seconds. The amplitude and frequency of fluctuations in heat flux from the heated slab surface and the efficiency at steady state was monitored for each of the six time steps. The results of these two stages of optimization are summarized in Table 4.8 and 4.9.

Table 4.8: Mesh Optimization Study Results

Mesh Size (# of CVs)	Run Type	Run Length (days)	Time Step Length (s)	Thermal Performance (%)
250,000	Transient	60	450	57
	Steady State	N/A	450	—
			3600	—
500,000	Transient	60	450	67.3
	Steady State	N/A	450	66.7
			3600	65.4
1,000,000	Transient	60	450	67.5
	Steady State	N/A	450	—
			3600	
2,000,000	Transient	60	450	61.1
	Steady State	N/A	450	59.2
			3600	60.1
7,000,000	Transient	60	450	54.0
	Steady State	N/A	450	55.4
			3600	—

Table 4.9: Time Step Optimization Results

Time Step Length (s)	Average Fluctuation Magnitude (W/m^2)	Maximum Fluctuation Magnitude (W/m^2)	Thermal Performance (%)
100	0.4	5	68.8
250	0.5	6	68.4
450	0.6	5	67.5
900	2.5	7	65.8
1800	3	7	66.2
3600	2	5	63.5

The 250,000 CV mesh was highly unstable in all simulations; an approximate system efficiency of 57% was observed for the transient simulation but no such approximation could be made for the steady state simulations with the same mesh. The computational mesh with 10^6 CVs ran reliably in transient simulations. However, it failed repeatedly in steady state simulations. The cause for these failures was unknown. Given the stability of its transient results, the 10^6 CV mesh was still considered in the mesh optimization process and it was used for the time step optimization whose results are provided in Table 4.9. Finally, the mesh with $7x10^6$ control volumes was stable for both transient and steady state simulations with a time step of 450 seconds, but was less stable when run with a time step of 3600 seconds.

Based on the results presented in Table 4.9, an optimal time step of 450 seconds was selected. Its average fluctuation magnitude value (W/m^2) was similar to those of time steps 100 and 250 seconds in length and much less than the average fluctuation magnitude values for the longer time steps.

Additionally, its maximum fluctuation (W/m^2) was among the lowest of all time step lengths assessed and its thermal performance (%) was reasonably close to that of the shorter time step simulations.

The extreme instability of simulations with the 250,000 CVs mesh discouraged the use of the mesh with 500,000 CVs, despite the relative stability of its simulations. Similarly, the 2 x 10^6 CV mesh was avoided due to the instability of the mesh with 10^6 CVs. This required the consideration of meshes with up to 10^7 CVs, which had not been previously included in the mesh optimization process. It was through this extension of the mesh optimization process that the optimal mesh size of 7 x 10^6 was found. The results for transient and steady state simulations using the final mesh and time step are provided in Table 4.9, with images of the final mesh available in Appendix E.3.

Heating Panel Output

Output of the heating panel in these simulations was discussed at length on page 76 (Section 3.4.3).

4.3.3 Radiation Modelling of ThermaRay's ESS in EXN/Aero

While EXN/Aero is capable of modelling all aspects of radiative heat transfer, including scattering, absorption, and emission within a medium, a simplified radiation model was used in the set of EXN/Aero simulations proposed here. As all vertical boundaries of the heated space in the computational domain are treated as symmetry planes, it was assumed that the net magnitude of scattering, absorption, and emission within the computational domain was negligible. As such, a modified radiation model based solely on the Stefan-Boltzmann Law as defined in Equation 4.5 was used, with a grey-body emissivity of 0.9 [83].

$$q_{rad} = \sigma\epsilon(T_C^4 - T_{ceiling}^4) \tag{4.5}$$

Secondary Radiation Model Validation

The second stage of validation for EXN/Aero's FVM-based radiation model consisted of the comparison of the radiative flux observed in a full-scale transient simulation with values from literature. The 2013 paper from Cholewa at al. [31] is the focus of this stage of validation due to its novel measurement technique and assessment of its results compared to prior related works. Other works will also be considered [29, 74, 86, 89, 90], values

from which are provided in Table 5.2. As reported in that table, Cholewa et al. [31] suggests a radiative flux between 5.4 and 6.2 W/m^{2}K should be observed. This validation was based on the EXN/Aero model methodology, each stage of which was described in the preceding sections.

The radiative flux from the concrete floor was steady at 66 W/m^2 as the system approached steady state during the first simulation. However, as the purpose of this simulation was solely to smooth out the temperature gradients within the computational domain, the temperature difference between the concrete floor and the ceiling 10 m above, was still quite high at nearly 23 °C. This equates to a h_r value of 2.9 W/m^{2}K. This was well below the expected range from Table 5.2. EXN/Aero's buoyancy and turbulence were not active during this first stage of the methodology. It was expected that incorporating these models, and by doing so balancing out the temperature gradient within the heated space, would increase the value of h_r. However, insufficient simulations were conducted to conclusively test this hypothesis.

Figure 5.10 displays the initial and final plots of the vertical temperature distribution through the center of the computational domain at the start and end of the first simulation, from the bottom of the 'undisturbed soil' layer on the left through to the ceiling at the right. As the buoyancy and turbulence models were not active during this first stage of the methodology, the sole mode of heat transfer present within the heated space was conduction. While the radiation model was active during all EXN/Aero simulations, it does not

impact the shape of the temperature distribution within the heated space, as described in Section 4.3.3. As conduction (governed by Fourier's Law, Equation 3.5) is linear, so too is the temperature gradient through the heated space on the right of Figure 5.10b on page 163.

Chapter 5

Results & Validation

5.1 1D Excel-Based Model

5.1.1 Verification & Validation

The results of the Excel-based model were used in the early development of the proposed set of EXN/Aero full-scale simulations for informal verification to ensure that no issues were present in the EXN/Aero solver. This attentiveness was necessary. The set of simulations that have been developed, tested, and proposed for the use of EXN/Aero to study the long-term, transient, three-dimensional behaviour of ThermaRay's ESS was the first time EXN/Aero has been used in the large scale analysis of a conjugate heat transfer based system. The quasi-1D mesh used in the '1D' simulations presented here was optimized based on the process discussed in Section 4.1.1. The resulting similarity between the Excel-based model and the quasi-1D EXN/Aero model is portrayed in Figure 5.1. A 0.72% average percent difference was achieved between the temperature values at each TES

layer interface between the Excel-based model and EXN/Aero results. The system's performance, measured by the percentage of heat from the panels passing upwards into the heated space above, was 90.9% based on EXN/Aero results, 3% more than the 87.8% predicted by the Excel-based model [49]. These preliminary simulations were performed to ensure that EXN/Aero's thermal modelling capabilities were functioning properly and to develop a stronger understanding of the approaches taken in the creation of the Excel-based model by the team at NSCC [49]. Once the five cases were completed, the same quasi-1D mesh was used to study EXN/Aero's contact resistance modelling capabilities, as discussed in Section 3.3.7.

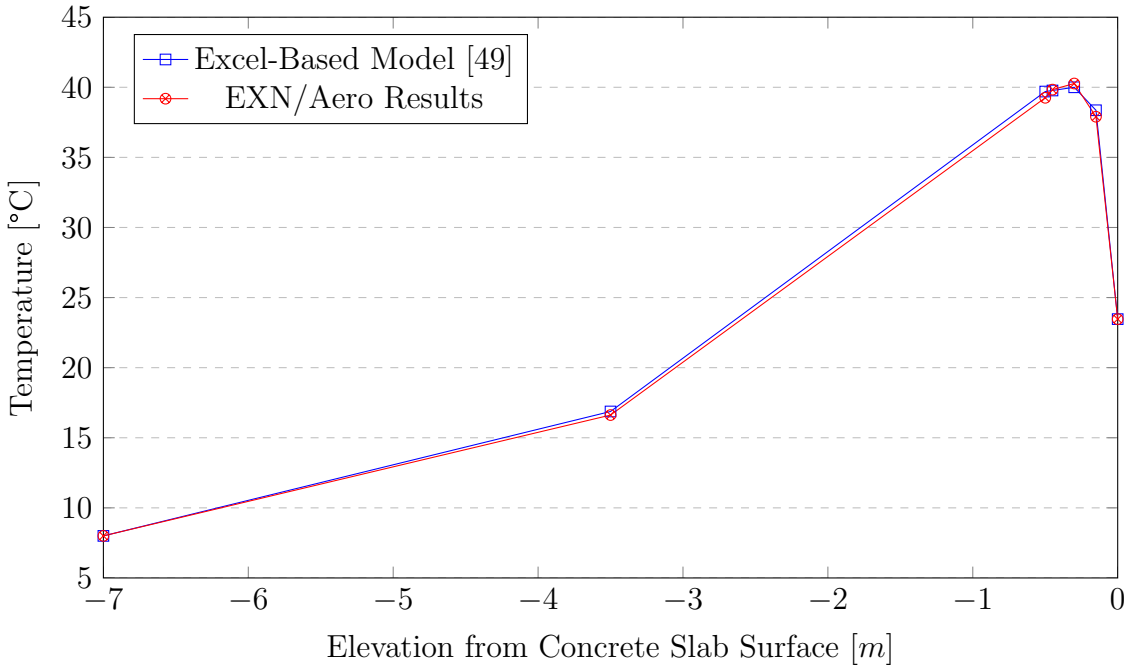

Figure 5.1: Verification of Excel-Based Model

5.1.2 1D Simulation Results & Discussion

The five 1D simulations described in Section 4.1.3 were run with EXN/Aero. The results are summarized in Table 5.1. These results, with an average difference of less than 0.1% to the results from the Excel-based model, are quite promising regarding the validation of the Excel-based model developed by Joseph et al. [49] at NSCC. This supports the comparison of results from the Excel-based model with those of the other simulations presented and proposed in this research.

Table 5.1: 1D Simulations - Performance Results

Case #	EXN/Aero Model Performance (%)	Excel-Based Model Performance (%)	Difference (%)
1	94.96	95.0	– 0.0385
2	92.87	92.9	– 0.0337
3	90.99	91.0	– 0.0060
4	89.63	89.6	+ 0.0317
5	88.33	87.8	+ 0.5344

The 1D simulation results, summarized in Table 5.1 and displayed in Figures 5.2 and 5.3, indicate a strong positive correlation between insulation thickness beneath the heating panel and system performance. However, the benefit for system performance decreases for each added unit thickness. The line of best fit (included in Figure 5.3) and its derivative for the 1D simulation results as presented in Figure 5.3 are provided in Equations 5.1 and 5.2,

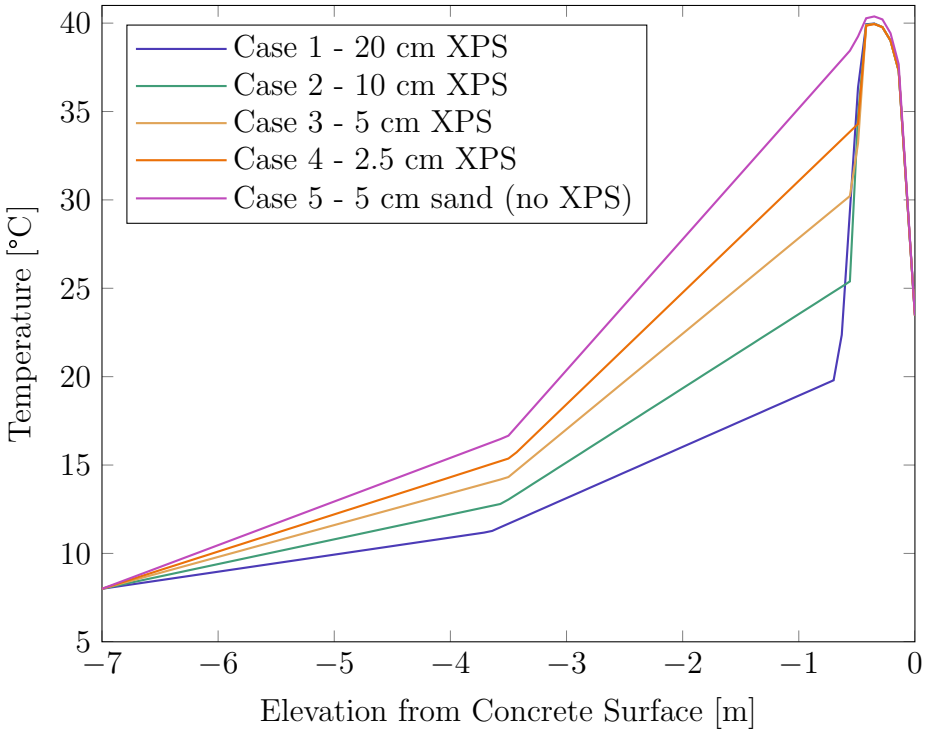

Figure 5.2: 1D Simulations - Temperature Results

respectively. These equations, with an R^2 value of nearly 1.0, indicate that additional XPS below the heating panel will no longer be beneficial to the system's performance beyond 23 cm of insulation. The horizontal asymptote is indicated by a dotted line in Figure 5.3. This relationship is further detailed and discussed in the section covering the results from the Simulink-based parametric studies, which showed a similar relationship between insulation below the heating panel and the system's long-term transient behaviour.

The conclusions from these simulations are two-fold. Installing the insulation required by the NBC, an RSI value of 1.32 which corresponds

to 3.8 cm of XPS [12], below the heating panels could improve the system's thermal performance. However, there is a limit to the benefits of insulation below the heating panels (as explained further in Section 5.5.1). Considering the cost of installing XPS across the entirety of a building's foundation, ThermaRay would likely be best suited to install the minimum required insulation thickness. Provided Codes Canada accepts the relocation of insulation from immediately below the concrete slab to below the heating panels, this would allow for ThermaRay to address the requirements of the NBC while improving their system's performance.

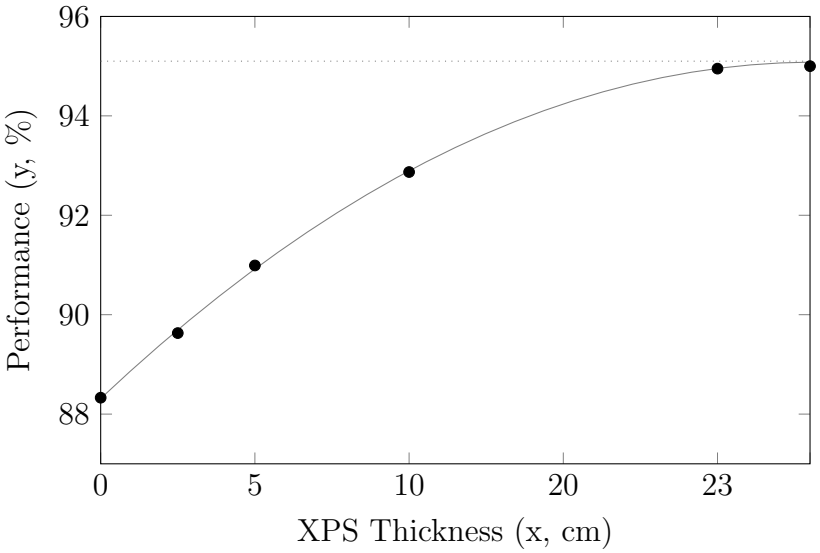

Figure 5.3: 1D Results: XPS vs. Performance

$$y = -0.0126x^2 + 0.584x + 88.314 \qquad (R^2 = 0.9996) \qquad (5.1)$$

$$y' = -0.0252x + 0.584 \tag{5.2}$$

5.2 Result Validation: Full-Scale Models

Validation of results for the full-scale models was based on values and equations from literature. Equations and suggested values for h_c, h_r, h_{tot}, and q_{floor} from studies by Cholewa et al. [31, 34], Zheng et al. [30], Seyam et al. [29], and Acikgoz et al. [74, 86] were beneficial for the validation of results. These equations and values are discussed in Sections 2.2 and 3.3, and summarized in Table 5.2. For sources that provided a range of values for the same variable, the recommended value is in parentheses.

Table 5.2: Validation Values from Literature

Reference Source	$\boldsymbol{h_{tot}}$, $\mathbf{W/m^2K}$	$\boldsymbol{h_r}$	$\boldsymbol{h_c}$
Acikgoz, 2015 [74]	9.53 – 10.26	5.45	3.5
Acikgoz, 2019 [86]	8.5 – 10.5 (9.5)	5.2 – 5.9 (5.5)	2.3 – 4.1 (3.3) $1.79(\Delta T_{ETS})^{0.28}$
Cholewa, 2013 [31]	8.7 $7.67(\Delta T_{ETS})^{0.1}$	5.4 – 6.2 (5.6)	2.2 – 3.5
EN 1264, 2008 [89, 90]	10.8	–	–
Seyam, 2014 [29]	4.47 (Computational) 5.38 (Experimental)	–	–

Reference Source	q_{tot}, W/m^2	q_r	q_c
Acikgoz, 2019 [86]	$7.16(\Delta T_{ETS})^{1.14}$	–	
Cholewa, 2013 [31]	25.1	18.7	6.4
EN 1264, 2008 [89, 90]	$8.92(\Delta T_{ETS})^{1.1}$	–	–
Seyam, 2014 [29]	–	46.9	–
Zheng, 2017 [30]	$29.166(\Delta T_a^{1.079} \cdot \Delta T_w^{0.023})$	–	–

5.3 Model Accuracy & Validation

Due to the lack of data available from full-scale installations of the ESS or even experimental results from sufficiently similar systems, quantification of the accuracy and precision of the models presented in this research is not possible. It is expected that the accuracy of each model corresponds to its computational demand, with the quasi-1D model being least accurate, the Simulink model being moderately accurate, and the full-scale EXN/Aero model being most accurate. The dependent factor here is the level of detail in the modelling of heat transfer within the heated space, with the full-scale EXN/Aero model being the sole model to include buoyancy modelling within the heated space. If buoyancy modelling could be incorporated into the Simulink model it would significantly increase its accuracy.

5.3.1 Simulink Model Accuracy & Assumptions

Given the importance of the Simulink model to addressing this research's primary objective, its accuracy must be considered more carefully. Table 5.3 provides an list of the key assumptions made in the development of the Simulink with the expected relative impact of each on the accuracy of the results. The basis for each assumption is provided thereafter.

Table 5.3: Simulink Model Assumptions

Assumption	**Significance**	**References**
k_{air} Constant	Low	Figure 5.10b [73]
h_c Constant	Medium	Section 3.3.2, Section 4.2.1, Page 92
q_{rad} from Roof Negligible	Low	Section 4.2.1, Page 94
Thermal Mass of XPS Negligible	Moderate	Table 3.2, A.1 [91, 92]
q_{cond} w/in TES region 2D at steady-state	Low	[23, 24]
$\Delta s_{gap} = 0.5$ mm	Low	Section 3.3.7, [82]
Air is a Non-Participating Medium (Radiation)	Low	Section 3.3.5, [93, 94]
Air Velocity ≤ 0.2 m/s	Low	Figures 5.11, 5.12, [29, 31, 57]

- k_{air}, the thermal conductivity of air within the heated space, is constant: This is justified by the difference in thermal conductivity of air over the range of temperatures observed through this research of 15 to 25 of just 0.0008 W/mK and the $\leq$1% contribution of conduction to the overall heat transfer rate through the heated space.

- h_c, the convective heat coefficient from the concrete slab surface into the heated space, is constant: The convection coefficient from the concrete slab into the heated space was carefully selected based primarily on Cholewa et al. [31]. The h_c values of between 2.5 and 3 W/m^{2}K were selected based on the assumption of an air velocity of less than 0.2 m/s, a selection supported by the findings presented from the second full-scale EXN/Aero simulation in Figures 5.11 and 5.12. These figures indicate that the average air velocity throughout the heated space is below 0.2 m/s, particularly near the surface of the concrete slab.
  - Furthermore, the ceiling temperature is an acceptable value for use as the far-field temperature for the calculation of convection through the heated space: Using the ceiling's inner temperature as the farfield temperature was considered acceptable due to the small difference between it and the floor's upper surface. The ratio between radiative and convective heat transfer was correct based on literature (60% radiation, 40% convection) as discussed in Section 5.6.
- q_{rad} from the roof's outer surface is negligible: This assumption was made to avoid needing to account for incoming solar radiation. In essence, the assumption is that the sum incoming and outgoing radiation is negligible when compared to convective losses to the environment. Given a roof temperature of $-5\,^{\circ}$C and a far-field exterior

air temperature (sky temperature for radiation) of $-10\,^{\circ}\mathrm{C}$, treating the roof as a blackbody with no incoming solar radiation, convection from the roof would still be seven-fold greater than radiation. This suggests the effect of this assumption on the accuracy of the model is minor, though future research could improve the model's accuracy by incorporating incoming and outgoing radiation from the roof's surface.

- The thermal mass of XPS is negligible: While the low thermal conductivity of XPS prevents it from being a widely used material for thermal storage, its specific heat capacity is significant - over twice that of the undisturbed soil layer. Its high specific heat capacity is the primary reason why it has the lowest thermal diffusivity of all TES layers, as shown in Table 3.2. This suggests that the thermal inertia of the XPS should be considered in future studies.

- q_{cond} within TES region is two-dimensional at steady-state: This was studied and confirmed in Wang et al. [23] and Zhou & He [24].

- The air gap between TES layers, used for calculating contact resistance, is 0.5 mm thick: While the results were heavily dependent on the assumed air gap thickness, the magnitude of contact resistance was varied in this research to determine the sensitivity of the system's performance to contact resistance and minimize the potentially negative impact of this assumption on the accuracy of the conclusions drawn from the results of this research.

- Air within the heated space is a non-participating medium for the purposes of radiation modelling: This is a commonly used assumption in peer-reviewed papers studying heat transfer within a radiantly heated space with moderate temperatures (Kuznetsov et al. [93] and Saravanan et al. [94], for example).
- Air velocity within the heated space has a magnitude less than 0.2 m/s: This assumption is thoroughly supported in Section 3.3.2.

5.4 Simulink Model Parametric Study: Results

5.4.1 Modified Parametric Study

The modified parametric study described on page 107 (Section 4.2.3) was primarily performed to study the effect of insulation, either above or below the heating panel, on the system's performance under a wide range of system states. The results for these two variables are summarized in Table 5.4 and plotted in Figures 5.4 and 5.5. Lines of best fit and R^2 values in Table 5.4 are based on the mean performance value for each value of a given variable, with the error bars in the figures having a magnitude of one standard deviation. All results from the modified parametric study are summarized and plotted in Appendix C.3. Error bars in figures depicting results from the modified

parametric study are equivalent to plus/minus one standard deviation for the mean value for each data point (+/– 1 σ).

Table 5.4: Modified Parametric Study Results

Variable	**Relationship**		
	Type	**Line of Best Fit**	**R^2 Value**
UpperInsulationThickness	Linear, Negative	y = -142.74x + 79.211	0.99
LowerInsulationThickness	Linear, Positive	y = 42.094x + 70.973	0.98

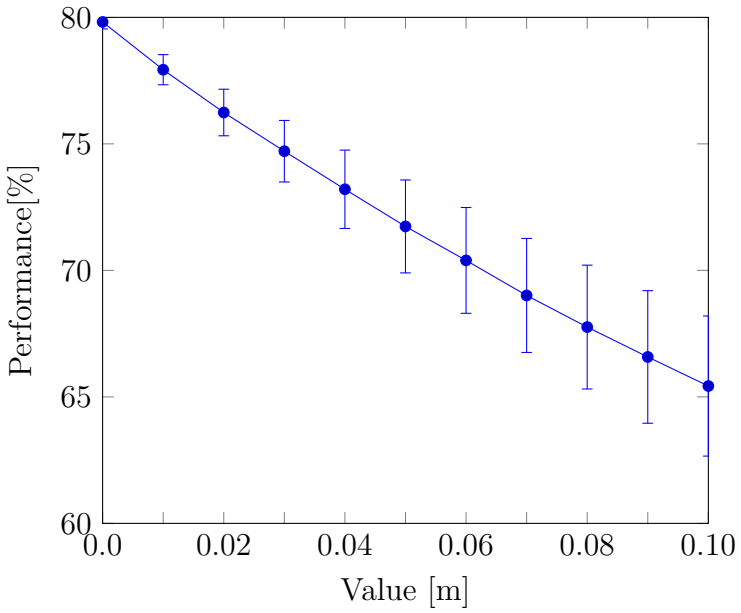

Figure 5.4: Results - UpperInsulationThickness

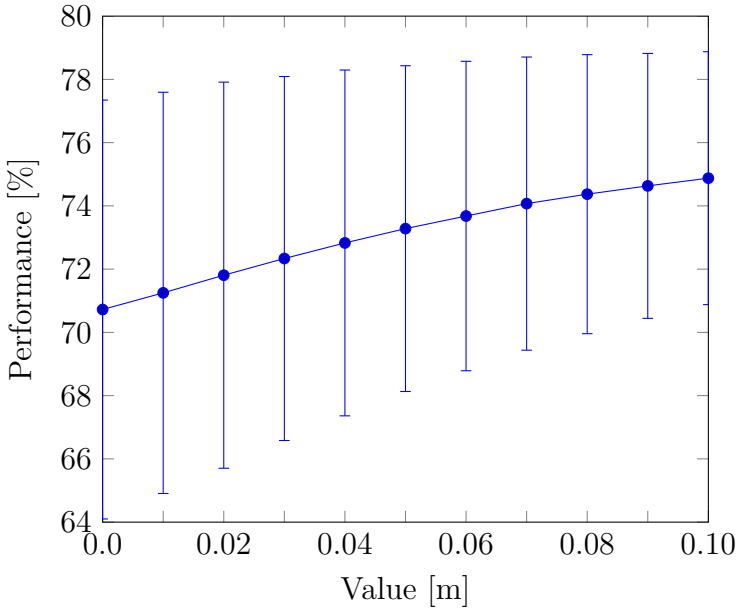

Figure 5.5: Results - LowerInsulationThickness

5.4.2 Standard Parametric Study

The standard parametric study was the primary source of results for all variables excluding "UpperInsulationThickness" and "LowerInsulationThickness", whose results were presented above, and "LowerIns_Layer", whose results were obtained through manually-set simulations (as described on page 110, Section 4.2.3). A standard parametric study was performed for these variables for two reasons; firstly, these variables are less pertinent to the primary research objective and therefore do not require as intensive study, and secondly, there was a concern that the effects of "UpperInsulationThickness" and "LowerInsulationThickness" on each of the other variables could

'cancel out', rendering their results less dependable. A standard parametric study would allow for each variable to be studied independently, providing ThermaRay with guidance on how they could alter their current installation practices, represented in the variables' default values. The results from the parametric study are summarized below, including "UpperInsulationThickness" and "LowerInsulationThickness" and the separately obtained "LowerIns_Layer" results. Plots for all results from the standard parametric study are provided in Appendix C.3, along with the same table as provided below for reference.

Table 5.5: Standard Parametric Study Results

Variable	**Relationship**	
	Type	**Line of Best Fit**
Air_Convection	Linear, Weak & Positive	y = 0.035x + 79.3
Ceiling_R_Value	Linear, Negative	y = -0.421x + 92.2
ConcreteSetpoint_Activate	Positive	–
ConcreteSurfaceSetpoint	Linear, Negative	y = -0.792x + 93.8
ContactResistanceOn	Weak & Negative	–
ContactResistanceValue	Linear, Weak & Negative	y = -26.2x + 80.0
Exterior_Air_Conv	Power, Weak & Positive	$y = 79.0\ x^{0.0014}$
HeaterFraction_Activate	Weak / No Correlation	–
HeaterRampDownTemp_Diff	Weak / No Correlation	–
LowerInsulationThickness	Asymptotic Linear, Positive	y = 17.2x + 79.4
LowerIns_Layer	Weak / No Correlation	–
MaxHeaterTemp	Asymptotic Linear, Negative	y = -0.036x + 81.0
SimLengthMonths	Linear, Week & Positive	y = 0.120x + 73.9
SimTimeStepMinutes	Linear, Weak & Negative	y = -0.0042x + 79.5
Soil_Temp_Full_Depth	Linear, Positive	y = 1.2259x + 69.7
UpperInsulationThickness	Asymptotic Linear, Negative	y = -174.19x + 78.67

5.5 Miscellaneous Results & Observations

5.5.1 Sub-Panel Insulation vs. Thermal Storage

Given the significant negative impact of insulation installed between the heating panel and the concrete slab on the system's performance, the logical next consideration was to instead consider installing the NBC-required insulation below the heating panel. However, doing so was shown to only provide a marginal benefit to the system - potentially not worth the cost of installing insulation across the entirety of a building's foundation. Based on previous research by Tahersima et al. [13, 26], it may be more energy efficient and economical to not install insulation across the entirety of the foundation but to instead increase the thickness of sub-grade insulation along the building's perimeter.

There are two competing factors at play when considering insulation installed beneath the heating panel. For one, increasing the overall thermal resistance between the heating panel and the bottom of the computational domain by introducing a layer of insulation is inherently beneficial as it encourages the flow of heat upwards towards the heated space. However, insulation also limits the functionality of all thermal mass located below it. In the case of the ESS, the majority of the system's thermal mass is situated within the undisturbed soil layer and so insulation between this layer and the

heating panel significantly reduces the thermal mass that is "available to" the system. Which of these factors was dominant over the other was unknown at the outset of this research. The 'LowerIns_Layer' variable was added to the parametric studies in an attempt to identify the dominant factor by varying the depth of insulation beneath the heating panel, represented by a point source of thermal resistance. Treating this insulation as a point source allowed for a more simple model to be used that allows for the thickness of the insulation and all TES layers to be held constant while the insulation's depth is varied. However, this invokes the assumption that the insulation's thermal mass is negligible. The accuracy of this assumption is discussed in Section 5.3.1.

Based on results of the 'LowerIns_Layer' variable in the standard parametric study, provided in Figure 5.6, it would seem that placing the insulation even lower in the foundation below the heating panel would have minimal impact on the system's performance. However, the difference between the three depths tested is just 10 cm. This is then insufficient to definitively state whether installing the NBC-required insulation further down would both meet the National Building Code while including more thermal mass between the heating panel and the insulation than in the simulations performed for this research. Therefore, further research on this matter is required. Additional research is also suggested regarding the inclusion of thicker insulation along the perimeter of ESS-heated buildings to address Codes Canada's energy efficiency concerns while maximizing the

thermal mass and inertia of the ESS.

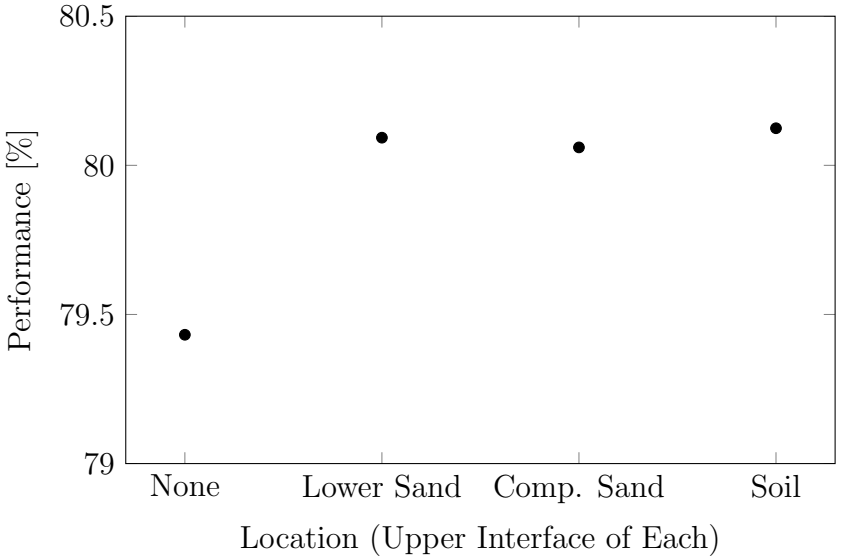

Figure 5.6: 'LowerIns_Layer' Results (SPS)

5.5.2 ESR Values

The "energy storage ratio", or ESR, was first mentioned on page 9 in the literature review. Equal to the ratio between energy passing into the heated space while the heating panel is active and all energy which passes into the heated space, the ESR was identified as a potential indicator of system performance. Accordingly, the ESR was calculated for each simulation in the standard parametric study. The results are plotted in Figure 5.7. While the average ESR was high, at 0.85, there appears to be no correlation between ESR and system performance. This high average ESR value was encouraging news for ThermaRay regarding the thermal performance of

their ESS. The primary method of determining system performance remains unaltered following this result.

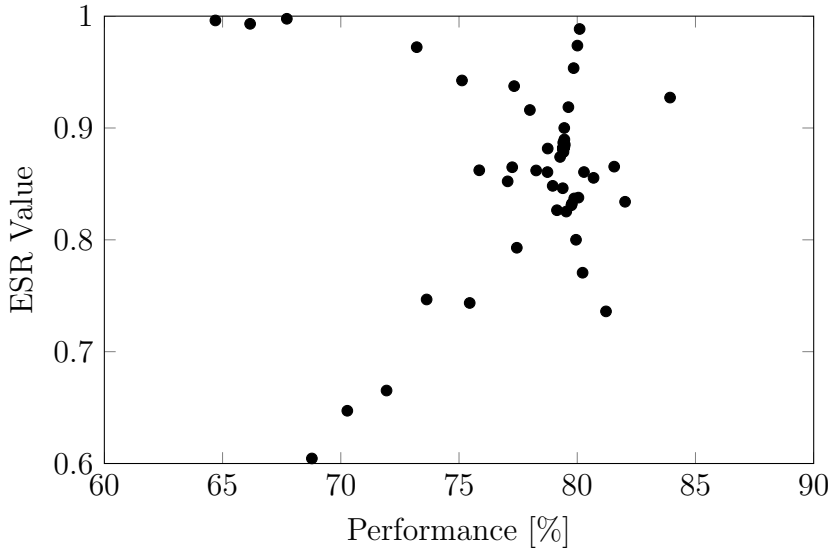

Figure 5.7: ESR Values vs. System Performance

Despite the lack of correlation between the ESR and system performance, there are mentionable patterns in Figure 5.7. Firstly, the handful of data points with particularly low performance values yet quite high ESR values are from the simulations with the highest thickness of insulation above the heating panel. This was to be expected, as increasing the thermal resistance between the concrete slab surface and the heating panel increases the Fourier Number (defined in Equation 5.3) of this region, not only reducing the total amount of heat reaching the heated space but increasing the delay between when heat enters the system through the heating panel and when it reaches the heated space. The former reduces the system performance while the

latter increases the ESR. Secondly, the data points with the lowest ESR values are from simulations with the highest ceiling R-values (R-50, R-55, and R-60). With less heat being lost through the ceiling, less heat is being drawn up from the TES region, decreasing system performance (and the heat load). Unlike insulation within the TES region, increasing the R-value of the ceiling does not impact the Fourier Number of the region between the heating panel and the concrete surface. As such, a higher ceiling R-value decreases both the ESR value and the system performance.

$$Fo = \frac{\text{Diffusive Transport Rate}}{\text{Storage Rate}} = \frac{\alpha t}{L^2} = \frac{kt}{c_p \rho L^2} \tag{5.3}$$

5.5.3 Compound Effect of Insulation Above & Below Heating Panel

The parametric studies above focused on the impact of insulation either above or below the heating panel. To study the impact of including insulation both above and below the heating panel, a subset of the data from the modified parametric study was extracted. The results are shown in Figure 5.8, with system performance indicated by colour. Results indicate that there is no unforeseen compound effect of installing insulation both above and below the heating panel. There may, however, be a compound effect on the thermal response time of the system. This was not directly considered in this research. Isolines on this figure would allow for the relationship between the

impact of insulation installed above and below on the system's performance for a given efficiency. The correlation between the slopes of these isolines and the thickness of insulation installed above the heating panel would be much stronger than that between the slopes and the thickness of insulation installed below the heating panel. This further stresses the importance for ThermaRay to receive permission to either not install the otherwise required insulation or to install it below the heating panel. It also supports further studies into whether increasing the thickness of insulation along a building's perimeter would address Codes Canada's concerns regarding thermal efficiency.

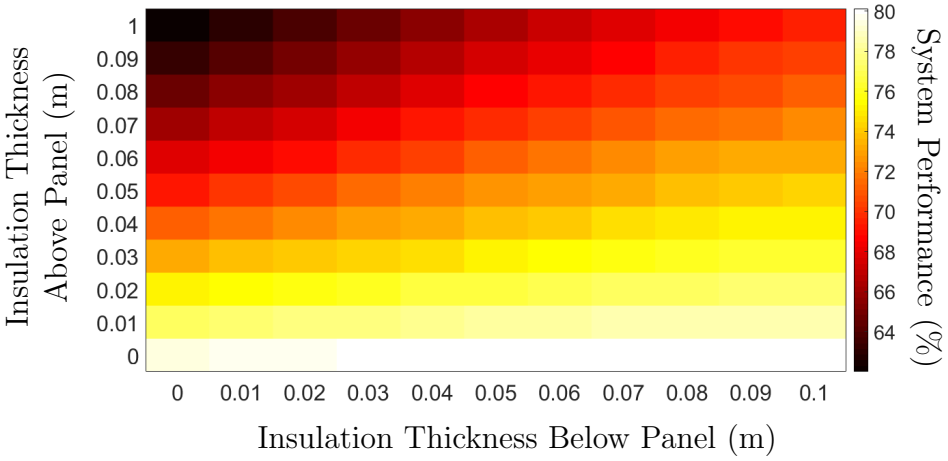

Figure 5.8: Compound Effect of Insulation Above & Below Heating Panel

5.6 Simulink Model Parametric Study: Model Validation

Radiation and h_{tot}

Based on the values from literature presented in Section 5.2, radiative flux (q_{rad}) was expected to represent between 60 and 65% of the total heat transfer from the concrete floor into the heated space (q_{tot}), with one article suggesting it may represent up to 75% [31, 74, 86]. Additionally, the overall heat transfer coefficient from the concrete slab into the heated space (h_{tot}) was expected to be in the range of 8.5 to 10.5 W/m^{2}K [31, 74, 86], with the exception of Seyam [29], who predicted a lower value of roughly 5 W/m^{2}K.

The results from the modified parametric study, representing the broadest range of results available from the Simulink model, are plotted in Figure 5.9. Specifically, the overall performance values are plotted against the radiation fraction ($\frac{q_{rad}}{q_{tot}}$), with the colour of each data point representing the value of h_{tot} (W/m^{2}K).

As demonstrated in Figure 5.9, the vast majority of data points have a radiation fraction value between 63 and 66% (0.63 and 0.66), with most being within the expected range of 60 and 65%. The highest radiation fraction values are from the simulations with the lowest h_c values, altered by the "Air_Convection" variable in the parametric study. A low h_c value would

decrease the heat transferred into the heated space by convection, increasing the temperature difference between the concrete slab and the ceiling above, increasing the radiative heat flux. Based on the relatively low value of h_{tot} of these simulations, it would appear this trade-off is detrimental to the system's performance. Similarly, the lowest radiation fraction values are from simulations with the highest h_c values. Unlike its counterpart, this trade-off appears to be beneficial for the system's performance as the data points with the lowest radiation fraction values have some of the highest h_{tot} values. This relationship between h_c at the concrete slab surface and the system's performance will be discussed further in 5.7.

Regarding h_{tot}, the average value of the data from the modified parametric study was 8.3 W/m^{2}K. This value was slightly below the expected range of 8.5 to 10.5 W/m^{2}K. Given the deviation of just 0.2 W/m^{2}K from the lower bound of the expected range, this was not particularly concerning. However, a low h_{tot} value suggests the presented system performance values may be artificially low.

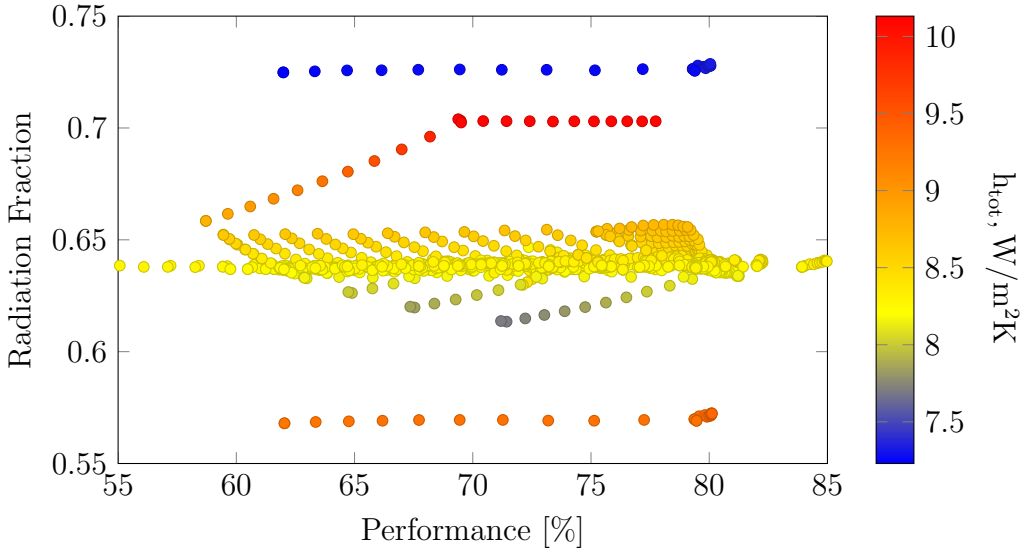

Figure 5.9: Simulink Model Results –
Performance and Radiation Fraction vs. h_{tot}

5.7 Simulink Model Parametric Study: Discussion

5.7.1 Modified Parametric Study

The modified parametric study focused on the primary objective of this research:

> "To examine the long-term transient performance of ThermaRay's ESS both with and without the currently required insulation between the concrete slab and unaltered soil below to support Code

Canada's decision as to whether such an exemption should be granted."

As such, the variables of interest were 'UpperInsulationThickness' and 'LowerInsulationThickness'. The results for these variables were summarized in Table 5.4 and visualized in Figures 5.4 and 5.5. The results of the modified parametric study indicate the affect of these variables on the system's performance over a variety of system arrangements and states; the scope was narrowed down to a more typical system arrangement and state in the standard parametric study, discussed in the subsequent section.

The results clearly indicate a strong negative correlation between the thickness (and presence) of insulation between the concrete slab and the heating element. This was the expected result, as such insulation would impede the passage of heat from the heating element upwards into the heated space. This was the strongest and most negative correlation found in this research project, with the slope of the line of best fit indicating a 1.5% decrease in system performance for every centimeter (cm) of insulation. This indicates that the insulation required by the NBC, with an RSI value of 1.32 corresponding to 3.8 cm of XPS [12], would decrease the system's performance by 5.5%. This is sigificant and would certainly be detrimental to the economic viability of ThermaRay's ESS in Canada. However, this suggests that if ThermaRay is unable to receive an exemption from the NBC-required insulation to either (a) not include the insulation or (b)

place it below the heating panel, there may still be economically viable opportunities for ThermaRay's ESS in Canada. This could include large industrial warehouses where forced air systems are inefficient due to the frequent use of large bay doors or in jurisdictions with time-of-use rates, as discussed in Section 1.

The relationship between the system's performance and insulation below the heating panel was more difficult to predict. While such insulation could improve performance by forcing more heat to pass upwards into the heated space, the same insulation would decrease the readily available TES region to between the concrete slab surface and the insulation below the heating panel. This would limit the availability of thermal energy storage below the insulation, potentially negatively impacting the system's long-term performance. To clarify, this limited 'availability' of TES due to the insulation is not due to any reduction in the thermal mass of TES materials within the system but the introduction of a thermal barrier between the heat source and the bulk of the thermal mass, which is within the undisturbed soil layer.

As displayed in Figure 5.5, it would appear that the benefit from heat flow from the heating panel being forced upwards by insulation below the heating panel appear to outweigh the cost of reducing the TES region. However, the correlation between insulation thickness (and presence) below the heating panel and the undisturbed soil below is much weaker than that described

above. For every centimeter of insulation placed below the heating panel, the system's performance improved by less than 0.5%, indicating a low sensitivity to performance improvement. If ThermaRay is permitted to include the NBC-required insulation below the heating panel rather than above, this would improve the system's performance by 1.6%. However, the relation does not appear to be infinitely linear; the benefit for system performance decreases for each added unit thickness. A similar pattern was found in the 1D simulations, as discussed in Section 5.1.2. Based on this, and the high cost of insulation, ThermaRay would be best suited to only install the required thickness of insulation below the heating panel. Furthermore, it would be ideal if ThermaRay could be granted permission to instead increase the thickness of insulation along the perimeter of ESS-heated buildings and exclude the currently required insulation across the entire foundation.

5.7.2 Standard Parametric Study

The scope of the standard parametric study (SPS) was more broad, covering the wide array of variables described in Section 4.2.2. The results for the SPS are summarized in Table 5.5 and visualized in Appendix C.3.2. The results for each variable were as follows:

- 'Air_Convection': The relation between the coefficient of convection at the surface of the concrete slab (h_c) and the system performance was first mentioned in Section 5.6, above. Figure 5.9 indicated that an

increase in the fraction of heat transfer from the heated slab surface in the form of convection was beneficial for the system's performance. This was further supported by the results of the SPS, with a weak yet positive linear correlation between h_c and system performance. As h_c increases with surface air velocity, this would suggest ThermaRay's ESS would perform best in buildings with sufficient air flow. This result is displayed in Figure C.25.

- 'Ceiling_R_Value': The relation between the R-value of the building's ceiling and the system's performance was contrary to the expected results. Based on discussions with ThermaRay and literature [33, 87], it was presumed an increase in ceiling R-value would be beneficial to the system's performance. This hypothesis was first mentioned on page 97. However, as visualized in Figure C.26, there was a clear negative correlation between the two variables in the SPS results. This can be explained by the fact that increasing the ceiling's R-value would have a similar impact to installing insulation between the concrete slab and the heating panel; it increases the thermal resistance along the heat's path from the heating panel to the exterior air. While increasing the ceiling's R-value is detrimental to the percentage of heat supplied to the system through the heating panel(s), well insulated buildings are still ideal for reducing the energy consumption and associated costs [87]. As shown in the work of Fontana [33], insulation is particularly important in spaces where the majority of the floor is exposed to the wall and

ceiling. Accordingly, industrial buildings with a significant portion of their floor exposed to the walls and ceiling should be especially attentive to the R-value of their building's envelope when incorporating ESS into the design of the building.

- 'ConcreteSetpoint_Activate': This variable was included to determine the impact of including or excluding the concrete surface temperature in the control of the ESS's heating panel control. The result, plotted in Figure C.27, indicate that the inclusion thereof is beneficial to the system's performance. While ThermaRay's ETS installations to date have included concrete surface temperature based heating panel control, this type of control was not included in the proposed EXN/Aero simulations, as mentioned in Section 3.4.3. This result suggests that the results from the proposed EXN/Aero simulations would then underestimate the system's performance.

- 'ConcreteSurfaceSepoint': With the previously mentioned concrete setpoint heating panel control active, this variable indicates the affect of the concrete slab surface temperature setpoint on the system's performance. The results, shown in Figure C.28, indicate the system performs best with a cooler floor temperature. This can be explained with the Fourier Law (Equation 3.5), which states an increase in temperature difference between two points increases the conduction of heat between the two points. Decreasing the floor surface temperature

increases the difference between its temperature and that of the heating panel, enhancing conduction upwards through the TES region and improving system performance.

- 'ContactResistanceOn' & 'ContactResistanceValue': The results for these two variables are plotted in Figure C.29 and C.30, respectively. They have been grouped here as they are indicators for the same relationship, that between the inclusion of contact resistance within the TES region and system performance. Both suggest a negative yet weak relationship between the inclusion (and significance) of contact resistance between each layer of the TES region and the system's performance. This was expected simply because there are more TES layer interfaces above the heating panel than below. As first mentioned on page 99 (Section 4.2.2), compaction of materials within the TES region could mitigate the impact of contact resistance on the system's performance.

- 'Exterior_Air_Conv': The results from this variable indicate that increasing the coefficient of convection from the exterior of the building's roof into the exterior air is beneficial to the system's performance. Like the results for 'Ceiling_R_Value', this is somewhat counter-intuitive as such an increase would cause an increase in the building's heat load. However, an increase in heat flux from the roof's outward surface would draw more heat up from the heating panel,

leading to an increase in system performance as measured in this research. With a difference in performance values of just 0.2% between the lowest and highest values, this relation is relatively weak, suggesting it does not play a significant part in the system's performance. This is visualized in Figure C.31.

- 'HeaterFraction_Activate' & 'HeaterRampDownTemp_Diff': The results from these variable at first appeared to be an error; enabling the heating panel to have a variable output had absolutely no impact on the system's performance. While this came as a surprise, it made sense upon review of a timeseries of heating panel output. The panel was only active in short bursts to 'top-up' the TES region. The brevity of these bursts speaks to why this variable had no impact on the system's performance. The results from these variables are plotted in Figures C.32 and C.33, respectively.

- 'LowerInsulationThickness': The positive and asymptotic relationship between this variable and the system's performance suggested in the modified parametric study was further revealed in the results of the standard parametric study, as shown in Figure C.34. From a thickness of 0 to 0.04 m (up to 4 cm), insulation below the heating panel was beneficial to the system's performance, which was increased by over 0.5%. However, beyond 0.04 cm (4 cm), further increase in insulation thickness had no significant effect on the system's

performance. This further supports the suggestion that ThermaRay should request permission from Codes Canada to install the required ∼4 cm of XPS insulation below the heating panel rather than above.

- 'LowerIns_Layer': The results from this variable, which changed the depth of insulation installed below the heating panel and are plotted in Figure C.35, indicate this depth does not have a significant impact on the system's performance. However, only interfaces between the heating panel and the upper surface of the 'undisturbed soil' TES were considered. This means a maximum depth of 0.3556 m was included in the study; further increasing the depth of this insulation may have a non-negligible effect on system performance. This indicates the previous suggestion regarding insulation below the heating panel can be appended to with a note that ThermaRay could install insulation at any of the TES interfaces below the heating panel and receive the benefits indicated by the 'LowerInsulationThickness' results.

- 'MaxHeaterTemp': The results from this variable are due to its effect on two temperature gradients, from the heating panel upwards to the exterior air and downwards from the heating panel to the isothermal point at the bottom of the 'undisturbed soil' TES layer. The closer the maximum heating panel temperature to the isothermal temperature at the bottom of the 'undisturbed soil' layer, the more significant the temperature gradient between the heating panel and

the exterior air is compared to that between the heating panel and this isothermal point. This has a slightly positive impact on the system's performance. Considering Figure 5.10, if the maximum heating panel temperature decreased to the isothermal temperature, the only remaining temperature gradient, and therefore the only direction of heat flux, would be between the heating panel and the exterior air. The ratio between the two temperature gradients decreases with an increase in the maximum heating panel temperature, hence the asymptotic nature of the relation.

- 'SimLengthMonths': The default value for this variable was chosen to be one year (12 months) to mitigate the impact of start-up fluctuations on the simulation results. No optimization or sensitivity study was performed. The results from this variable indicate that the system's performance improves over time. This could be due to the long-term establishment of thermal energy storage throughout the TES region, particularly within the 'undisturbed soil' region which is nearly 7 m thick and would thus require a significant length of time to experience a change in temperature. This is further explained by the thermal diffusivity time constant of the 'undisturbed soil' TES region, defined and presented on page 39 (Section 3.3.1). The improvement of the ESS's performance over time is also contrary to the long-term performance of traditional forced-air systems, which can decrease over time from 'wear-and-tear' and the build-up of dust and other blockages

in ducting. This result is good news for ThermaRay, as it suggests their hypothesis that the majority of heat "lost" to the soil beneath an ESS-heated building is eventually recovered and passed into the heated space, particularly in regions distant from the building's perimeter. Further study with a domain of study which represents the undisturbed soil more accurately than a layer of soil with an isothermal surface at its full depth would be required to further test this hypothesis.

- 'SimTimeStepMinutes': The length of the simulation's time step had little to no impact on the simulation's results for the Simulink model, as shown in Figure C.38. Varying the time step length from 5 to 20 minutes had a 0.05% impact on the system's performance. The difference in performance value between 10 and 15 minutes is less than that between either 5 to 10 minutes or 15 to 20 minutes. This suggests values in the 10 to 15 minute range minimize the impact of the time step on the system's performance, supporting the selection of 10 minutes as the default time step length.

- 'Soil_Temp_Full_Depth': This is yet another variable whose results are aligned with the expectations set out by Fourier's Law (Equation 3.5). Decreasing the isothermal temperature at the bottom-most point of the 'undisturbed soil' layer renders the temperature gradient between it and the heating panel more steep. This increases the conductive heat flux downwards from the panel, decreasing system performance.

This suggests that ThermaRay's ESS would be best suited for locations with a large seasonal temperature variance. In such an environment the hot summers would raise the soil temperature, increasing the ESS's performance in the winter, while the cold winter air temperatures would provide a steep temperature gradient between the heating panels and the exterior air during the heating season. This result also supports ThermaRay's hypothesis that the majority of heat "lost" to the soil beneath an ESS-heated building is eventually recovered or otherwise contributes to the system's long-term performance.

- 'UpperInsulationThickness': As in the results from the MPS, the results of the SPS indicate a strong negative correlation between the thickness (and presence) of insulation installed between the concrete slab and the heating panel. Moreover, the SPS indicates an even stronger negative correlation than its more broad predecessor. For every centimeter (cm) of insulation, the system's performance fell by roughly 1.75%, a relationship 20% stronger than that found through the MPS. This further supports the importance of ThermaRay receiving permission from Codes Canada to either exclude insulation from its TES region (other than along the perimeter of a building) or to instead install the required insulation below the heating panel.

This concludes the discussion of the results from the parametric studies. Recommendations drawn from these results are provided in Chapter 6.

5.8 EXN/Aero Simulations: Results

Two simulations were performed and their results presented here to demonstrate the first two simulations described in Section 4.3. The third simulation was not completed to its prescribed length; however, results from the culmination of the second simulation indicate that the set of simulations would provide a system performance value within the range of values obtained through the parametric studies detailed in Section 4.2.3.

First Simulation (Initialization)

The smooth temperature gradient established by this simulation is demonstrated in Figure 5.10. The simple yet essential objective of using an effective thermal conductivity value, as presented in Section 3.3.4, was achieved. The final temperature field of the first simulation was used as the initial temperature field for the second simulation.

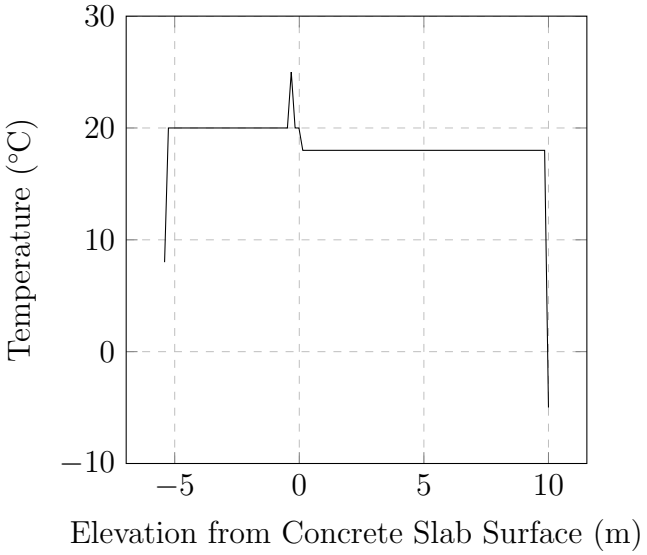

(a) Initial Temperature Distribution

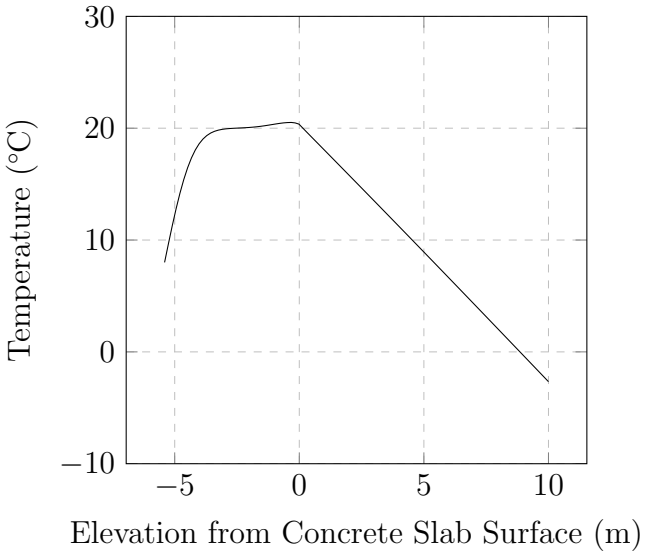

(b) Final Temperature Distribution

Figure 5.10: Temperature Distributions - Stage 1

Second Simulation (Buoyancy & Turbulence)

The buoyancy field produced by this simulation with the settings provided is displayed in Figures 5.11 and 5.12. As mentioned in Section 4.3, these figures were produced from simulations ran with EXN/Aero's κ-ω turbulence model. To consider the effect of turbulence model selection on the simulation's outputs, EXN/Aero's κ-ω SST turbulence model was tested as well, the buoyancy fields from which are provided in Figures 5.13 and 5.14. The expectation was that the κ-ω SST model would out-perform its predecessor, the κ-ω turbulence model [75].

Based on existing literature, the formation of a single Rayleigh-Bénard convection cell spanning the height of the heated space was expected given the high Rayleigh Number [95]. Without outside influence or sudden blockage, these cells typically space the entire vertical column of a fluid. It was then surprising to find two Rayleigh-Bénard convection cells in the velocity field produced by the κ-ω SST turbulence model, while the κ-ω model produced the expected single cell.

The κ-ω turbulence model led to the development of a single Rayleigh-Bénard convection cell, as expected from literature [95] and displayed in Figures 5.11 and 5.12. Air in the heated space moves through the cell based on these steps, starting from the top of the heated space:

1. Warm air, rising from the heated slab below along the left of the figures, encounters the cool ceiling.
2. Cooling as it passed along the ceiling from left to right of the figures, and therefore becoming more dense, the air begins to descend.
3. Air continues to accelerate downwards until it is impeded by the concrete floor.
4. Passing over the warm concrete floor from right to left, air begins to warm and become lighter.
5. Upon reaching a critical point near the bottom left of the heated space in Figure 5.11, the warmed air begins to rise.
6. Warmed air continues to rise until it is impeded by the ceiling, and the cycle continues.

It was noted in the discussion of results from the parametric studies that improving convection at the floor surface was notably beneficial to the system's performance. As noted in literature, the establishment of Rayleigh-Bénard convection cells boosts convection into the heated space, improving system performance [75,95]. This further supports the importance of accurately modelling turbulent, buoyancy-driven flow within the heated space when using CFD-CHT to assess the performance of radiant heat systems.

While further study into the formation of Rayleigh-Bénard convection cells above radiant floors would be beneficial to our understanding of radiant heating system's thermodynamic behaviour, this was not the study's purpose. As such, the model which produced a single Rayleigh-Bénard convection cell was selected for the set of simulations proposed in this research.

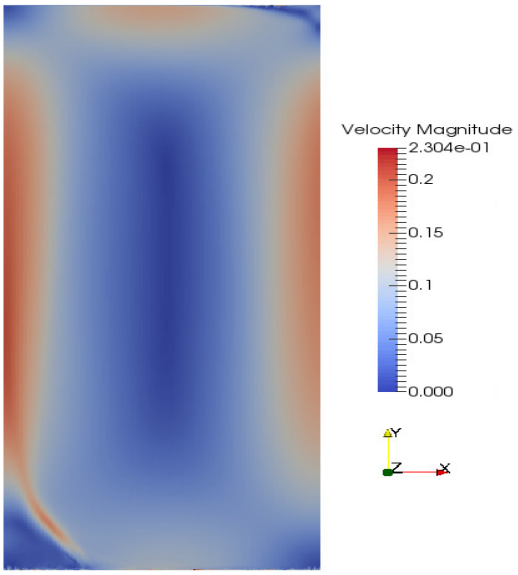

Figure 5.11: Buoyancy Field: Velocity Magnitude (κ-ω)

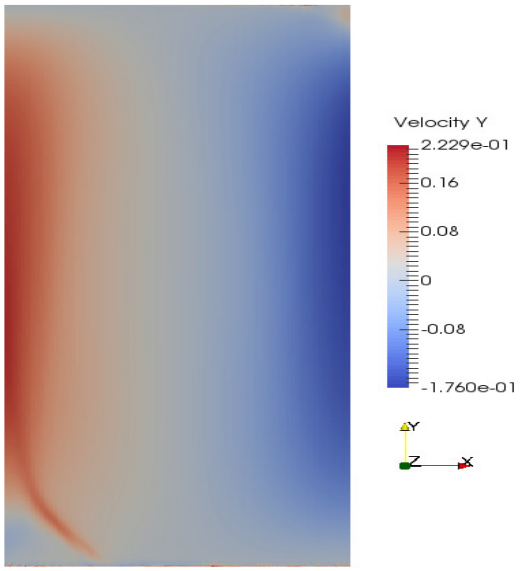

Figure 5.12: Buoyancy Field: Velocity in Y (Vertical, κ-ω)

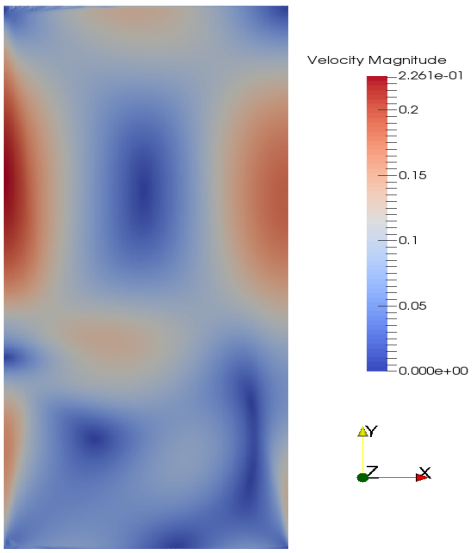

Figure 5.13: Buoyancy Field: Velocity Magnitude (κ-ω SST)

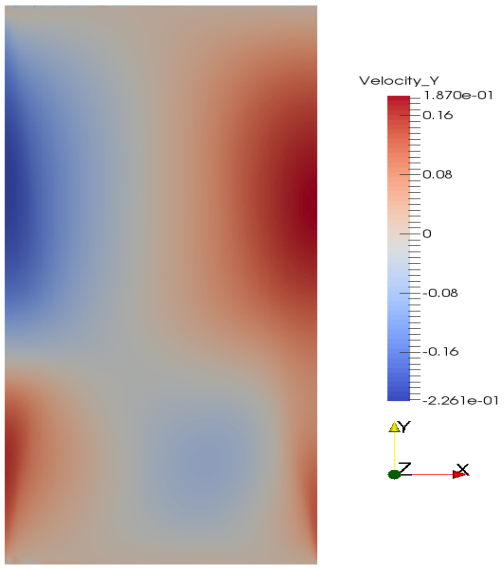

Figure 5.14: Buoyancy Field: Velocity in Y (Vertical, κ-ω SST)

Third Simulation: Complete CFD/CHT

The purpose of this simulation was to address the research's primary objective by studying how ThermaRay's ESS performs on a long-term, transient basis with all forms of heat transfer considered. The previous simulations established the temperature field within the TES region and both the temperature and velocity fields within the heated space. During this simulation, the system's performance over up to two months is simulated with the velocity field 'frozen' and the heating panel cycling on a 24 hour basis. Unfortunately, due to unforeseen circumstances, a complete final simulation was not performed during this project. However, the third presribed simulation was run for a duration sufficiently long for three 24-hour cycles to take place. Figures 5.15 and 5.16 are from the first 'on' and 'off' portions of the first cycle, respectively. They demonstrate that the transient heater control was functional and its impact on the temperature field immediately surrounding the heating panel. A portion of the Rayleigh-Bénard convection cell formed during the second simulation (described in the preceding section) is faintly visible near the concrete-air interface above the leftmost edge of the heating panel in both figures.

This duration was not sufficient for the system to achieve a reasonably steady state for evaluation using the EXN/Aero-specific performance method prescribed in Sectin 3.5. While formal system performance evaluation was not feasible, the same informal method for performance evaluation used

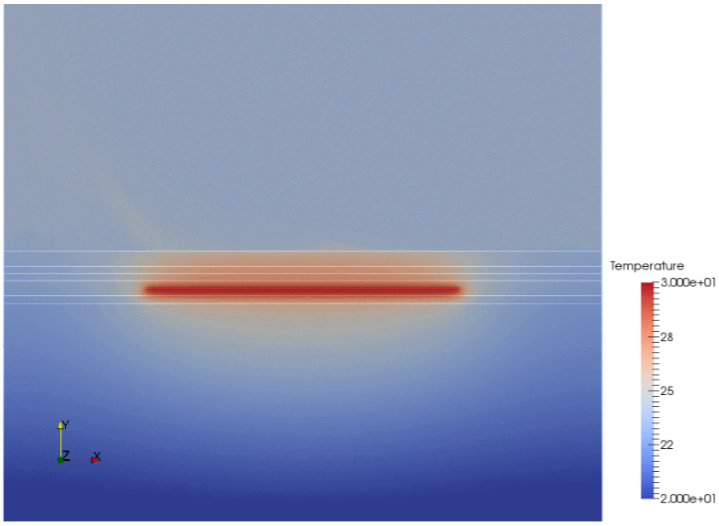

Figure 5.15: Transient Heating Control Demonstration - 'On'

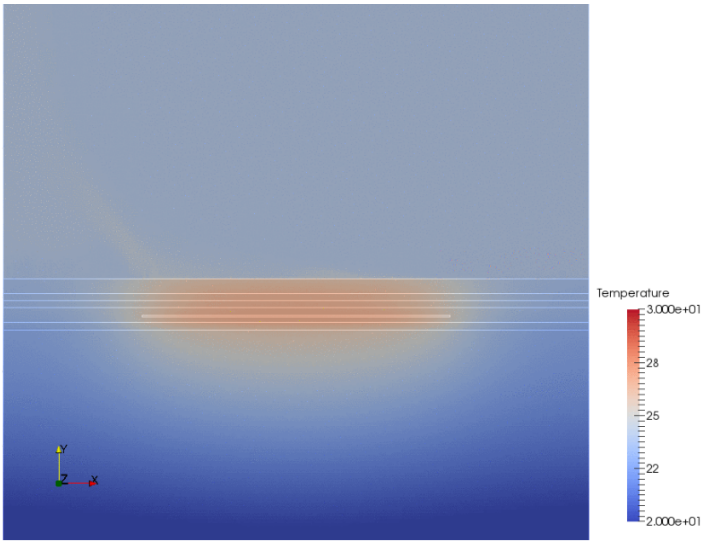

Figure 5.16: Transient Heating Control Demonstration - 'Off'

during the mesh optimization process (refer to Section 4.3.2) was used at the outset of the third simulation. This method, based on the percentage of heat transfer leaving the 'sand layer' passing upwards (see Equation 4.4),

indicated 84% of heat flow from the 'sand' layer of the TES region was passing upwards at the outset of the third simulation. This is within the range of values found during the parametric studies, albeit higher than the majority of performance values obtained in the majority of parametric study simulations.

5.9 EXN/Aero Simulations: Discussion

While a complete set of the proposed simulations was not performed, results from instances of the first two simulations indicate that all capabilities of EXN/Aero to study ThermaRay's ESS that were tested and validated for this research performed as expected. As the final simulation's settings are essentially a mixture of those from the previous two simulations, it is expected that a set of simulations as described in Section 4.3 could be completed without issue.

Chapter 6

Conclusions

Three models have been created for the purpose of long-term transient analysis of ThermaRay's ESS. A quasi-1D model was built in EXN/Aero to verify an existing Excel-based model and test EXN/Aero's CHT modelling capabilities. Upon the successful completion of this first stage of the research, the testing of EXN/Aero's full suite of CFD-CHT modelling capabilities began. This included conjugate heat transfer at the concrete slab surface, modelling buoyancy, turbulence, and radiation within the heated space, transient control of the heating panel, and contact resistance between the TES layers. A set of three simulations to be run in EXN/Aero was then developed and tested. These simulations would first establish a smooth temperature gradient across the computational domain from which the buoyancy model could be launched to establish the velocity field within the heated space. In the final simulation, the buoyancy-driven velocity field was 'frozen' and the heating panel cycling based on a 24-hour cycle. The set of three EXN/Aero simulations was demonstrated, indicating the model was ready to perform long-term transient assessments of ThermaRay's ESS.

A third model, produced in Simulink, was built due to the rather high computation demand of the proposed simulations to allow for a variety of parameters to be tested much faster than if the same testing was to be done with the proposed set of EXN/Aero simulations. Two sets of parametric studies, one focused on the NBC-mandated sub-slab insulation and one focused on other variables of interest to ThermaRay, were conducted using the Simulink model. Results were validated based on values from literature and have been used to formulate the observations, recommendations, and conclusions below.

A few key observations were made from the results of these models:

- First and foremost, results from the quasi-1D model and both parametric studies conducted with the Simulink model showed that insulation below the heating panel improves the system's performance, up to a thickness of 4 centimetres. Results from the parametric studies also indicated insulation between the concrete slab and heating panel was severely detrimental to the system's performance, whether insulation was also installed beneath the heating panel or not.

- Contrary to expectations, increasing the total R-value of the building's ceiling/roof assembly had a negative impact on the system's performance, albeit less severe than installing insulation between the concrete slab and the heating panel. This was due to the manner in which the system's performance was calculated in this research; well-

insulated buildings are still ideal for radiant heat systems to reduce heat losses. A system performance evaluation approach that is instead focused on the amount of heat required to meet an occupant-set temperature setpoint would more accurately portray the effect of ceiling R-value on the system's performance.

- The parametric studies, particularly the SPS, clearly indicated the system's performance improves over time. This behaviour is unlike most conventional heating systems, which usually degrade with time. This supports ThermaRay's belief that the majority of heat "lost" to the soil beneath a building (beyond the 7 m included in the computational domain used in this research) is eventually recovered or at least contributes to the system's long-term performance. The sole remaining significant cause of heat loss beneath the heated concrete slab would be through the perimeter of the building's foundation.

- Improving convection from the concrete slab surface was found to be more beneficial than increasing the radiative flux, suggesting that ground-level air flow is important for the thermal performance of sub-grade radiant heat systems and for accurately modelling these systems. The Rayleigh-Bénard convection that developed during the second of the three EXN/Aero simulations proposed in this research plays an important part in this modelling as it significantly increases convection at the floor surface.

- While the minimum concrete surface temperature recorded during the majority of Simulink simulations was within roughly 1.1 °C of the setpoint temperature, as per the transient heating panel control algorithm, that same algorithm could be detrimental to occupant comfort under certain circumstances. Prohibiting the heating panel from providing heat to the system for half of any given 24-hour period, to replicate system control in a jurisdiction with time-of-use electricity rates, made it possible for the concrete surface temperature to fall well below the setpoint temperature. This was one of the contributing factors which led 21 of the 1968 simulations performed for the two parametric studies to experience concrete slab surface temperatures below 15 °C.

These observations come at the end of a two year research project during which numerous obstacles and unforeseen changes to the scope were encountered. Some of these challenges included, in no particular order:

- Acquisition of the necessary data was difficult. The pursuit of thermal property data for the TES layers and soil temperature data down to an isothermal point for a Canadian location was particularly arduous. The sources found for this data span several decades and continents, leading to uncertainty regarding the impact of using the data in a single system on the accuracy of the models' results.
- This being the first industry-partnered application for several of these

capabilities and the on-going nature of EXN/Aero's development added to this research's level of difficulty and the uncertainty as to the appropriate scope of the research. This led to the continual adjustment of the research's scope.

- The fact that this was the first industry-partnered application of EXN/Aero's full suite of CFD-CHT capabilties also contributed to uncertainty regarding the computational resources required to perform full-scale, long-term, transient simulations modelling ThermaRay's ESS in EXN/Aero. This led to the development of the Simulink model when it became clear that a thorough parametric study using a full-scale model would not be feasible with EXN/Aero. The Simulink model and its parametric studies were not within the original scope of the project, yet they became a significant source of results for the research presented here.

The following recommendations have been drawn from the above observations and challenges, and from relevant findings in existing literature:

- Prior to further in-depth study of ThermaRay's ESS, more reliable and recent data should be acquired, ideally with all data originating from the same location. On that topic, ThermaRay has installed a number of sensors in an ETS installation site in Quebec. While data from this site is expected to include heat fluxes and temperature from throughout the system, the precise nature of this data is unknown and the data was

unavailable upon the project's completion. This inhibited definitive calculation of the models' accuracy.

- Further study should include more accurate representation of the lower limit of the "undisturbed soil" layer, which was treated in this research as an isothermal surface. As the parametric studies indicated the system's performance improves over time, studying the multi-year evolution of the temperature field at depths greater than 5 meters below the concrete slab would be necessary to definitively quantify thermal losses beneath the concrete slab and within the foundation's perimeter.

- While this research focused on the effect of various parameters on the system's long-term performance in terms of energy "lost" to the soil beneath an ESS-heated building, future studies could instead focus on the effect thereof on the system's thermal response. This would provide a stronger understanding of the benefits of the system's thermal mass and its relationship with other system parameters, including the inclusion of sub-grade insulation.

- Variations in the thickness and composition of each TES layer should be studied, including insulation materials other than XPS (within any limitations set by the NBC) to optimize the design of the TES region. Similarly, the effect of varying the thickness of sub-grade perimeter should be studied, which would require a significantly larger computational domain.

- Further study should be performed into the thermal inertia of the ESS and each of its TES layers, including the insulation. This would inform further development of the system and other radiant heating and cooling systems, providing a clearer picture of the contribution of thermal mass and inertia to system performance. The addition of a cost function with and without TOU rates to this analysis would be expected to further indicate the benefits of the system's thermal mass and inertia.

- ThermaRay should permit heating panel activation during periods when heating panels would otherwise be off due to the time-of-use based control if the concrete slab temperature reaches a preset temperature. This would address the aforementioned concern regarding the floor temperature decreasing beyond the bounds of occupant comfort during designated 'off' periods.

- Buoyancy modelling, or an otherwise more accurate model of convection through the heated space, should be added to the Simulink model to provide a more accurate yet computationally efficient means of thoroughly studying the ESS's performance.

- Studying the affect of different k_{eff} values, as calculated in Section 3.3.4, on the results of the first full-scale EXN/Aero would be beneficial for the continued development of EXN/Aero's CFD-CHT capabilities and of the proposed EXN/Aero simulations.

- Soil temperature data from various locations throughout Canada should be considered in any future studies of ThermaRay's ESS as the parametric studies performed here indicated it is a factor impacting the system's performance. This should include one location from each of the climate zones included in the NBC.

- A system performance evaluation approach that is instead focused on the amount of heat required to meet an occupant-set temperature setpoint would more accurately portray the effect of ceiling R-value on the system's performance. Such an evaluation approach would be recommended for any further studies of ThermaRay's ESS and other radiant heat systems with significant thermal mass.

- Model predictive control (MPC) and the integration of a PI controller (and other continuous control approaches) should be studied as a potential means to improve the ESS's performance, as indicated in literature [24, 41–47]. While more complex control approaches should be considered and studied, fluctuations in the concrete surface in Simulink simulations using the discrete control approach currently used by ThermaRay had over-shoots of less than one degree (1 °C), a reasonably small value given the simplicity of the control approach.

- ThermaRay should request one of two permissions from Codes Canada:

  - That ThermaRay be permitted to install the required insulation beneath the heating panels in their ESS. This would improve the

system's thermal performance as the original regulation intented, rather than being detrimental to the system's performance, or

  - That ThermaRay be permitted to exclude the sub-slab insulation that is otherwise required for heated slabs on the grounds that its inclusion would be detrimental to the system's performance, in contrast with the regulation's intentions.

- Future studies should focus more directly on the comparison between ThermaRay's ESS and traditional hydronic systems to get to the heart of Codes Canada's concerns regarding the ESS. This would likely necessitate the parallel development of a whole-building, full-scale model of both types of systems.

In conclusion, this research project accomplished what it set out to achieve in its primary objctive. It also contributed to the existing knowledge base in the field of radiant system modelling and facilitated future analyses of ThermaRay's ESS. The affect of insulation at various depths and thicknesses installed across the footprint of a building heated by ThermaRay's ESS was studied through the development and utilization of three models and two sets of parametric studies. Furthermore, a full-scale model of a typical installation of ThermaRay's ESS in an industrial building was produced. Finally, a set of simulations that together allow for the long-term, transient performance of the system to be analyzed under a wide variety of circumstances. This will allow for more in-depth assessment of ThermaRay's ESS and other radiant

systems to be performed in the future.

Bibliography

[1] ThermaRay Inc., "ThermaRay - Electric Radiant Heating Systems," 2018.

[2] J. Yap and R. Circ, *Guide to Classifying Industrial Property.* Urban Land Institute, 2nd ed., 2003.

[3] G. Williams and L. Gold, "Ground Temperatures," tech. rep., Division of Building Research, National Research Council Canada, Ottawa, ON, 1976.

[4] ThermaRay Inc., "ThermaRay Earth Storage System: Installation Guide," 2017.

[5] Departments of the U.S. Army and the Air Force, "Concrete Floor Slabs on Grade Subjected to Heavy Loads," tech. rep., Washington, DC, 1987.

[6] The Engineering Toolbox, "Concrete Slab Thickness," 2009.

[7] E. Kuznetsova, "Properties of the crushed rocks used as frost protection layer of the Norwgian roads: field and laboratory investigations," tech. rep., Norwgian University of Science and Technology, Trondheim, Norway, 2014.

[8] M. S. Kersten, "Thermal properties of soils," *Engineering Experiment Station Bulletins*, vol. 52, no. 21, 1949.

[9] I. Hamdhan and B. Clarke, "Determination of thermal conductivity of coarse and fine sand soils," in *Proceedings of World Geothermal ...*, 2010.

[10] M. N. Alban, "Literature Study on Radiant Heating in a Thermally Comfortable Indoor Environment: A Summary Report," tech. rep., KU Leuven, Leuven, Belgium, 2010.

[11] Canadian Commision on Building and Fire Codes, "National Building Code of Canada - Section 9.36.2.7," 2010.

[12] Codes Canada, "National Building Code of Canada," tech. rep., National Research Council Canada, 2015.

[13] M. Tahersima, P. Tikalsky, and R. Revankar, "An experimental study on using a mass radiant floor with geothermal system as thermal battery of the building," *Building and Environment*, vol. 133, pp. 8–18, apr 2018.

[14] G. Henze, C. Felsmann, D. Kalz, and S. Herkel, "Primary energy and comfort performance of ventilation assisted therm-active building system in continental climates," *Energy and Buildings*, vol. 40, no. 2, pp. 99–111, 2008.

[15] K.-N. Rhee and K. W. Kim, "A 50 year review of basic and applied research in radiant heating and cooling systems for the built environment," *Building and Environment*, vol. 91, pp. 166–190, 2015.

[16] M. Bojić, D. Cvetković, V. Marjanović, M. Blagojević, and Z. Djordjević, "Performances of low temperature radiant heating systems," *Energy and Buildings*, vol. 61, pp. 233–238, 2013.

[17] J. Babiak, *REHVA Guidebook No. 7 - Low temperature heating and high temperature cooling*. 2007.

[18] C. Karmann, S. Schiavon, and F. Bauman, "Thermal comfort in buildings using radiant vs. all-air systems: A critical literature review," *Building and Environment*, vol. 111, pp. 123–131, 2017.

[19] T. Imanari, T. Omori, and K. Bogaki, "Thermal comfort and energy consumption of the radiant ceiling panel system.: Comparison with the conventional all-air system," *Energy and Buildings*, vol. 30, no. 2, pp. 167–175, 1999.

[20] D. Olsthoorn, F. Haghighat, A. Moreau, and G. Lacroix, "Abilities and limitations of thermal mass activation for thermal comfort, peak shifting and shaving: A review," *Building and Environment*, vol. 118, pp. 113–127, 2017.

[21] J. Le Dréau and P. Heiselberg, "Energy flexibility of residential buildings using short term heat storage in the thermal mass," *Energy*,

vol. 111, pp. 991–1002, 2016.

[22] P. Chuangchid and M. Krarti, "Foundation heat loss from heated concrete slab-on-grade floors," *Building and Environment*, vol. 36, no. 5, pp. 637–655, 2001.

[23] D. Wang, Y. Liu, Y. Wang, and J. Liu, "Numerical and experimental analysis of floor heat storage and release during an intermittent in-slab floor heating process," *Applied Thermal Engineering*, vol. 62, no. 2, pp. 398–406, 2014.

[24] G. Zhou and J. He, "Thermal performance of a radiant floor heating system with different heat storage materials and heating pipes," *Applied Energy*, vol. 138, pp. 648–660, 2015.

[25] R. Zeng, X. Wang, W. Xiao, Y. Zhang, Q. Zhang, and H. Di, "Thermal performance of phase change material energy storage floor for active solar water-heating system," *Frontiers of Energy and Power Engineering in China*, vol. 4, no. 2, pp. 185–191, 2010.

[26] M. Tahersima and P. Tikalsky, "Experimental and numerical study on heating performance of the mass and thin concrete radiant floors with ground source systems," *Construction and Building Materials*, vol. 178, pp. 360–371, 2018.

[27] A. Laouadi, "Development of a radiant heating and cooling model for building energy simulation software," *Building and Environment*,

vol. 39, no. 4, pp. 421–431, 2004.

[28] T. L. Ritter and B. Kilkis, "An analytical model for the design of in-slab electric heating panels," (United States), American Society of Heating, Refrigerating and Air-Conditioning Engineers, Inc., Atlanta, GA (United States), 1998.

[29] S. Seyam, A. Huzayyin, H. El-Batsh, and S. Nada, "Experimental and numerical investigation of the radiant panel heating system using scale room model," *Energy and Buildings*, vol. 82, pp. 130–141, 2014.

[30] X. Zheng, Y. Han, H. Zhang, W. Zheng, and D. Kong, "Numerical study on impact of non-heating surface temperature on the heat output of radiant floor heating system," *Energy and Buildings*, vol. 155, pp. 198–206, 2017.

[31] T. Cholewa, M. Rosiński, Z. Spik, M. R. Dudzińska, and A. Siuta-Olcha, "On the heat transfer coefficients between heated/cooled radiant floor and room," *Energy and Buildings*, vol. 66, pp. 599–606, 2013.

[32] X. Wu, J. Zhao, B. W. Olesen, L. Fang, and F. Wang, "A new simplified model to calculate surface temperature and heat transfer of radiant floor heating and cooling systems," *Energy and Buildings*, vol. 105, pp. 285–293, 2015.

[33] L. Fontana, "Thermal performance of radiant heating floors in furnished enclosed spaces," *Applied Thermal Engineering*, vol. 31,

no. 10, pp. 1547–1555, 2011.

[34] T. Cholewa, R. Anasiewicz, A. Siuta-Olcha, and M. A. Skwarczynski, "On the heat transfer coefficients between heated/cooled radiant ceiling and room," *Applied Thermal Engineering*, vol. 117, pp. 76–84, 2017.

[35] R. Li, T. Yoshidomi, R. Ooka, and B. W. Olesen, "Field evaluation of performance of radiant heating/cooling ceiling panel system," *Energy and Buildings*, vol. 86, pp. 58–65, 2015.

[36] M. Corcione, L. Fontana, and G. Moncada Lo Giudice, *Riscaldamento a pavimento radiante. Uno studio teorico sul comportamento termico*, vol. 3. jan 2001.

[37] M. Corcione, L. Fontana, and G. Moncada Lo Giudice, "A parametric analysis on the effects of furnishings upon the performance of radiant floor-panel heating systems," in *Proceedings of the 7th REHVA World Congress and Clima 2000 Naples 2001 Conference*, (Naples, IT), pp. 59–68, CLIMA 2000, sep 2001.

[38] Y. Luo, L. Zhang, Z. Liu, Y. Wang, F. Meng, and L. Xie, "Modeling of the surface temperature field of a thermoelectric radiant ceiling panel system," *Applied Energy*, vol. 162, pp. 675–686, 2016.

[39] Y. Luo, L. Zhang, Z. Liu, J. Wu, Y. Zhang, and Z. Wu, "Three dimensional temperature field of thermoelectric radiant panel system:

Analytical modeling and experimental validation," *International Journal of Heat and Mass Transfer*, vol. 114, pp. 169–186, 2017.

[40] Y. Luo, L. Zhang, Z. Liu, Y. Wang, J. Wu, and X. Wang, "Dynamic heat transfer modeling and parametric study of thermoelectric radiant cooling and heating panel system," *Energy Conversion and Management*, vol. 124, pp. 504–516, 2016.

[41] S. Li, J. Joe, J. Hu, and P. Karava, "System identification and model-predictive control of office buildings with integrated photovoltaic-thermal collectors, radiant floor heating and active thermal storage," *Solar Energy*, vol. 113, pp. 139–157, 2015.

[42] A. Afram and F. Janabi-Sharifi, "Theory and applications of HVAC control systems A review of model predictive control (MPC)," *Building and Environment*, vol. 72, pp. 343–355, 2014.

[43] J. Široký, F. Oldewurtel, J. Cigler, and S. Prívara, "Experimental analysis of model predictive control for an energy efficient building heating system," *Applied Energy*, vol. 88, no. 9, pp. 3079–3087, 2011.

[44] Y. Yu, V. Loftness, and D. Yu, "Multi-structural fast nonlinear model-based predictive control ofahydronic heating system," *Building and Environment*, vol. 69, pp. 131–148, 2013.

[45] J. Romaní, L. F. Cabeza, and A. de Gracia, "Development and experimental validation of a transient 2D numeric model for radiant

walls," *Renewable Energy*, vol. 115, pp. 859–870, 2018.

[46] T. H. Pedersen, R. E. Hedegaard, K. F. Kristensen, B. Gadgaard, and S. Petersen, "The effect of including hydronic radiator dynamics in model predictive control of space heating," *Energy and Buildings*, vol. 183, pp. 772–784, 2019.

[47] H. Tang, P. Raftery, X. Liu, S. Schiavon, J. Woolley, and F. S. Bauman, "Performance analysis of pulsed flow control method for radiant slab system," *Building and Environment*, vol. 127, pp. 107–119, 2018.

[48] H. Eure, "Improving HVAC With PID and VFDs," 2008.

[49] A. Joseph, J. Thomson, H. Ajlani, and M. Barrett, "1-Dimensional Thermal Model for Radiant Panel Applications: Final Report," tech. rep., Nova Scotia Community College, 2017.

[50] G. D. Raithby, "Discussion of the finite-volume method for radiation, and its application using 3d unstructured meshes," *Numerical Heat Transfer, Part B: Fundamentals*, vol. 35, no. 4, pp. 389–405, 1999.

[51] MathWorks, "What is MATLAB?," 2019.

[52] MathWorks, "Simulink," 2019.

[53] A. Gerber, K. Wilcox, and J. Zhang, "Benchmarking of a Massively Parallel Hybrid CFD Solver for Ocean Applications," in *Proceedings*

of the ASME 2013 32nd International Conference on Ocean, Offshore, and Arctic Engineering, (Nantes, France), ASME, 2013.

[54] L. Careto, A. Gosman, S. Patankar, and D. Spalding, "Two calculation procedures for steady, three-dimensional flow with recirculation," in *Proceedings of the 3rd International Conference on Numerical Methods in Fluid Dynamics*, (Paris), 1972.

[55] F. Motasemi and A. G. Gerber, "Multicomponent conjugate heat and mass transfer in biomass materials during microwave pyrolysis for biofuel production," *Fuel*, vol. 211, no. March 2017, pp. 649–660, 2018.

[56] F. Incropera, D. DeWitt, T. Bergman, and A. Lavine, *Fundamentals of Heat and Mass Transfer*. Wiley, 2006.

[57] American Society of Heating Refrigeration and Air Conditioning Engineers (ASHRAE), "ANSI/ASHRAE Standard 62.1-2013 Ventilation for acceptable indoor air quality," 2013.

[58] H. B. Awbi, H. B. Awbi, A. Hatton, and A. Hatton, "Natural convection from heated room surfaces," *Energy and Buildings*, vol. 30, pp. 233–244, 1999.

[59] T. Min, L. Schutrum, G. Parmelee, and J. Vouris, "Natural Convection and Radiation in a Panel Heated Room," tech. rep., Heating Piping and Air Conditioning (HPAC), 1956.

[60] A. Koca, Z. Gemici, Y. Topacoglu, G. Cetin, R. C. Acet, and B. B. Kanbur, "Experimental investigation of heat transfer coefficients between hydronic radiant heated wall and room," *Energy and Buildings*, vol. 82, pp. 211–221, 2014.

[61] M. De Carli, M. Scarpa, R. Tomasi, and A. Zarrella, "DIGITHON: A numerical model for the thermal balance of rooms equipped with radiant systems," *Building and Environment*, vol. 57, pp. 126–144, 2012.

[62] D. D. Gray and A. Giorgini, "The validity of the boussinesq approximation for liquids and gases," *International Journal of Heat and Mass Transfer*, vol. 19, no. 5, pp. 545–551, 1976.

[63] COMSOL Inc., "The Boussinesq Approximation," 2017.

[64] R. Doyle, T. L. Jeans, A. G. L. Holloway, and D. Fieger, "URANS simulations of an axisymmetric submarine hull undergoing dynamic sway," *Ocean Engineering*, vol. 172, pp. 155–169, 2019.

[65] M. C. Bettle, A. G. Gerber, and G. D. Watt, "Unsteady analysis of the six DOF motion of a buoyantly rising submarine," *Computers & Fluids*, vol. 38, no. 9, pp. 1833–1849, 2009.

[66] "HVAC Analysis of an Operating Room," 2019.

[67] A. Lockwood, "CFD in the Cloud," 2018.

[68] V. Panjkovic and J. Truelove, "Computational Fluid Dynamics Modelling of Iron Flow and Heat Transfer in the Iron Blast Furnace Hearth," in *Second International Conference on CFD in the Minerals and Process Industries*, (Melbourne, Australia), 1999.

[69] Q. Chen and W. Xu, "Simplified Method for Indoor Airflow Simulation," in *Proceedings of CLIMA 2000 World Congress*, (Brussels, Belgium), 2000.

[70] N. A. M. Amin, F. Bruno, and M. Belusko, "Effective thermal conductivity for melting in PCM encapsulated in a sphere," *Applied Energy*, vol. 122, pp. 280–287, 2014.

[71] H. Taheri, F. Schmidt, and M. Gabi, "Numerical Investivation of Effective Heat Conductivity of Fluid in Charging Process of Thermal Storage Tank," *Open Jounral of Fluid Dynamics*, vol. 5, no. 1, p. 12, 2015.

[72] K. A. Brucker and J. Majdalani, "Effective thermal conductivity of common geometric shapes," *International Journal of Heat and Mass Transfer*, vol. 48, no. 23-24, pp. 4779–4796, 2005.

[73] J. Holman, *Heat Transfer*. New York, NY: McGraw-Hill, 10th ed., 2010.

[74] O. Acikgoz, "A novel evaluation regarding the influence of surface emissivity on radiative and total heat transfer coefficients in radiant

heating systems by means of theoretical and numerical methods," *Energy and Buildings*, vol. 102, pp. 105–116, 2015.

[75] X. Li and J. Tu, "Evaluation of the eddy viscosity turbulence models for the simulation of convectionradiation coupled heat transfer in indoor environment," *Energy and Buildings*, vol. 184, pp. 8–18, 2019.

[76] S. H. Kim and K. Y. Huh, "Assessment of the finite-volume method and the discrete ordinate method for radiative heat transfer in a three-dimensional rectangular enclosure," *Numerical Heat Transfer, Part B: Fundamentals*, vol. 35, no. 1, pp. 85–112, 1999.

[77] P. Hassanzadeh and G. D. Raithby, "Finite-volume solution of the second-order radiative transfer equation: Accuracy and solution cost," *Numerical Heat Transfer, Part B: Fundamentals*, vol. 53, no. 4, pp. 374–382, 2008.

[78] J. Y. Murthy and S. R. Mathur, "Computational Heat Transfer in Complex Systems: A Review of Needs and Opportunities," *Journal of Heat Transfer*, vol. 134, no. 3, p. 031016, 2012.

[79] X. Li, Y. Yan, and J. Tu, "Evaluation of models and methods to simulate thermal radiation in indoor spaces," *Building and Environment*, vol. 144, no. August, pp. 259–267, 2018.

[80] K.-B. Cheong and T.-H. Song, "Examination of Solution Methods for the Second-Order Discrete Ordinate Formulation," *Numerical Heat*

Transfer, vol. 27, no. 2, pp. 155–173, 1995.

[81] International Organization for Standardization, "Thermal insulation Heat transfer by radiation Physical quantities and definitions," 1989.

[82] G. Mittal, H. Lapp, and J. Townsend, "Feasibility of Drying Wheat with Various Solid Heat Transfer Media," *Journal of Canadian Agricultural Engineering*, vol. 27, pp. 121–125, 1985.

[83] Mikron Instrument Company, "Table of Emissivity of Various Surfaces," 2019.

[84] F. Rowley, A. Algren, and J. Blackshaw, "Surface Conductances as Affected by Air Velocity, Temperature, and Character of Surface," *ASHVE Transcript*, vol. 36, p. 429, 1930.

[85] WindFinder, "Ottawa Airport," 2019.

[86] O. Acikgoz, Y. Karakoyun, Z. Yumurtac, N. Dukhan, and A. S. Dalklç, "Realistic experimental heat transfer characteristics of radiant floor heating using sidewalls as heat sinks," *Energy and Buildings*, vol. 183, pp. 515–526, 2019.

[87] D. Cvetković and M. Bojić, "Optimization of thermal insulation of a house heated by using radiant panels," *Energy and Buildings*, vol. 85, pp. 329–336, 2014.

[88] B. W. Olesen, "Thermal comfort requirements for floors occupied by

people with bare feet," *ASHRAE Transactions*, vol. 2451, pp. 41–57, 1977.

[89] EN1264-2, "Water-based surface embedded heating and cooling systems - Part 2: Floor heating prove methods for the determination of thermal output using calculations and test methods," 2008.

[90] EN 12645, "Water based surface embedded heating and cooling systems Part 5: heating and cooling surfaces embedded in floors, ceilings, and walls," 2008.

[91] Owens Corning Foam Insulation LCC, "Foamular Extruded Polystyrene (XPS) Insulation SI and I-P Units for Selected Properties," tech. rep., 2011.

[92] B. S. Hemingway and R. A. Robie, "Heat capcity of polystyrene from 275 to 315 K," tech. rep., United States Department of the Interior - US Geological Survey, Reston, VA, 1994.

[93] G. V. Kuznetsov, N. I. Kurilenko, and A. E. Nee, "Mathematical modelling of conjugate heat transfer and fluid flow inside a domain with a radiant heating system," *International Journal of Thermal Sciences*, vol. 131, pp. 27–39, 2018.

[94] S. Saravanan and N. Raja, "Combined radiation-convection in an air filled enclosure with in-line heaters," *International Communications in Heat and Mass Transfer*, vol. 110, p. 104399, 2020.

[95] J. G. Maveety and J. R. Leith, "Heat transfer in Rayleigh-Bénard convection with air in moderate size containers," *International Journal of Heat and Mass Transfer*, vol. 41, no. 4, pp. 785–796, 1998.

[96] The Engineering Toolbox, "Specific Heat of Solids," 2003.

[97] Concrete Block Association, "A Guide to Selection & Specification," 2017.

[98] Concrete Block Association, "External Walls Thermal Performance," 2017.

[99] P. P and A. P, "Comparison of thermal properties of three texturally different soils under two compaction levels," *African Journal of Agricultural Research*, vol. 8, no. 28, pp. 3679–3687, 2013.

[100] S. L. Manzello, S. H. Park, T. Mizukami, and D. P. Bentz, "Measurement of Thermal Properties of Gypsum Board at Elevated Temperatures," in *Proceedings of the Fifth International Conference on Structures in Fire*, (Singapore), National Institute of Standards and Technology, 2008.

[101] O Reg. 332/12 S.9.15.4.2.(1), "Ontario Building Code."

[102] K. Cavanaugh, M. Bradfield, T. Bremner, K. Callahan, E. Hill, T. Holm, W. McCall, D. Musser, J. Ries, S. Rowe, J. Speck, S. Spinney, A. Sukenik, R. Valore, and M. Van Geem, "Guide to Thermal

Properties of Concrete and Masonry Systems," tech. rep., American Concrete Institute, 2002.

[103] Environment Canada, "Historical Data - Ottawa, ON," 2018.

Appendices

Appendix A

Supplementary Data Table(s)

Table A.1: TES Layer Details

Layer & Sources	**L [m]**	**k [W/mK]**	**ρ [kg/m^3]**	**c_p [J/kgK]**
Heated Space [4, 56]	10	0.02624	1.177	1.0049
Concrete Slab [4, 5, 96–98]	0.1016	0.75	1400	750
Compacted Granular Rock [4, 7, 8]	0.0508	2.0	2700	729
Compacted Fill [4, 8, 99]	0.0508	1.15	1616.27	1237.4
Sand [4, 9]	0.1016	0.27	1700	800
Panels [4, 100]	0.0127	0.258	711	1089
Compacted Sand [4, 8]	0.0508	0.30	28.9	711.7
Undisturbed Soil [3, 8]	6.6444	0.72	1893.1	747.3
XPS Insulation [91, 92]	Varies	0.029	28.9	1500

Appendix B

1D Simulations

Table B.1: 1D Mesh Reference Case Mesh Dimensions

Block	**Depth-wise Dimension**	**Depth (m)**
Concrete Slab	121	0.15
Upper Sand	121	0.15
Heater	5	0.005
Lower Sand	121	0.15
XPS / Sand	41	0.05
Soil	2401	3.0
Granite	2797	3.5

Note: 'Dimension' here refers to the number of computational mesh lines in the given direction. A depth-wise dimension of 5 indicates a mesh block with four control volumes along its depth.

B.1 Reference Case Data

Table B.2: 1-Dimensional Model Reference Case – Layers [49]

Layer	**Thermal Conductivity** (W/mK)	**Thickness (m)**
Room Air	5.00	4.00
Medium Density Concrete	0.55	0.15
Dry Sand	5.00	0.15
Heater	-	-
Dry Sand	5.00	0.2
Moist Soil	1.00	3.00
Granite	3.00	6.00 (max)

Table B.3: 1-Dimensional Model – Excel Model Constants [49]

Variable	**Value**
Panel Setpoint Temperature	40 °C
Room Setpoint Temperature	18 °C
Film Free Resistance at Slab to Room	0.1 m^2K/W
Constant Seasonal Ground Temperature Depth	7 m
Ground Temperature at Full Depth	8 °C
Foundation Perimeter Heat Transfer	0 W (Adiabatic)

B.2 Boundary Conditions

Table B.4: 1D Mesh Boundary Conditions

BC Location	BC Type	Variable	Value
Room/Concrete Slab Interface	Wall	Surface Heat Transfer Coefficient	10 W/m^{2}K
		Farfield Temperature	18°C
Exterior Vertical Walls	Wall	Heat Transfer Rate	0 W (Adiabatic)
Block Interfaces	BC Connectivity	Wall Energy Option	Pure Conduction
Granite/Undisturbed Soil Interface	Wall	Wall Temperature	8°C

Table B.5: 1D Model Heater Output

Case #	Volumetric Heat Output (kW m^{-3})
1	11.50
2	11.76
3	12.00
4	11.19
5	12.70

B.2.1 Simulation Mesh

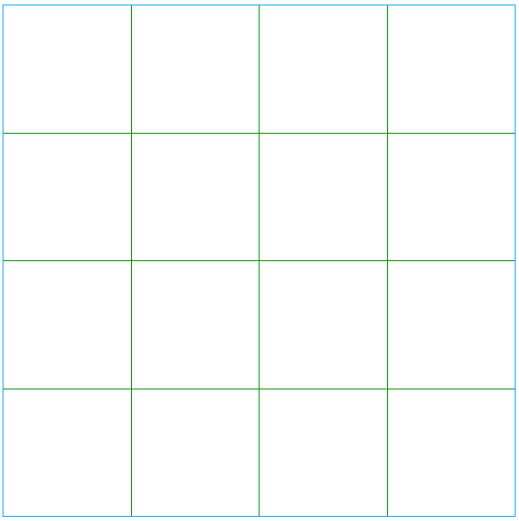

Figure B.1: 1D Simulation Mesh - Top View

Appendix C

MATLAB/Simulink Model

C.1 Simulink Model Components & Control Logic

The following table summarizes the figures that follow it, which represent various aspects of the Simulink model. For an overview of the blocks used from Simulink's "Thermal" library, refer to Table 4.2. Some signal blocks have been excluded to improve the aesthetic and readability of the figures, including selected GoTo, From, Display, ToWorkspace, and Scope blocks.

Table C.1: MATLAB Component Blocks - Overview

Figure Number	**Description**
Figure C.1	Top-level view of the system.
Figure C.2	Subsystem representing the TES region from the bottom of the undisturbed soil layer up to the bottom of the heating panel.
Figure C.3	Typical subsystem for a TES layer with conduction and thermal mass blocks.
Figure C.4	Typical subsystem for a TES layer with a temperature sensor.
Figure C.5	Subsystem for calculating contact resistance for TES region below the heating panel.
Figure C.6	Subsystem used for dynamic control of the heating panel output.
Figure C.7	Subsystem for calculating the heating panel's variable output, when permitted.
Figure C.8	Subsystem representing the TES region from the top of the heating panel up to the surface of the concrete slab.
Figure C.9	Detailed view of the top-level Simulink model from the heating panel surface up to the concrete surface, through the heated space and ceiling into the exterior air.

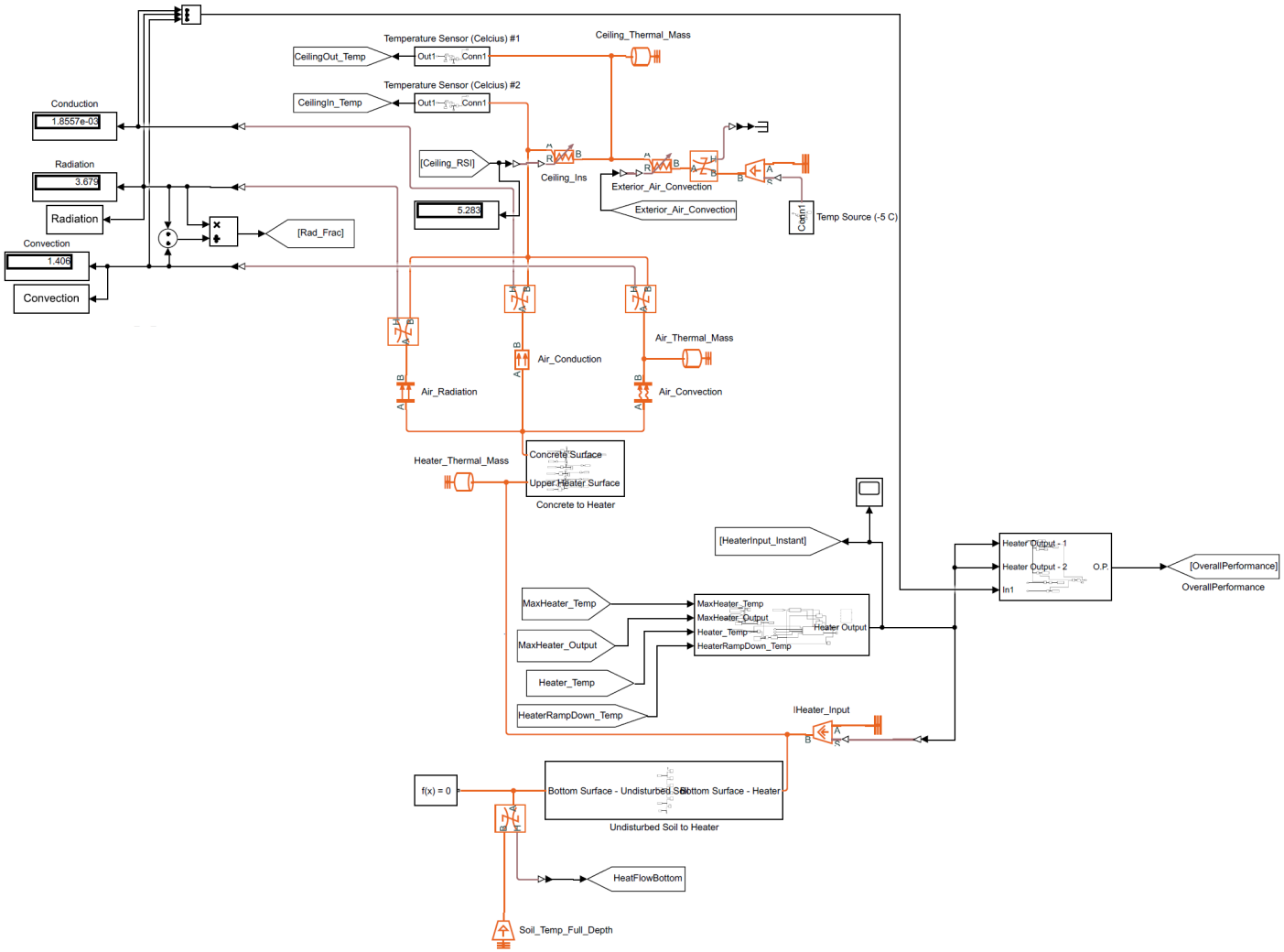

Figure C.1: Model: Top-Level View

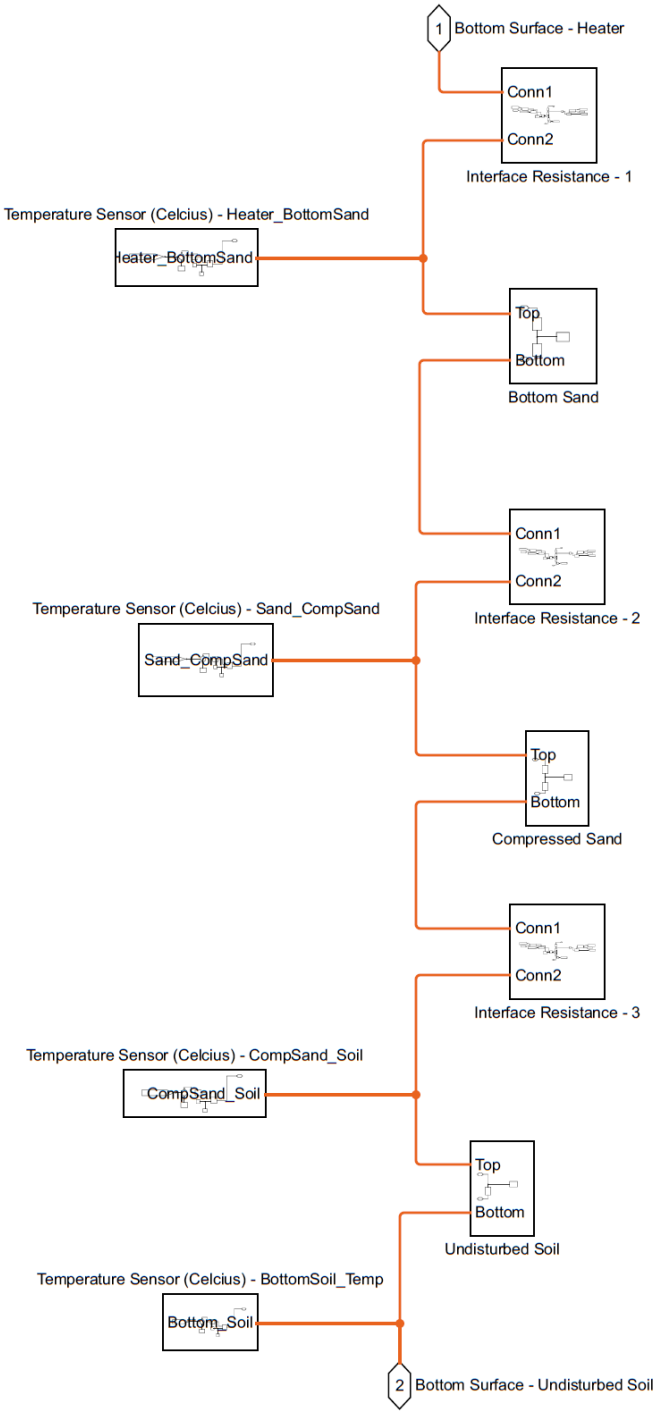

Figure C.2: Subsystem - Soil to Heating Panel

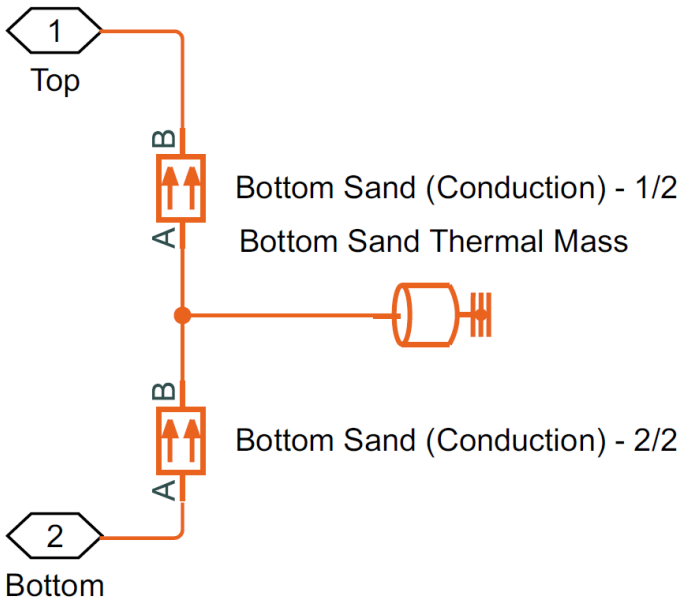

Figure C.3: Subsystem - TES Layer (Conduction and Thermal Mass)

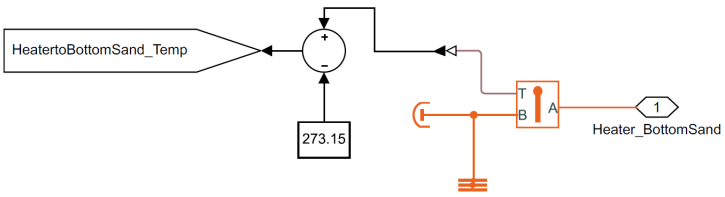

Figure C.4: Subsystem: TES Layer (Temperature Sensor)

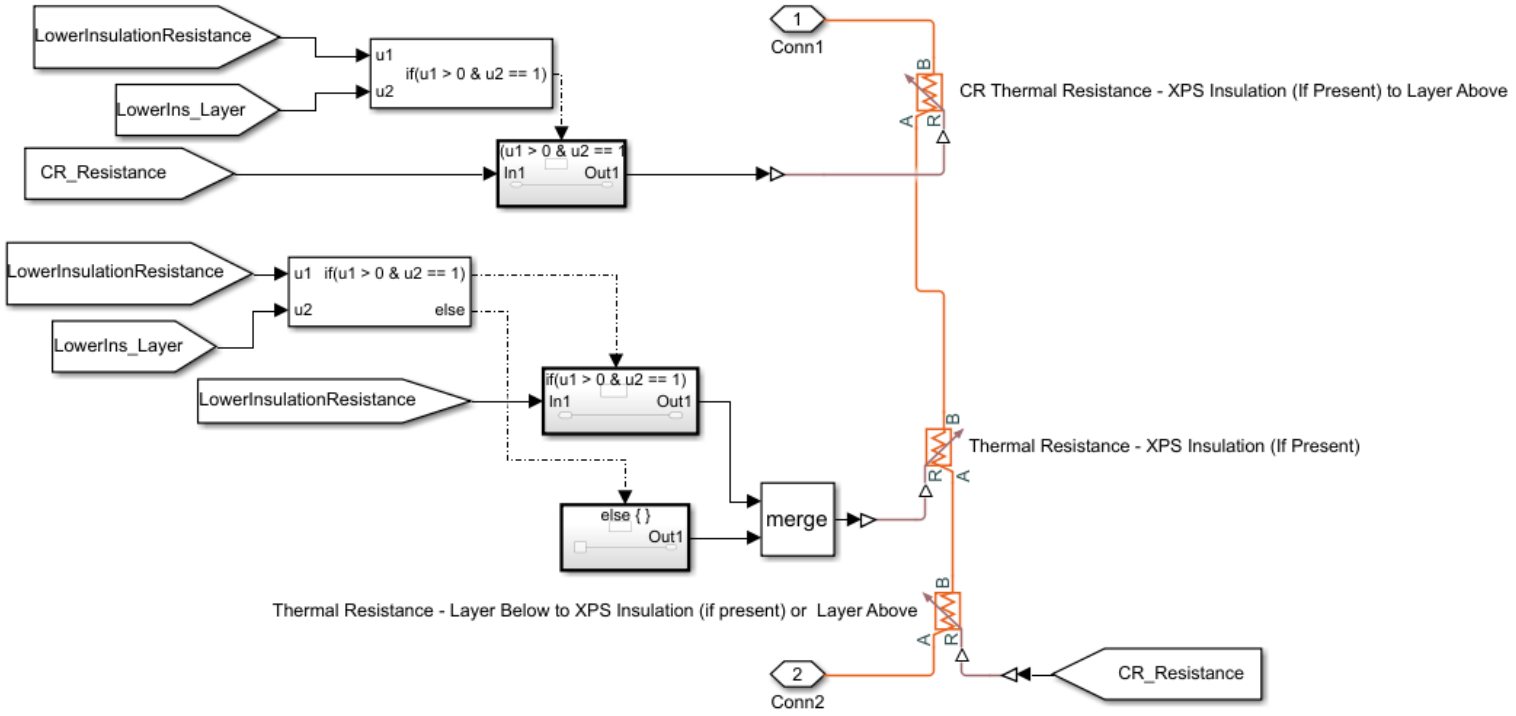

Figure C.5: Subsystem - Interface Resistance

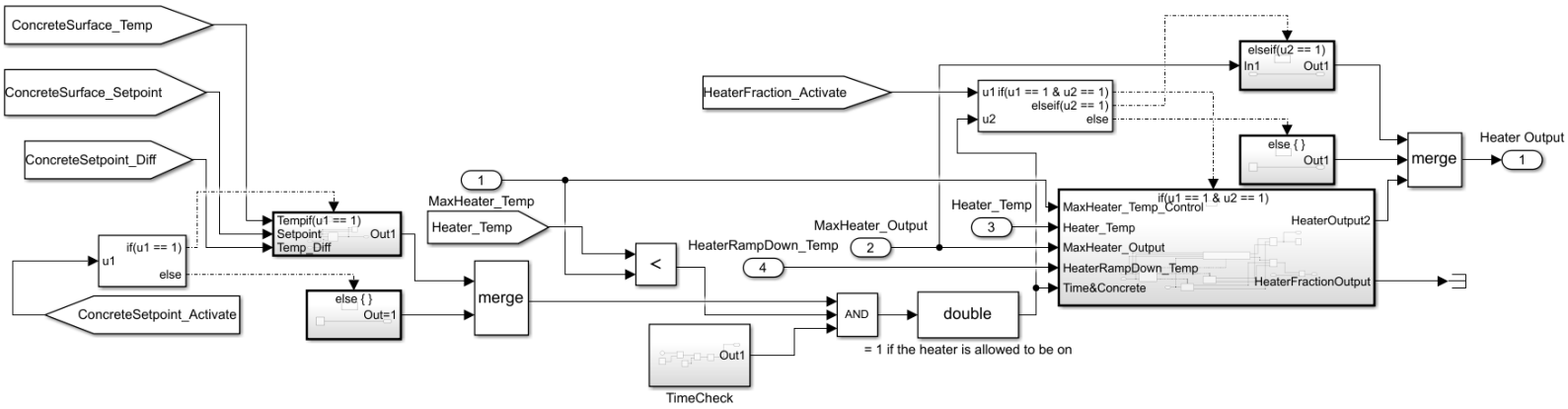

Figure C.6: Subsystem: Heating Panel Control

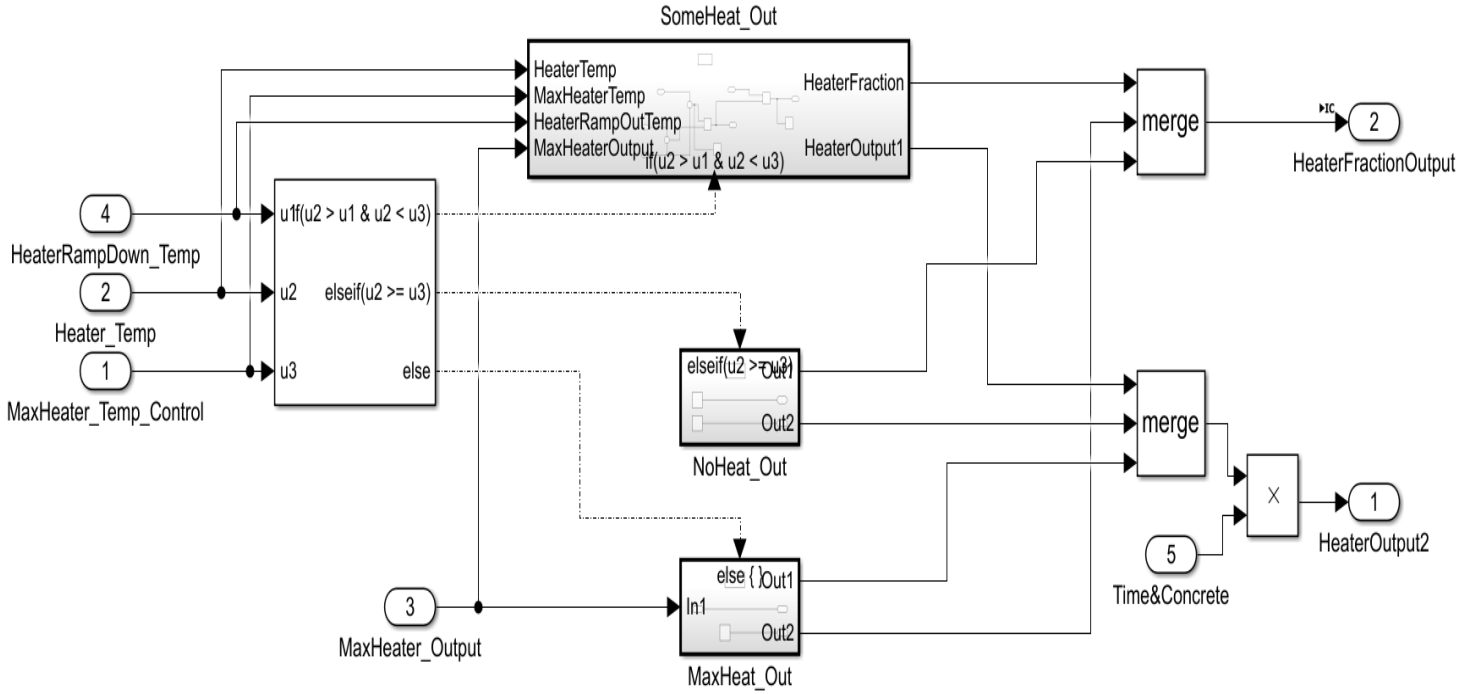

Figure C.7: Subsystem - Heating Panel Variable Output Calculator

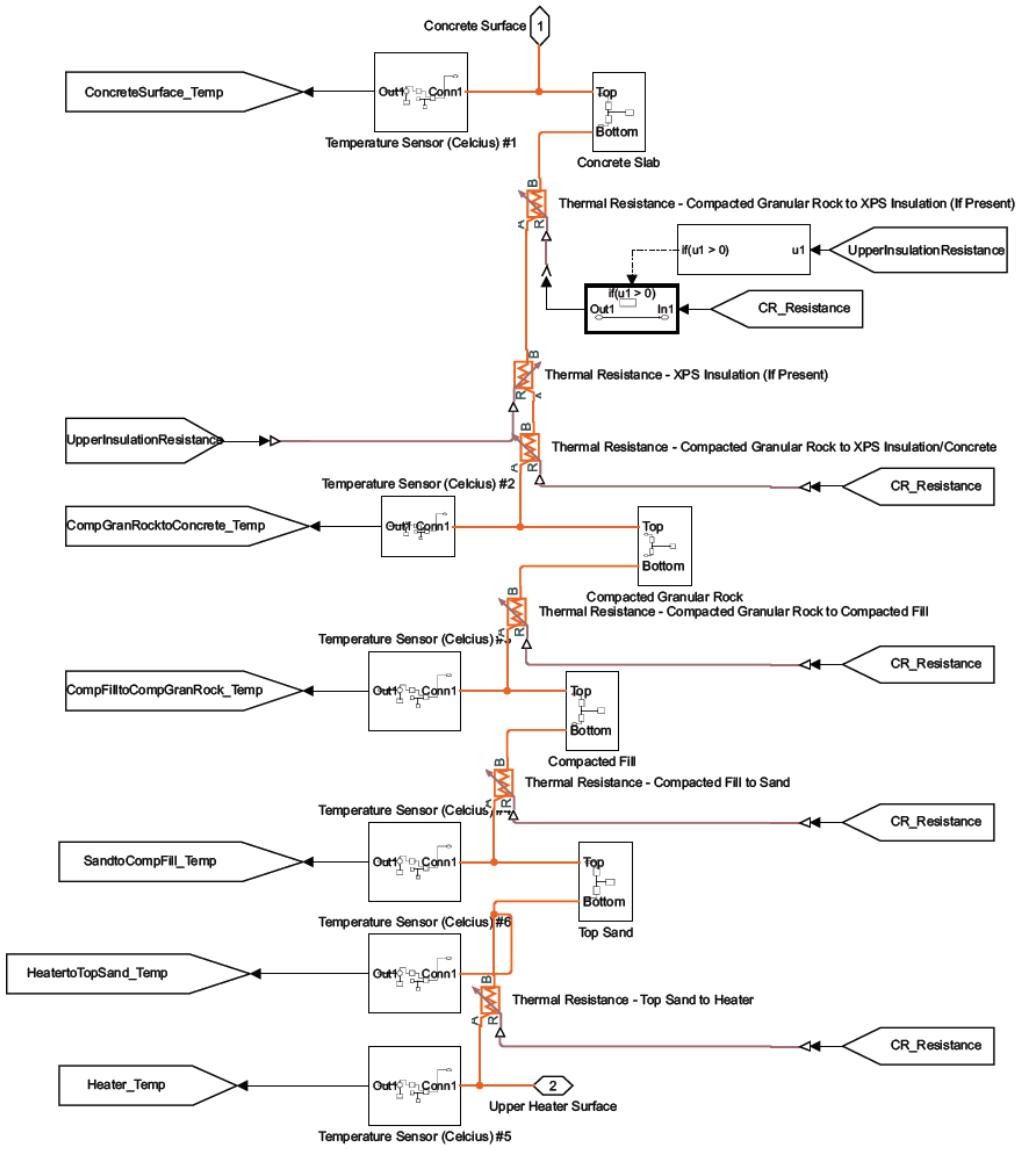

Figure C.8: Subsystem - Heating Panel to Concrete

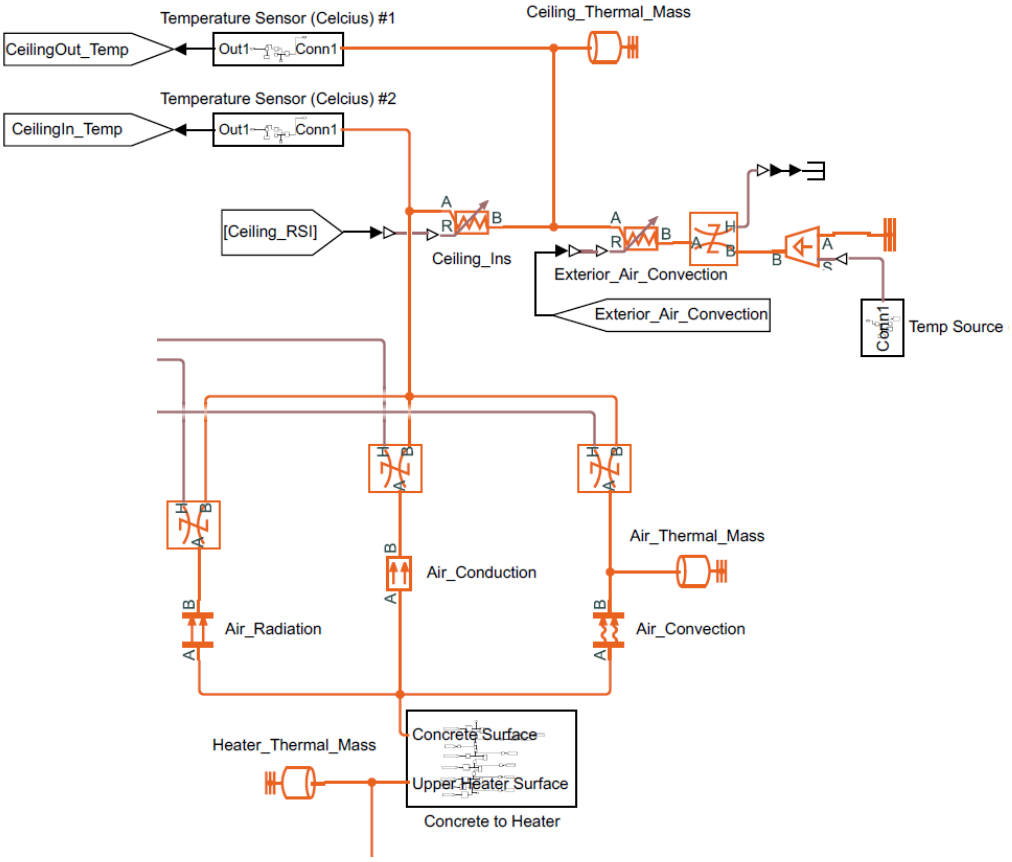

Figure C.9: System View - Heater to Air

C.2 MATLAB Code

This section provides all MATLAB code used to control the Simulink model and analyze the parametric study results. All code is commented thoroughly.

C.2.1 Parametric Study Control Code

```
clear;clc; tic;
% Clears Workspace prior to new simulations, starts sim timer
numSim = 1;
% Sets number of simulations performed
open_system('ThermaRay2.slx');
% Opens the ThermaRay2 Simulink model

%% Obtain Variable Names & Defaults:
SimulationRequests = readtable('SimulationRequests.xlsx');
% Read in requested simulations (all variables that will or
% could be varied and their default values)
DataIn.Number = height(SimulationRequests);
% Set the number of variables included in the Simulation
% Requests spreadsheet
DataIn.Names = string(table2array(SimulationRequests(:,1)));
% Set the name of each variable
DataIn.Components = strings(DataIn.Number,1);
% Preallocate string array for Component name of each variable
```

```
19 DataIn.Mins = table2array(SimulationRequests(:,2));
20 % Set the minimum value of each variable, as specified in the
21 % Simulation Requests spreadsheet
22 DataIn.Maxs = table2array(SimulationRequests(:,3));
23 % Set the maximum value of each variable, as specified in the
24 % Simulation Requests spreadsheet
25 DataIn.Step = table2array(SimulationRequests(:,4));
26 % Set the step size for each variable, as specified in the
27 % Simulation Requests spreadsheet
28 DataIn.Defaults = table2array(SimulationRequests(:,5));
29 % Set the default value of each variable, as specified in the
30 % Simulation Requests spreadsheet
31 DataIn.Primary = string(table2array(SimulationRequests(:,6)));
32 % Determine which variables were specified as "Primary"
33 % variables, variables that for each value tested, all other
34 % tested variables will be varied across each variable's
35 % specified range
36
37 %% Set Default Values
38 for i = 1:DataIn.Number
39 % Cycles through each variable to set component names, defaults
40 DataIn.Components(i) = strcat("ThermaRay2/",DataIn.Names(i));
41 % Set the component name for each variable
42 DataIn.NumSim(i) = numel([DataIn.Mins(i):DataIn.Step(i): ...
43     DataIn.Maxs(i)]);
44 % Determine the number of simulations each variable will
45 % require (doesn't consider the effect of "Primary Variables")
```

```
46      switch DataIn.Names(i)
47          % Switches through the variable names
48      case "SimLengthMonths"
49          % Simulation length must be set separately as
50          % it is a global simulation variable
51          SimLengthSeconds = ...
52              string(DataIn.Defaults(i)*2628000);
53          % Obtains the default simulation length in seconds
54          set_param('ThermaRay2','StopTime',SimLengthSeconds);
55          % Sets simulation length to the default value
56          SimLengthPosition = i;
57          % Saves the position of simulation length within the
58          % list of variables
59      case "SimTimeStepMinutes"
60          % Simulation time step must be set separately
61          % as it is a global simulation variable
62          TimeStepSeconds = string(DataIn.Defaults(i)*60);
63          % Obtains the default simulation time step in seconds
64          set_param('ThermaRay2','FixedStep',TimeStepSeconds);
65          % Sets simulation time step to the default value
66          SimTimeStepPosition = i;
67          % Saves the position of simulation time step within
68          % the list of variables
69      case "ContactResistanceOn"
70          % Set "ContactResistanceOn" separately as is handy
71          % to know the position of this variable within the list
72          set_param('ThermaRay2/ContactResistanceOn/', ...
```

```
73              'value',string(DataIn.Defaults(i)));
74          % Sets "ContactResistanceOn" to its default value
75          ContactResistanceOnPosition = i;
76          % Saves the position of "ContactResistanceOn" within
77          % the list of variables
78      case "Air_Convection"
79          set_param('ThermaRay2/Air_Convection/', ...
80              'heat_tr_coeff',string(DataIn.Defaults(i)));
81          % Sets the default value of the coefficient of
82          % heat transfer for convection through the heated space
83      case "Soil_Temp_Full_Depth"
84          set_param('ThermaRay2/Soil_Temp_Full_Depth', ...
85              'temperature',string(DataIn.Defaults(i)));
86          % Sets the default full depth soil temperature
87          % (bottom of domain)
88      otherwise
89          set_param(DataIn.Components(i),'Value', ...
90              string(DataIn.Defaults(i)));
91          % Sets default values for all other variables
92      end
93  end
94
95  %% Estimate Number of Sims Required
96  numSimTotal = 0;
97  for i = 1:DataIn.Number
98      if DataIn.Primary(i) == "Yes"
99  % If variable (i) is a primary variable:
```

```
100         numSimTotal = numSimTotal + ((sum(DataIn.NumSim(:)) ...
101             -DataIn.NumSim(i))*DataIn.NumSim(i)) + 1;
102     else % Otherwise:
103         numSimTotal = numSimTotal + DataIn.NumSim(i);
104     end
105 end
106
107 %% Setup the data tables for performance and temperature
108 varNames = {'Run_Number','Sim_Length_Months', ...
109     'Sim_Time_Step_Minutes','Variable_Changed', ...
110     'Variable_Value','Overall_Performance', ...
111     'Radiation_Fraction','Primary_Variable', ...
112     'Primary_Variable_Value','Radiation','Convection','ESR'};
113     % Specify variables to be included in DataTable
114 varTypes = {'double','double','double','string','double', ...
115     'double','double','string','string','double','double', ...
116     'double'};
117     % Specifies variable type for each column of DataTable
118 DataTable = table('Size',[numSimTotal 12],'VariableTypes', ...
119     varTypes,'VariableNames',varNames);
120     % Pre-allocates and formats DataTable
121 varNames_Temperatures = {'Run_Number','Soil_BottomTemp', ...
122     'CompSand_SoilTemp','Sand_CompSandTemp', ...
123     'Heater_BottomSandTemp','HeaterTemp', ...
124     'Heater_TopSandTemp','Sand_CompFillTemp', ...
125     'CompFill_CompGranRockTemp','CompGranRock_ConcreteTemp',...
126     'ConcreteTemp','CeilingInTemp','CeilingOutTemp','ExtTemp'};
```

```
127     % Sets variable names for the temperature table
128 varTypes_Temperatures = {'double','double','double',...
129     'double','double','double','double','double','double', ...
130     'double','double','double','double','double'};
131     % Set variable types for the temperature table
132 TempsTable = table('Size',[numSimTotal 14],'VariableTypes',...
133     varTypes_Temperatures,'VariableNames',...
134     varNames_Temperatures);
135     % Preallocate and formate the temperature table
136 varNames_Values = {'Run_Number','MaxHeaterTemp', ...
137     'ConcreteSurfaceSetpoint','LowerInsulationThickness', ...
138     'UpperInsulationThickness','ContactResistanceOn', ...
139     'ContactResistanceValue','SimLengthMonths', ...
140     'SimTimeStepMinutes','Air_Convection', ...
141     'Soil_Temp_Full_Depth','HeaterRampDownTemp_Diff', ...
142     'ConcreteSetpoint_Activate','LowerIns_Layer', ...
143     'HeaterFraction_Activate','Exterior_Air_Conv', ...
144     'Ceiling_R_Value'};
145 % Sets variable names for the values table
146 varTypes_Values = {'double','double','double','double', ...
147     'double','double','double','double','double','double',...
148     'double','double','double','double','double','double', ...
149     'double'};
150 % Set variable types for the values table
151 ValuesTable = table('Size',[numSimTotal 17],'VariableTypes',...
152     varTypes_Values,'VariableNames',varNames_Values);
153 % Preallocate and formate the values table
```

```
154 numTimeSteps = (str2double(SimLengthSeconds)/ ...
155     str2double(TimeStepSeconds))+1;
156     % Set the number of time steps in each simulation
157 numTimeSteps_half = fix(numTimeSteps/2);
158     % Determine the midpoint of the simulation
159 %% Perform Initial Simulation with Default Values
160
161 sim('ThermaRay2');
162 % Performs the first run,
163 % with all variables set to their defaults
164
165 SaveDataTable;
166 % Saves the first row of the data table
167 SaveTempTable;
168 % Saves the current row of the temp. table
169 % See separate code at the bottom for these two .m files
170 ValuesTable(numSim,:) = getparam(DataIn);
171 % Saves the current variable values in the Values table
172 numSim = numSim + 1;
173 % Keep track of the number of simulations performed, in part
174 % as the current numSim value is the current row for the
175 % data and temperature tables.
176
177 %% Vary Parameters Based on "SimulationRequests" Spreadsheet
178 waiting = waitbar(0,'Please wait...');
179 % Starts the waitbar window
180 for i = 1:DataIn.Number
```

```
181     % Walk through each variable in the list of variables
182     if DataIn.Primary(i) == "Yes"
183         % If the current variable was specified as a
184         % Primary Variable
185         for j = DataIn.Mins(i):DataIn.Step(i):DataIn.Maxs(i)
186             % Walk through from the variable's minimum to its
187             % maximum by its specified step
188         switch DataIn.Names(i)
189                 % This should ensure that the primary value is
190                 % walking through its values as it should...
191         case "SimLengthMonths"
192         set_param("ThermaRay2",'StopTime',string(j*262800));
193         case "SimTimeStepMinutes"
194         set_param("ThermaRay2",'FixedStep',string(j*60));
195         case "Air_Convection"
196         set_param('ThermaRay2/Air_Convection/', ...
197             'heat_tr_coeff',string(j));
198         case "Soil_Temp_Full_Depth"
199         set_param('ThermaRay2/Soil_Temp_Full_Depth', ...
200             'temperature',string(j));
201         otherwise
202         set_param(DataIn.Components(i),'Value',string(j));
203         end
204
205         for k = 1:DataIn.Number
206         % Walk through each variables in the list of variables
207             if i ≠ k
```

```
208             % Skip the primary variable's default value
209             % as it has already been performed
210
211             % These six next lines obtain the name, minimum,...
212             % maximum, step size, default value, and ...
213             % component name of the current variable (k)
214             keyVariable.Name = DataIn.Names(k);
215             keyVariable.Min = table2array...
216                 (SimulationRequests(k,2));
217             keyVariable.Max = table2array...
218                 (SimulationRequests(k,3));
219             keyVariable.Step = table2array...
220                 (SimulationRequests(k,4));
221             keyVariable.Default = DataIn.Defaults(k);
222             keyVariable.Component = DataIn.Components(k);
223
224             for keyVariableValue = keyVariable.Min : ...
225                     keyVariable.Step : keyVariable.Max
226                 % This for loop walks through the current
227                 % variable (k)'s values, from min to max
228                 switch keyVariable.Name
229                 % Check the name of the current variable,
230                 % set the variable to the current value,
231                 % run the simulation, saves the results
232                 case "SimLengthMonths"
233                 set_param("ThermaRay2",'StopTime', ...
234                     string(keyVariableValue*262800));
```

```
235                 sim('ThermaRay2');
236                 numTimeSteps = ((keyVariableValue*262800)/ ...
237                     str2double(TimeStepSeconds))+1;
238                 % Set the number of time steps in each sim
239                 numTimeSteps_half = fix(numTimeSteps/2);
240                 SaveDataTableSimLength; % Save performance data
241                 SaveTempTable; % Save temperature data
242                 ValuesTable(numSim,:) = getparam(DataIn);
243                 % Saves the current variable values
244                 % in the Values table
245                 numTimeSteps = (str2double(SimLengthSeconds)...
246                     /str2double(TimeStepSeconds))+1;
247                 % Set the number of time steps in each sim
248                 numTimeSteps_half = fix(numTimeSteps/2);
249                 set_param("ThermaRay2",'StopTime',SimLengthSeconds);
250                 case "SimTimeStepMinutes"
251                 set_param("ThermaRay2",'FixedStep', ...
252                     string(keyVariableValue*60));
253                 sim('ThermaRay2');
254                 numTimeSteps = (str2double(SimLengthSeconds)...
255                     /(keyVariableValue*60))+1;
256                 % Set the number of time steps in each sim
257                 numTimeSteps_half = fix(numTimeSteps/2);
258                 SaveDataTableTimeStep;
259                 % Saves the first row of the data table
260                 SaveTempTable;
261                 % Saves the current row of the temp. table
```

```
262                 ValuesTable(numSim,:) = getparam(DataIn);
263                 % Saves the current variable values
264                 % in the Values table
265                 numTimeSteps = (str2double(SimLengthSeconds)...
266                     /str2double(TimeStepSeconds))+1;
267                 % Set the number of time steps in each sim
268                 numTimeSteps_half = fix(numTimeSteps/2);
269                 set_param("ThermaRay2",'FixedStep',...
270                     TimeStepSeconds);
271                 case "Air_Convection"
272                 set_param('ThermaRay2/Air_Convection/',...
273                     'heat_tr_coeff',string(keyVariableValue));
274                 sim('ThermaRay2');
275                 SaveDataTable;
276                 % Saves the first row of the data table
277                 SaveTempTable;
278                 % Saves the current row of the temp. table
279                 ValuesTable(numSim,:) = getparam(DataIn);
280                 % Saves the current variable values
281                 % in the Values table
282                 set_param('ThermaRay2/Air_Convection/', ...
283                     'heat_tr_coeff',string(keyVariable.Default));
284                 case "Soil_Temp_Full_Depth"
285                 set_param('ThermaRay2/Soil_Temp_Full_Depth',...
286                     'temperature',string(keyVariableValue));
287                 sim('ThermaRay2');
288                 SaveDataTable;
```

```
289                 % Saves the first row of the data table
290                 SaveTempTable;
291                 % Saves the current row of the temp. table
292                 ValuesTable(numSim,:) = getparam(DataIn);
293                 % Saves the current variable values
294                 % in the Values table
295                 set_param('ThermaRay2/Soil_Temp_Full_Depth',...
296                     'temperature',string(keyVariable.Default));
297                 otherwise
298                 set_param(keyVariable.Component,'Value',...
299                     string(keyVariableValue));
300                 sim('ThermaRay2');
301                 SaveDataTable;
302                 % Saves the first row of the data table
303                 SaveTempTable;
304                 % Saves the current row of the temp. table
305                 ValuesTable(numSim,:) = getparam(DataIn);
306                 % Saves the current variable values
307                 % in the Values table
308                 set_param(keyVariable.Component,'Value',...
309                     string(keyVariable.Default));
310                 end
311             numSim = numSim + 1;
312             end
313             waitbar(numSim / numSimTotal)
314         end
315         end
```

```
316         end
317     switch DataIn.Names(i)
318         % This ensures that the primary value is set back
319         % to its default value
320         case "SimLengthMonths"
321             set_param("ThermaRay2",'StopTime',string ...
322                 (DataIn.Defaults(i)*2628000));
323         case "SimTimeStepMinutes"
324             set_param("ThermaRay2",'FixedStep',string ...
325                 (DataIn.Defaults(i)*60));
326         case "Air_Convection"
327             set_param('ThermaRay2/Air_Convection/', ...
328                 'heat_tr_coeff',string(DataIn.Defaults(i)));
329         case "Soil_Temp_Full_Depth"
330             set_param('ThermaRay2/Soil_Temp_Full_Depth', ...
331                 'temperature',string(DataIn.Defaults(i)));
332         otherwise
333             set_param(DataIn.Components(i),'Value',string(j));
334     end
335     else
336         % If it is not a primary variable
337         % there is no need to cycle through all primary
338         % variable values, so just one simulation is run
339         keyVariable.Name = DataIn.Names(i);
340         % See above for comments, same steps taken
341         keyVariable.Min = table2array(SimulationRequests(i,2));
342         keyVariable.Max = table2array(SimulationRequests(i,3));
```

```
343         keyVariable.Step =table2array(SimulationRequests(i,4));
344         keyVariable.Default = DataIn.Defaults(i);
345         keyVariable.Component = DataIn.Components(i);
346
347         for keyVariableValue = keyVariable.Min : ...
348                     keyVariable.Step : keyVariable.Max
349                 % This for loop walks through the current
350                 % variable (k)'s values, from min to max
351                 switch keyVariable.Name
352                 % Check the name of the current variable,
353                 % set the variable to the current value,
354                 % run the simulation, saves the results
355                 case "SimLengthMonths"
356                 set_param("ThermaRay2",'StopTime', ...
357                     string(keyVariableValue*262800));
358                 sim('ThermaRay2');
359                 numTimeSteps = ((keyVariableValue*262800)/ ...
360                     str2double(TimeStepSeconds))+1;
361                 % Set the number of time steps in each sim
362                 numTimeSteps_half = fix(numTimeSteps/2);
363                 SaveDataTableSimLength; % Save performance data
364                 SaveTempTable; % Save temperature data
365                 ValuesTable(numSim,:) = getparam(DataIn);
366                 % Saves the current variable values
367                 % in the Values table
368                 numTimeSteps = (str2double(SimLengthSeconds)...
369                     /str2double(TimeStepSeconds))+1;
```

```
370                 % Set the number of time steps in each sim
371                 numTimeSteps_half = fix(numTimeSteps/2);
372                 set_param("ThermaRay2",'StopTime',...
373                     SimLengthSeconds);
374                 case "SimTimeStepMinutes"
375                 set_param("ThermaRay2",'FixedStep', ...
376                     string(keyVariableValue*60));
377                 sim('ThermaRay2');
378                 numTimeSteps = (str2double(SimLengthSeconds)...
379                     /(keyVariableValue*60))+1;
380                 % Set the number of time steps in each sim
381                 numTimeSteps_half = fix(numTimeSteps/2);
382                 SaveDataTableTimeStep;
383                 SaveTempTable;
384                 ValuesTable(numSim,:) = getparam(DataIn);
385                 % Saves the current variable values
386                 % in the Values table
387                 numTimeSteps = (str2double(SimLengthSeconds)...
388                     /str2double(TimeStepSeconds))+1;
389                 % Set the number of time steps in each sim
390                 numTimeSteps_half = fix(numTimeSteps/2);
391                 set_param("ThermaRay2",'FixedStep',...
392                     TimeStepSeconds);
393                 case "Air_Convection"
394                 set_param('ThermaRay2/Air_Convection/',...
395                     'heat_tr_coeff',string(keyVariableValue));
396                 sim('ThermaRay2');
```

```
397                 SaveDataTable;
398                 % Saves the first row of the data table
399                 SaveTempTable;
400                 % Saves the current row of the temp. table
401                 ValuesTable(numSim,:) = getparam(DataIn);
402                 % Saves the current variable values
403                 % in the Values table
404                 set_param('ThermaRay2/Air_Convection/', ...
405                 'heat_tr_coeff',string(keyVariable.Default));
406                 case "Soil_Temp_Full_Depth"
407                 set_param('ThermaRay2/Soil_Temp_Full_Depth',...
408                     'temperature',string(keyVariableValue));
409                 sim('ThermaRay2');
410                 SaveDataTable;
411                 % Saves the first row of the data table
412                 SaveTempTable;
413                 % Saves the current row of the temp. table
414                 ValuesTable(numSim,:) = getparam(DataIn);
415                 % Saves the current variable values
416                 % in the Values table
417                 set_param('ThermaRay2/Soil_Temp_Full_Depth',...
418                     'temperature',string(keyVariable.Default));
419                 otherwise
420                 set_param(keyVariable.Component,'Value',...
421                     string(keyVariableValue));
422                 sim('ThermaRay2');
423                 SaveDataTable;
```

```
424                 % Saves the first row of the data table
425                 SaveTempTable;
426                 % Saves the current row of the temp. table
427                 ValuesTable(numSim,:) = getparam(DataIn);
428                 % Saves the current variable values
429                 % in the Values table
430                 set_param(keyVariable.Component,'Value',...
431                     string(keyVariable.Default));
432                 end
433             numSim = numSim + 1;
434         end
435         waitbar(numSim / numSimTotal)
436     end
437 end
438
439 DataTablennz = DataTable(1:nnz(table2array(DataTable(:,1))),:);
440 % Saves the non-zero rows of the DataTable as an array
441 DataTableUnique = unique(DataTablennz(:,2:11),'rows','stable');
442 % Removes non-unique rows from DataTable,
443 % maintaining the order of rows
444 TempTablennz = ...
445     TempsTable(1:nnz(table2array(TempsTable(:,1))),:);
446 TempTableUnique = unique(TempTablennz(:,2:14),'rows','stable');
447 FileNameTable = ['SimResults-DataTable_', ...
448     datestr(now, 'dd-mmm-yyyy'),'.xlsx'];
449 % Sets the file name of the DataTable's .XLSX output file
450 writetable(DataTableUnique,FileNameTable);
```

```
% Saves the DataTable as an Excel spreadsheet
FileNameTempTable = ['SimResults-TempTable_', ...
    datestr(now, 'dd-mmm-yyyy'),'.xlsx'];
% Sets the file name of the TempTable's .XLSX output file
writetable(TempTableUnique,FileNameTempTable);
% Saves the TempTable as an Excel spreadsheet
FileNameMAT = ...
    ['SimResults-Workspace_',datestr(now, 'dd-mmm-yyyy')];
% Sets the file name of the DataTable .MAT output file
FileNameValues = ['SimResults-ValuesTable_', ...
    datestr(now, 'dd-mmm-yyyy'),'.xlsx'];
% Sets the file name of the Values Table's .XLSX output file
writetable(table2array(ValuesTable),FileNameValues);
% Saves the Values Table as an Excel spreadsheet
save(FileNameMAT);
% Saves the workspace as a .MAT file
toc;
% Stops the clock, outputs the total time

%-------------------------------------------------------------

% SaveDataTable.m:

DataTable(numSim,:) = {numSim, ...
    DataIn.Defaults(SimLengthPosition),...
    DataIn.Defaults(SimTimeStepPosition),"None",0, ...
    mean(OverallPerformance.Data(numTimeSteps_half: ...
```

```
478      numTimeSteps)),mean(Rad_Frac.Data(numTimeSteps_half: ...
479      numTimeSteps)),"None.","--",mean(Radiation.Data ...
480      (numTimeSteps_half:numTimeSteps)),mean(Convection.Data ...
481      (numTimeSteps_half:numTimeSteps))};
482
483  % SaveDataTableSimLength.m:
484
485  DataTable(numSim,:) = {numSim,keyVariableValue, ...
486      DataIn.Defaults(SimTimeStepPosition), ...
487      keyVariable.Name,keyVariableValue, ...
488      mean(OverallPerformance.Data ...
489      (numTimeSteps_half:numTimeSteps)), ...
490      mean(Rad_Frac.Data(numTimeSteps_half:numTimeSteps)),...
491      "None.","--",mean(Radiation.Data ...
492      (numTimeSteps_half:numTimeSteps)),...
493      mean(Convection.Data(numTimeSteps_half:numTimeSteps)), ...
494      mean(ESR.data(numTimeSteps_half:numTimeSteps))};
495
496  % SaveDataTableTimeStep.m:
497
498  DataTable(numSim,:) = {numSim, ...
499      DataIn.Defaults(SimLengthPosition),keyVariableValue, ...
500      keyVariable.Name,keyVariableValue, ...
501      mean(OverallPerformance.Data ...
502      (numTimeSteps_half:numTimeSteps)), ...
503      mean(Rad_Frac.Data(numTimeSteps_half:numTimeSteps)), ...
504      DataIn.Names(i),string(j),mean(Radiation.Data ...
```

```
505      (numTimeSteps_half:numTimeSteps)),mean(Convection.Data ...
506      (numTimeSteps_half:numTimeSteps)),mean(ESR.data ...
507      (numTimeSteps_half:numTimeSteps))};
508
509  % SaveTempTable.m:
510
511  TempsTable(numSim,:) = {numSim,mean(Soil_BottomTemp.Data ...
512     (numTimeSteps_half:numTimeSteps)), ...
513     mean(CompSand_SoilTemp.Data ...
514     (numTimeSteps_half:numTimeSteps)), ...
515     mean(Sand_CompSandTemp.Data ...
516     (numTimeSteps_half:numTimeSteps)), ...
517     mean(Heater_BottomSandTemp.Data ...
518     (numTimeSteps_half:numTimeSteps)), ...
519     mean(HeaterTemp.Data(numTimeSteps_half:numTimeSteps)), ...
520     mean(Heater_TopSandTemp.Data ...
521     (numTimeSteps_half:numTimeSteps)), ...
522     mean(Sand_CompFillTemp.Data ...
523     (numTimeSteps_half:numTimeSteps)), ...
524     mean(CompFill_CompGranRockTemp.Data ...
525     (numTimeSteps_half:numTimeSteps)), ...
526     mean(CompGranRock_ConcreteTemp.Data ...
527     (numTimeSteps_half:numTimeSteps)), ...
528     mean(ConcreteTemp.Data(numTimeSteps_half:numTimeSteps)),...
529     mean(CeilingInTemp.Data(numTimeSteps_half:numTimeSteps)),...
530     mean(CeilingOutTemp.Data...
531     (numTimeSteps_half:numTimeSteps)),...
```

```
532     mean(ExtTemp.Data(numTimeSteps_half:numTimeSteps))};
533
534
535 function params = getparam(DataIn)
536 % This function is used each time a simulation is performed
537
538 params = zeros(1,DataIn.Count);
539 % Allocate/clear the variable 'params'
540
541 for n = 1:DataIn.Count
542 % Cycle through all variables that are included in the
543 % parametric study and therefore changed frequently
544     switch DataIn.Names(n)
545 % This switch-case code saves the current value of
546 % variable 'n' in the params array
547         case "SimLengthMonths"
548             params(n) = get_param("ThermaRay2",'StopTime');
549         case "SimTimeStepMinutes"
550             params(n) = get_param("ThermaRay2",'FixedStep');
551         case "Air_Convection"
552             params(n) = get_param ...
553                 ('ThermaRay2/Air_Convection/','heat_tr_coeff');
554         case "Soil_Temp_Full_Depth"
555             params(n) = ...
556                 get_param('ThermaRay2/Soil_Temp_Full_Depth',...
557                 'temperature');
558         otherwise
```

```
559             params(n) = ...
560                 get_param(DataIn.Components(n),'Value');
561     end
562 end
563 % The function's output, params, is called and saved
564 % each time a simulation is performed.
565 end
```

C.2.2 Parametric Study Data Analysis Code

```
%% DataProcess.m:
% Processes results from the simulink model and outputs
% plots for each parametric study variable

clc;clear;close all;
% Start fresh
try
    % Delete GoFigure.m, if it exists.
    delete('GoFigure.m')
catch
    warning('GoFigure.m does not exist.')
end

%% Load simulation results and sort them by "Variable_Changed"
load('SimResults-Workspace_05-Nov-2019.mat','DataTableUnique');
% Load data from most recent simulation results (manually edit)
sortDataTable = sortrows(DataTableUnique,3);
% Sort data based on column 3, "Variable_Changed"
sortData = table2array(sortDataTable);
% Convert the data table to an array for manipulation

sortDataTablePrimary = sortrows(DataTableUnique,7);
sortDataPrimary = table2array(sortDataTablePrimary);
%% Section: General Results
```

```
% (ignores whether a result involves a primary variable)
j = 0;
% Preallocate variable j as counter
Variable.Current(:) = sortData(:,3);
% Saves the ``Variable Changed''
% from the sorted data table
for i = 1:height(sortDataTable)
    % Run through this For loop for all sims in the loaded data
    if i≥2 && Variable.Current(i) ≠ Variable.Current(i-1)
        % If this isn't the first simulation being considered
        % and the "Variable_Changed" value for simulation i
        % is NOT the same as simulation i-1, then...
        Variable.End(j) = i-1;
        % That IF means that the "Variable_Changed" value has
        % just changed, so the last variable just ended.
        j = j + 1;
        % Add one to counter j, as one more value of
        % "Variable_Changed" has been encountered
        Variable.Start(j) = i;
        % Simulations for the current "Variable_Changed"
        % value start at data point "i"
        Variable.Name(j) = Variable.Current(i);
        % Set the name of Variable j as the current
        % "Variable_Changed" value
    elseif i == 1
        % If this is the first simulation,
        % then do all of the previous stuff...
```

```
52          j = j + 1;
53          % Except the "Variable.End" line,
54          % as there is no previous "Variable_Changed"
55          Variable.Start(j) = i;
56          Variable.Name(j) = Variable.Current(i);
57      end
58  end
59  Variable.End(j) = i;
60  % The last value of "Variable_Changed" ends at
61  % the last value of "i".
62
63  for i = 1:j
64      % This for loop uses the text from 'GoFigureText.txt'
65      % for each variable encountered in the earlier loop
66      if i == 1
67          % If we're working on the first variable (j = 1),
68          % set up the start of the script.
69          stringtext = string(['for i = 1:j' newline ...
70          'Variable.Mean(i) = mean(str2double(sortData' ...
71          '(Variable.Start(i):Variable.End(i),5)));' ...
72          newline 'if contains(string(Variable.Name(i)),' ...
73          '"None") == 0' newline 'switch Variable.Name(i)' ...
74          newline]);
75              % Setup the script, including the start of the
76              % for loop walking through all variables.
77      end
78      if Variable.Name(i) ≠ "None."
```

```
79          % If the "Variable_Changed" value for "i" is not "None"
80          newText = regexprep(string(fileread...
81              ('GoFigureText.txt')),"VARIABLE", ...
82              string(Variable.Name(i)));
83          % Replace "VARIABLE" with the current variable name
84          % in the "GoFigureGeneralText.txt" file
85          stringtext = append(stringtext,newText);
86          % Append the current edited copy of the
87          % "GoFigureGeneralText.txt" to the script text.
88      end
89  end
90
91  stringtext = append(stringtext,[newline 'end' newline 'end' ...
92     newline 'end']);
93  % Finish off the script's text with a couple "end"'s
94
95  % These next four lines save the script's text as an -.m file
96  edit GoFigure.m
97  FID = fopen('GoFigure.m','w');
98  fprintf(FID,'%s',stringtext);
99  fclose(FID);
100
101 GoFigure
102 % Run the script. Uses the current workspace:
103 % (counter "j", structure "Variable", data "sortDataTable")
```

This is the 'GoFigureText.txt' file used in the "DataProcess.m" code.

```
% This txt file is used by "DataProcess.m", with the word in caps lock
replaced by each variable in the simulation dataset

case "VARIABLE"
% For each variable...
VARIABLE.Data = sortDataTable(Variable.Start(i):Variable.End(i),:);
% Extract data for current variable
VARIABLE.Sorted = sortrows(VARIABLE.Data,4);
% Sort extracted data table based on column 4, "Value"
VARIABLE.SortedArray = table2array(VARIABLE.Sorted);
% Convert extracted data table to array
m = 0;
% Start counter "m"
for k = 1:height(VARIABLE.Sorted)
% Start for loop, from 1 to number of simulations fo current variable
VARIABLE.Value(k) = table2array(VARIABLE.Sorted(k,4));
% The k'th value of the .Value array is the k'th value of the sorted
% extracted data table, column 4, "Value"

if k >= 2 && VARIABLE.Value(k) ~= VARIABLE.Value(k-1)
% Similar structure to one in DataProcess.m,
% if this is not the first simulation and the current value of the
```

```
% .Value array is different from the last...
VARIABLE.End(m) = k-1;
% Save the end point of the last value of the variable
m = m + 1;
% Increase the counter, indicating the number of values of the variable
VARIABLE.Start(m) = k;
% Save the start point of the current value of the variable
VARIABLE.Step = VARIABLE.Value(k) - VARIABLE.Value(k-1);
% Save the step size of the variable
elseif k == 1
% If this is the first value of the variable...
m = m + 1;
% Increase the counter, indicating the number of values of the variable
VARIABLE.Start(m) = k;
% Save the start point of the current value of the vari-able
end
end
VARIABLE.Min = min(VARIABLE.Value);
% Save the minimum value of the current variable
VARIABLE.Max = max(VARIABLE.Value);
% Save the maximum value of the current variable
VARIABLE.End(numel(VARIABLE.Start)) = numel(VARIABLE.Value);
% Save the last end value
```

```
for n = 1:numel(VARIABLE.Start)
% This goes through each grouping of variables and calculates
% the mean and standard deviation of each
VARIABLE.Mean(n) = mean(str2double ...
((VARIABLE.SortedArray(VARIABLE.Start(n):VARIABLE.End(n),5))));
VARIABLE.StdDev(n) = std(str2double ...
((VARIABLE.SortedArray(VARIABLE.Start(n):VARIABLE.End(n),5))));
end

figure('Name','VARIABLE');
% This plots the mean and standard deviation
% at each value of the variable
try
% Using a "try / catch" structure as the insulation thickness variables
% were being problematic. Sometimes "None." would sneak through, too.
errorbar(VARIABLE.Min:VARIABLE.Step:VARIABLE.Max, ...
VARIABLE.Mean,VARIABLE.StdDev);
catch
if contains(Variable.Name(i),"Insulation") == 1
errorbar(round(VARIABLE.Min,2):round(VARIABLE.Step,2): ...
round(VARIABLE.Max,2),VARIABLE.Mean,VARIABLE.StdDev);
else
```

```
warning('Cannot produce plot with VARIABLE.');
end
end
```

C.3 MATLAB/Simulink Model Results

C.3.1 Modified Parametric Study (MPS)

This appendix builds on Section 5.4.1, summarizing and plotting the results from the modified parametric study for all variables. Plots are provided with error bars equal to one standard deviation from the mean performance value for each data point.

Table C.2: Modified Parametric Study Results

Variable	**Relationship**		
	Type	**Line of Best Fit**	**R^2 Value**
Air_Convection	Weak / No Correlation	–	–
Ceiling_R_Value	Linear, Negative	y = -0.353x + 86.3	1
ConcreteSetpoint_Activate	Positive	–	–
ConcreteSurfaceSetpoint	Linear, Negative	y = -0.455x + 83.0	0.99
ContactResistanceOn	Weak & Negative	–	-
ContactResistanceValue	Linear, Negative	y = -21.0x + 75.2	1
Exterior_Air_Conv	Power, Weak & Positive	$y = 75.1\ x^{0.0012}$	0.92
HeaterFraction_Activate	Weak & Positive	–	–
HeaterRampDownTemp_Diff	Weak / No Correlation	–	–
LowerInsulationThickness	Linear, Positive	y = 42.1x + 71.0	0.98
MaxHeaterTemp	Negative (for 20-30 °C)	–	–
SimLengthMonths	Weak / No Correlation	–	–
SimTimeStepMinutes	Weak / No Correlation	–	–
Soil_Temp_Full_Depth	Linear, Positive	y = 1.04x + 66.5	1
UpperInsulationThickness	Linear, Negative	y = -143x + 79.2	0.99

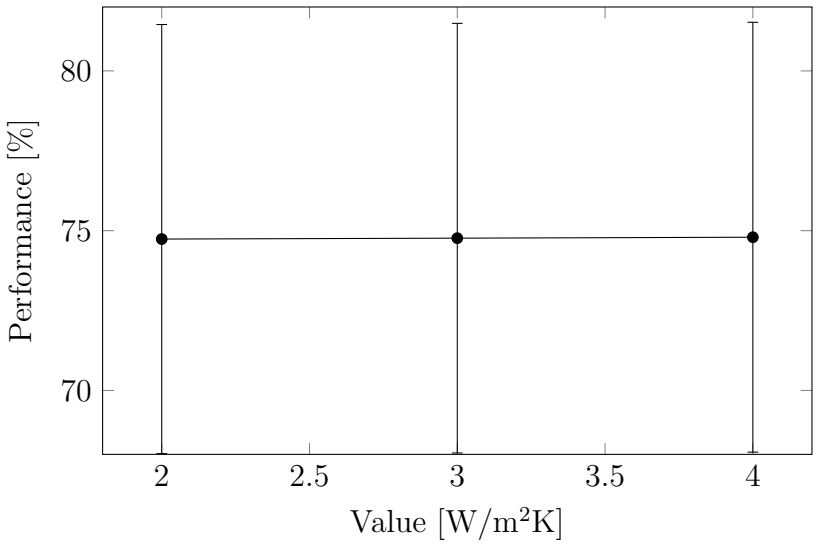

Figure C.10: MPS Results - Air_Convection

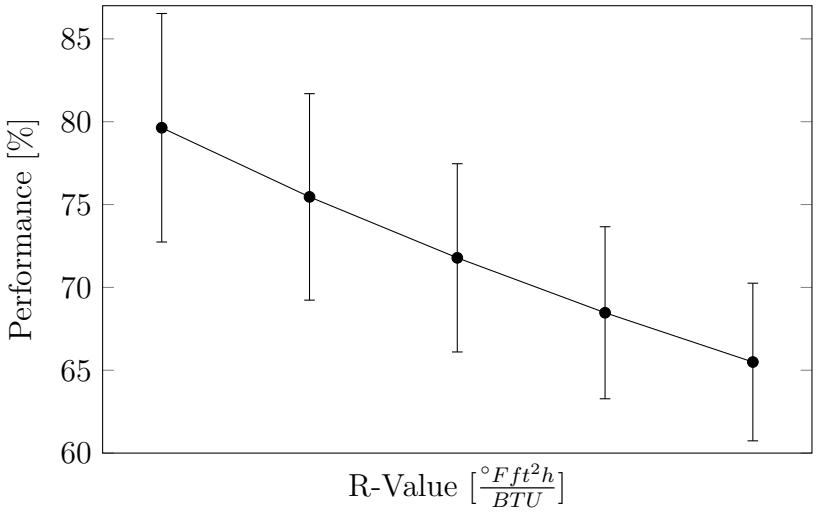

Figure C.11: MPS Results - Ceiling_R_Value

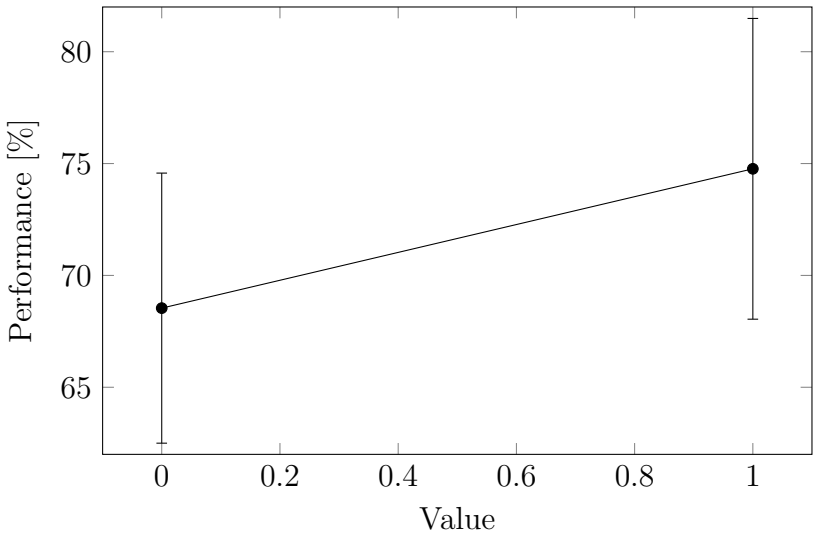

Figure C.12: MPS Results - ConcreteSetpoint_Activate

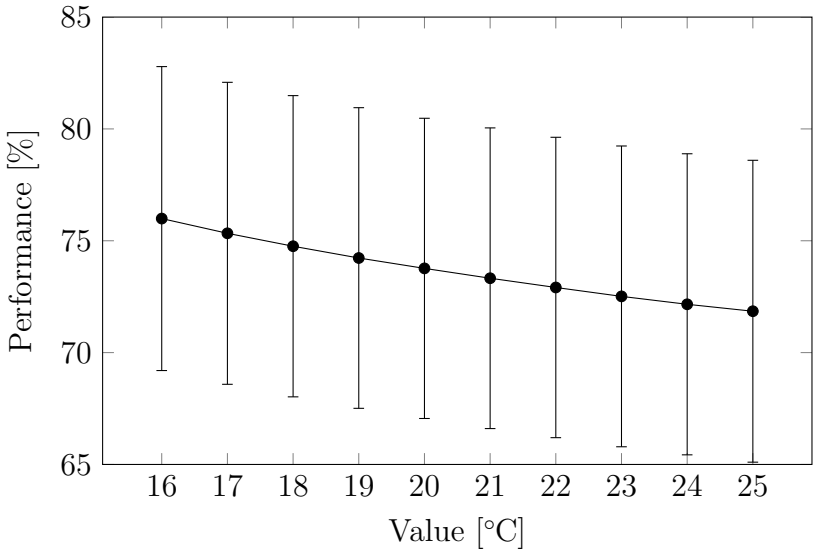

Figure C.13: MPS Results - ConcreteSurfaceSetpoint

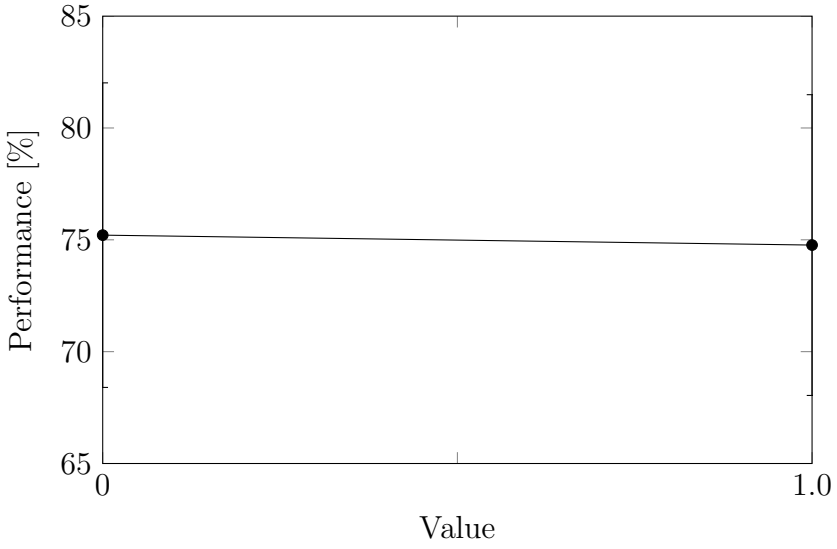

Figure C.14: MPS Results - ContactResistanceOn

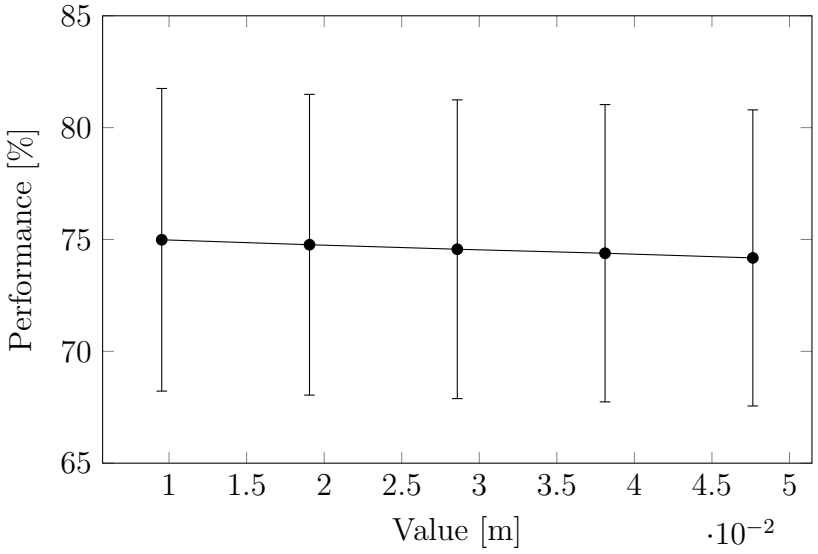

Figure C.15: MPS Results - ContactResistanceValue

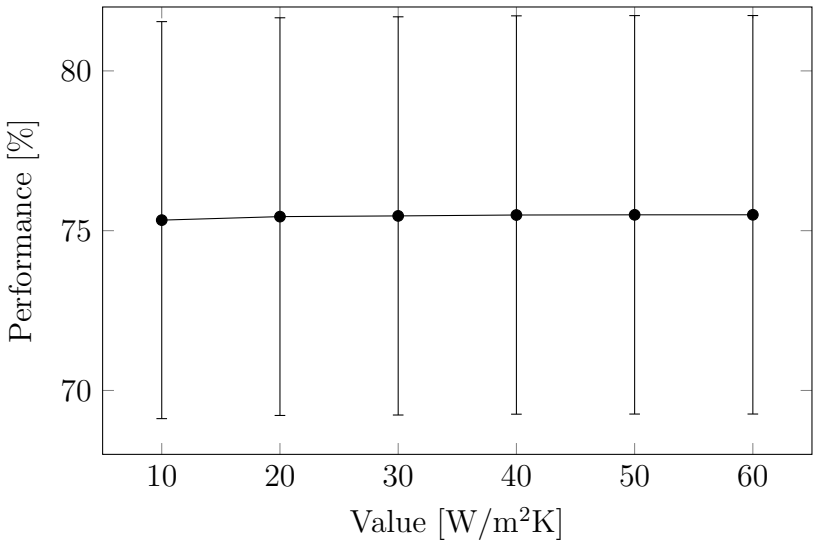

Figure C.16: MPS Results - Exterior_Air_Conv

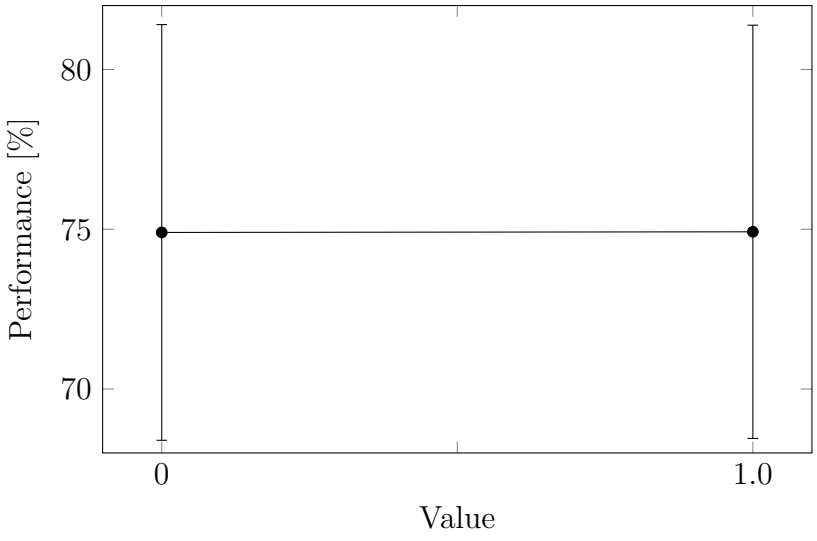

Figure C.17: MPS Results - HeaterFraction_Activate

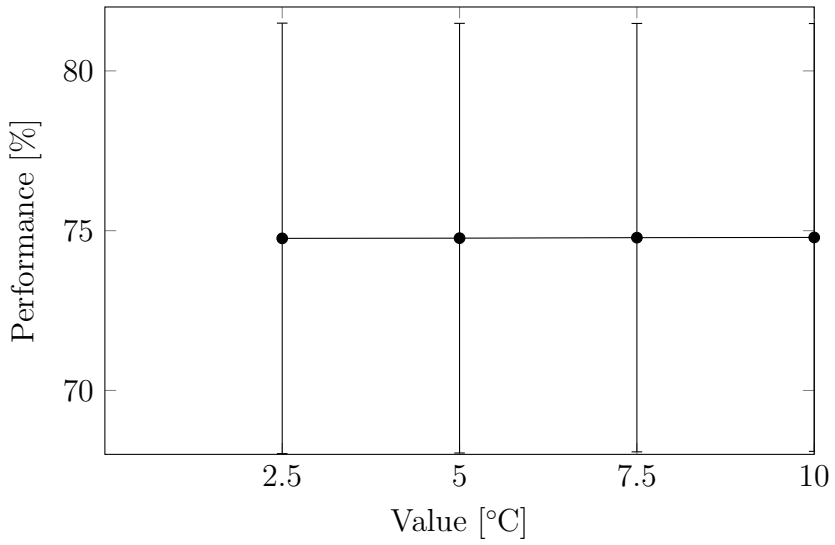

Figure C.18: MPS Results - HeaterRampDownTemp_Diff

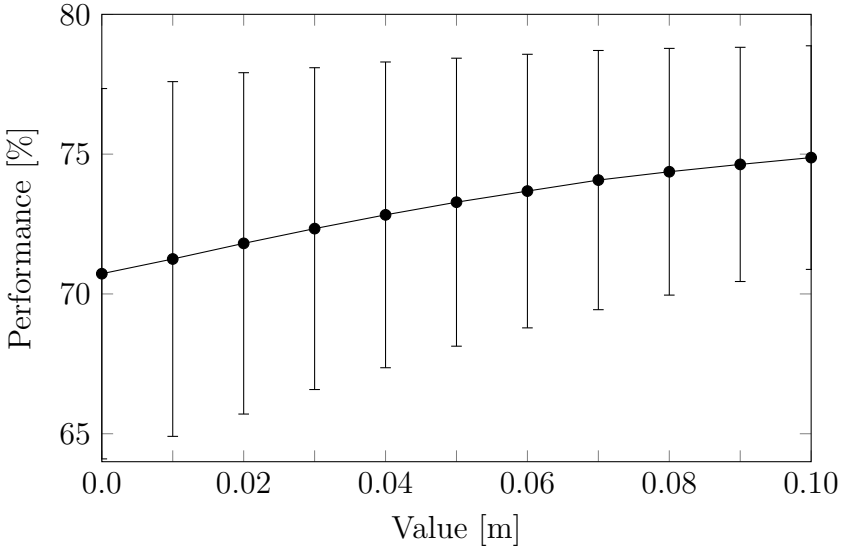

Figure C.19: MPS Results - LowerInsulationThickness

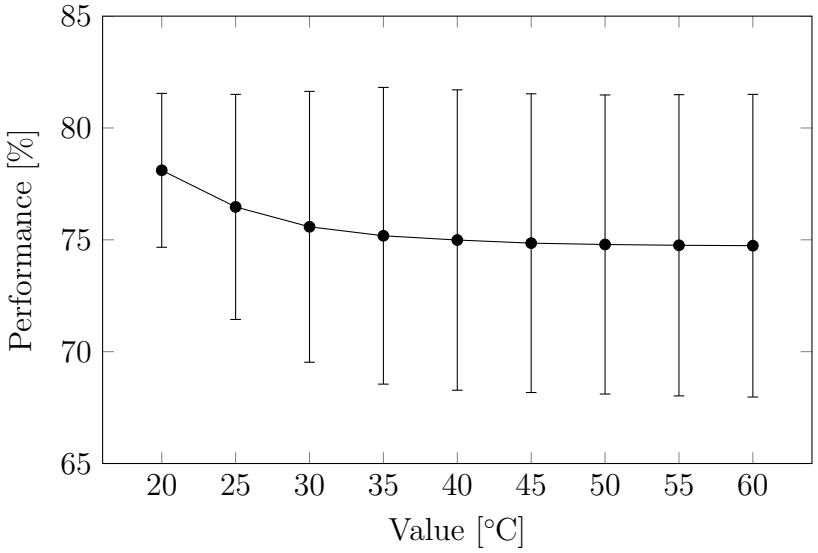

Figure C.20: MPS Results - MaxHeaterTemp

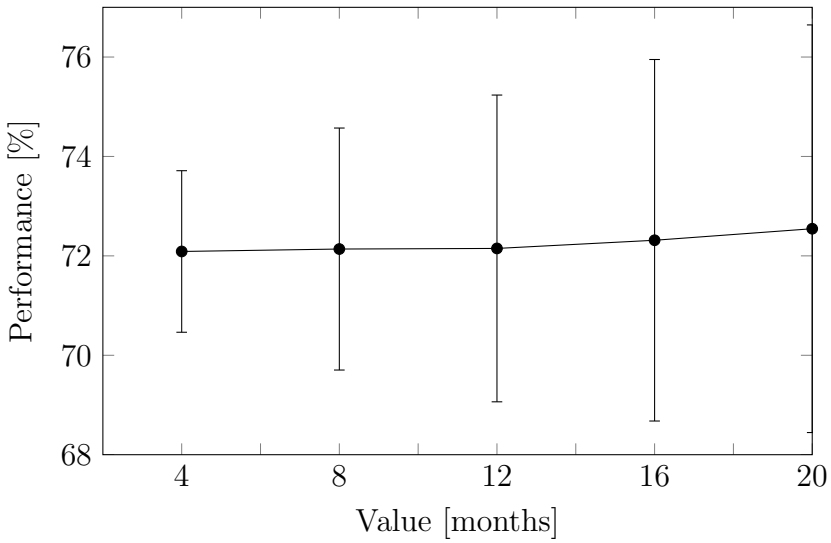

Figure C.21: MPS Results - SimLengthMonths

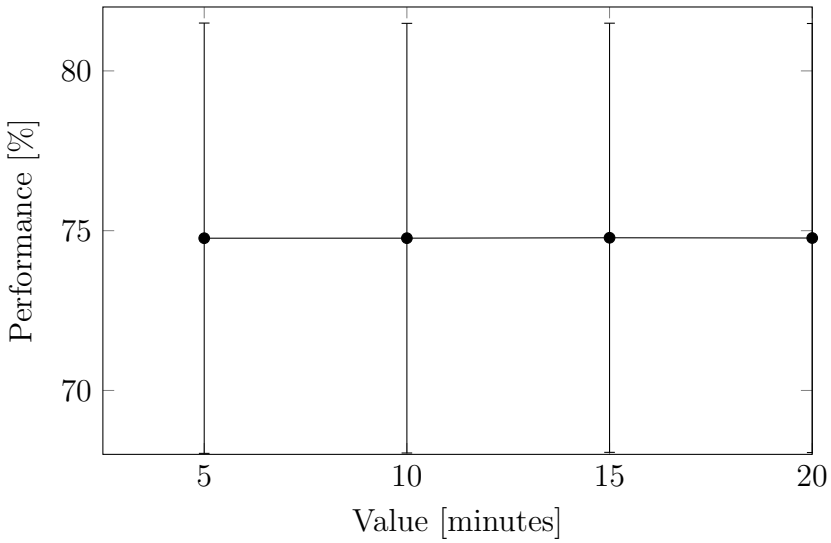

Figure C.22: MPS Results - SimTimeStepMinutes

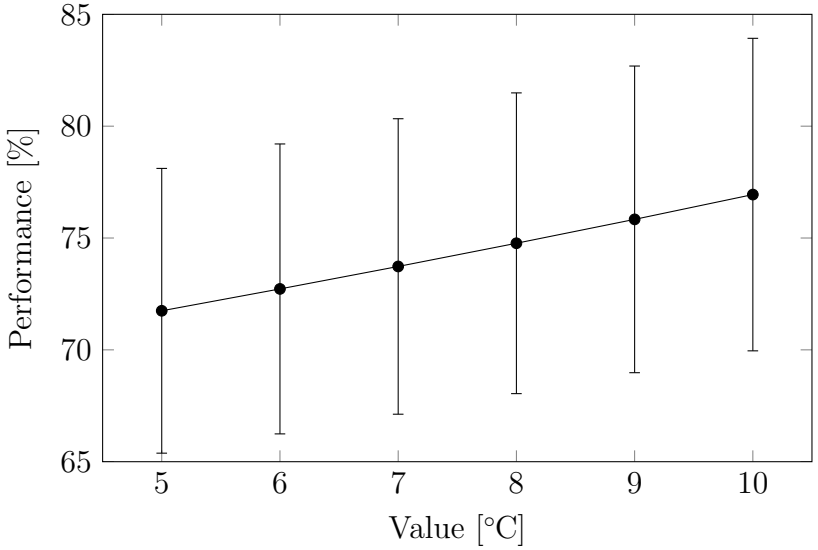

Figure C.23: MPS Results - Soil_Temp_Full_Depth

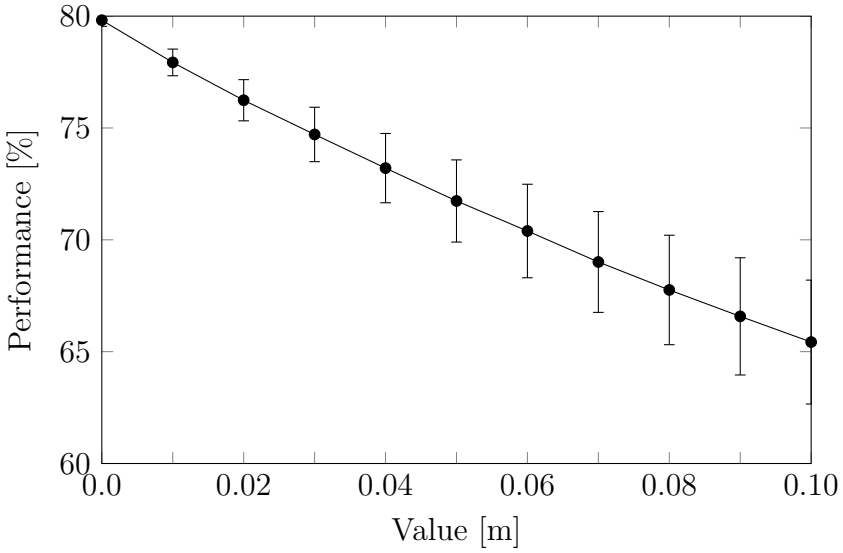

Figure C.24: MPS Results - UpperInsulationThickness

C.3.2 Standard Parametric Study (SPS)

This appendix builds on Section 5.4.2, summarizing and plotting the results from the standard parametric study for all variables. When available, the line of best fit for each variable is provided in the corresponding plot.

Table C.3: Standard Parametric Study Results

Variable	**Relationship**	
	Type	**Line of Best Fit**
Air_Convection	Linear, Weak & Positive	y = 0.035x + 79.3
Ceiling_R_Value	Linear, Negative	y = -0.421x + 92.2
ConcreteSetpoint_Activate	Positive	–
ConcreteSurfaceSetpoint	Linear, Negative	y = -0.792x + 93.8
ContactResistanceOn	Weak & Negative	–
ContactResistanceValue	Linear, Weak & Negative	y = -26.2x + 80.0
Exterior_Air_Conv	Power, Weak & Positive	$y = 79.0\ x^{0.0014}$
HeaterFraction_Activate	Weak / No Correlation	–
HeaterRampDownTemp_Diff	Weak / No Correlation	–
LowerInsulationThickness	Asymptotic Linear, Positive	y = 17.2x + 79.4
LowerIns_Layer	Weak / No Correlation	–
MaxHeaterTemp	Asymptotic Linear, Negative	y = -0.036x + 81.0
SimLengthMonths	Linear, Week & Positive	y = 0.120x + 73.9
SimTimeStepMinutes	Linear, Weak & Negative	y = -0.0042x + 79.5
Soil_Temp_Full_Depth	Linear, Positive	y = 1.2259x + 69.7
UpperInsulationThickness	Asymptotic Linear, Negative	y = -174.19x + 78.67

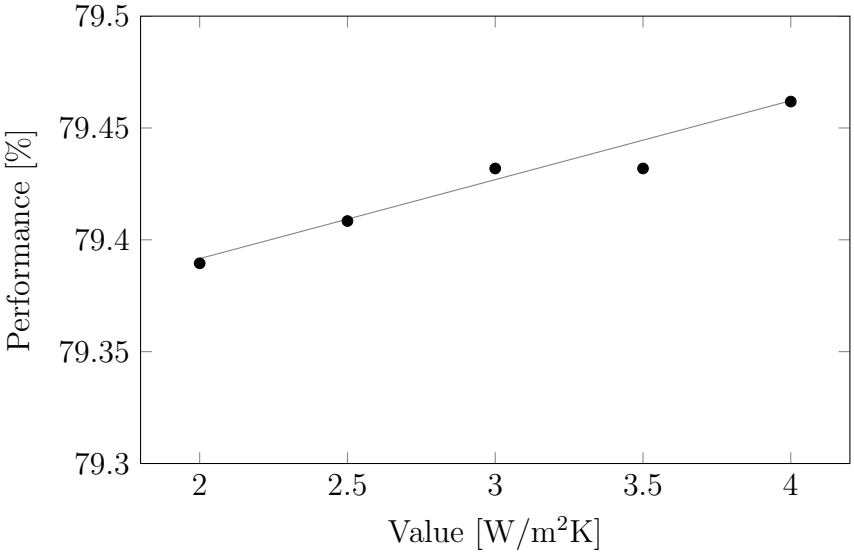

Figure C.25: SPS Results - Air_Convection

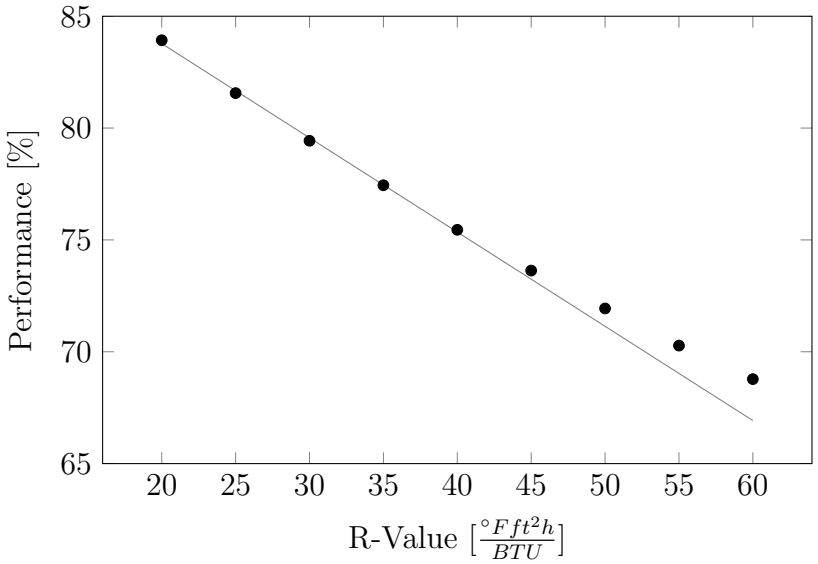

Figure C.26: SPS Results - Ceiling_R_Value

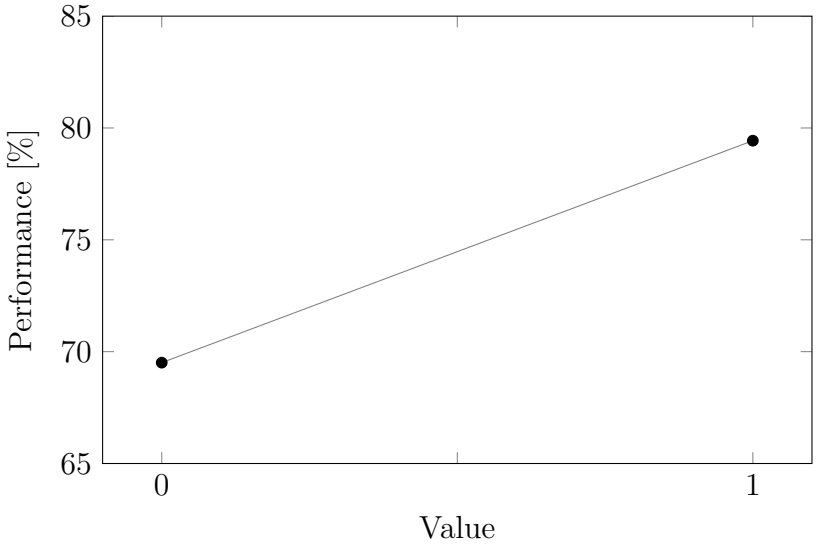

Figure C.27: SPS Results - ConcreteSetpoint_Activate

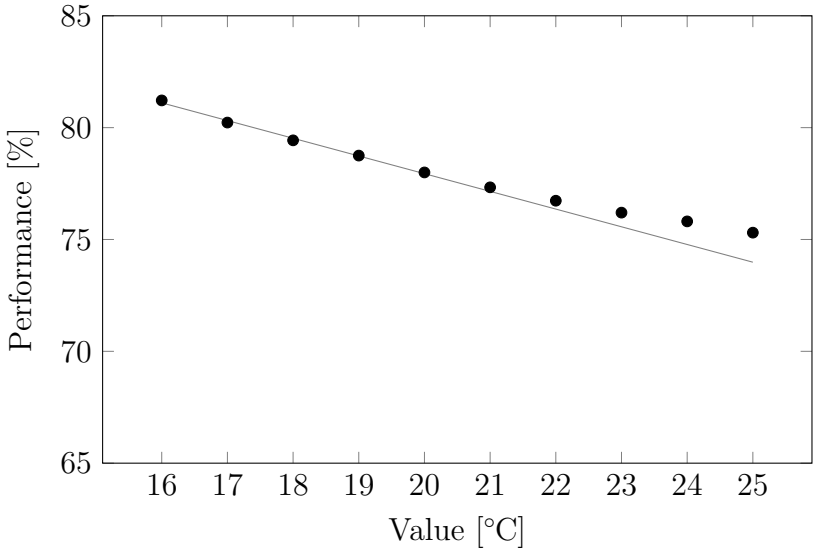

Figure C.28: SPS Results - ConcreteSurfaceSetpoint

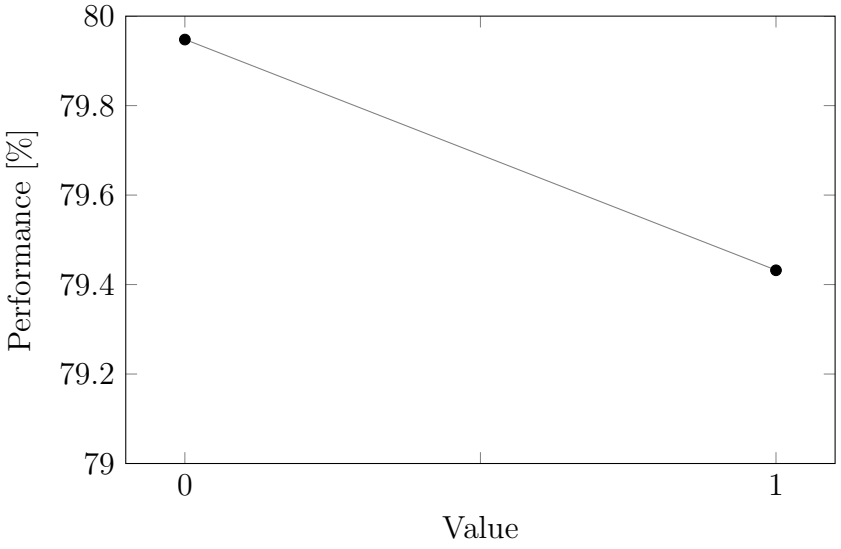

Figure C.29: SPS Results - ContactResistanceOn

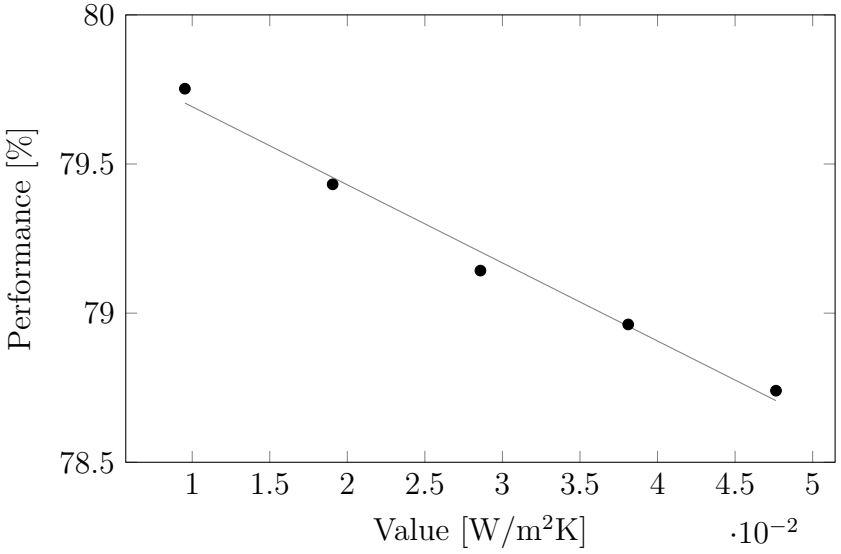

Figure C.30: SPS Results - ContactResistanceValue

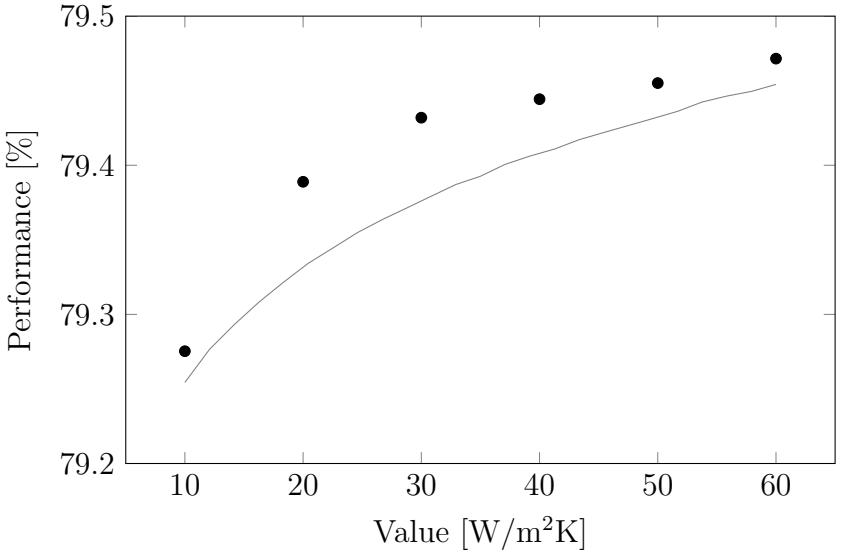

Figure C.31: SPS Results - Exterior_Air_Conv

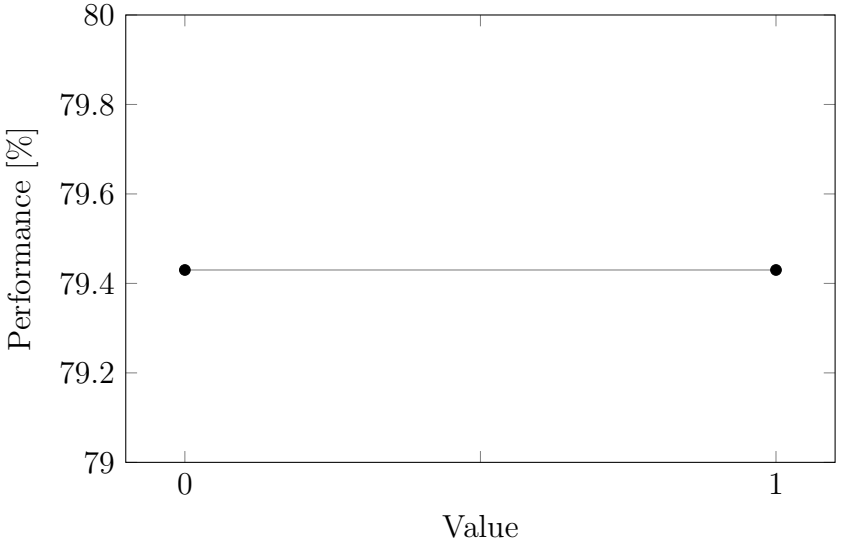

Figure C.32: SPS Results - HeaterFraction_Activate

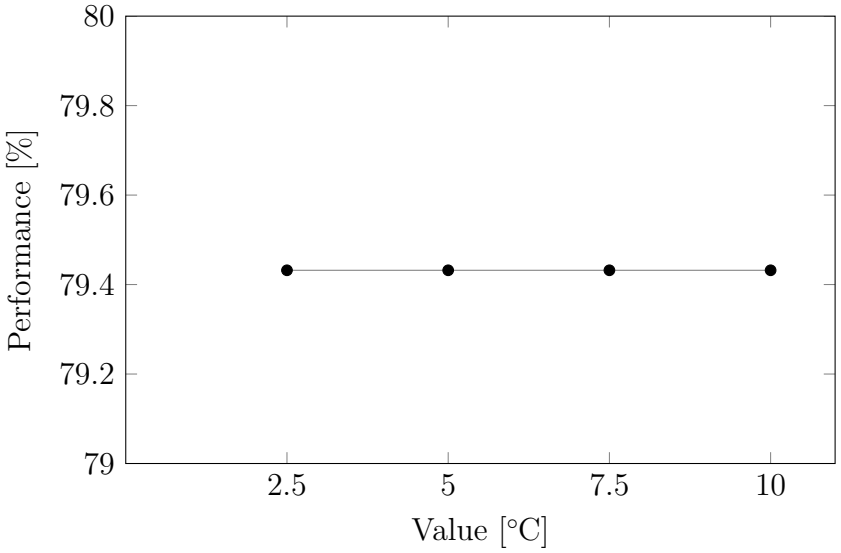

Figure C.33: SPS Results - HeaterRampDownTemp_Diff

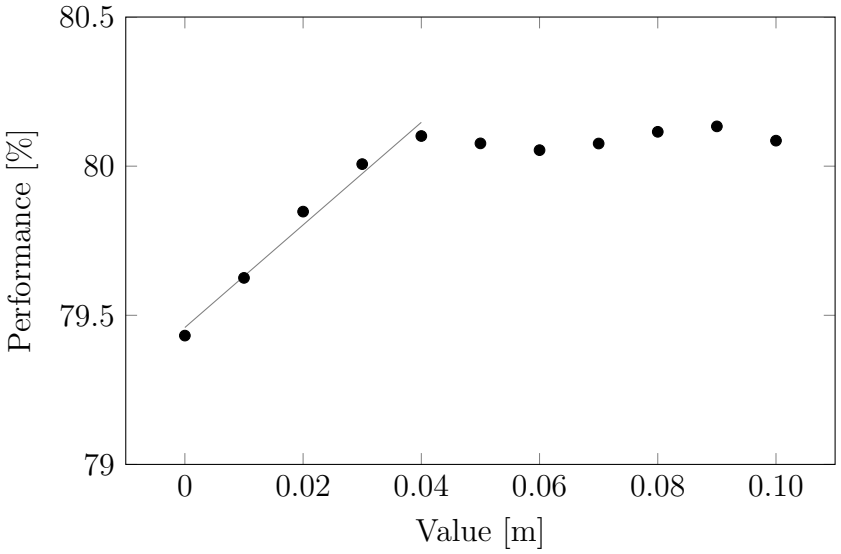

Figure C.34: SPS Results - LowerInsulationThickness

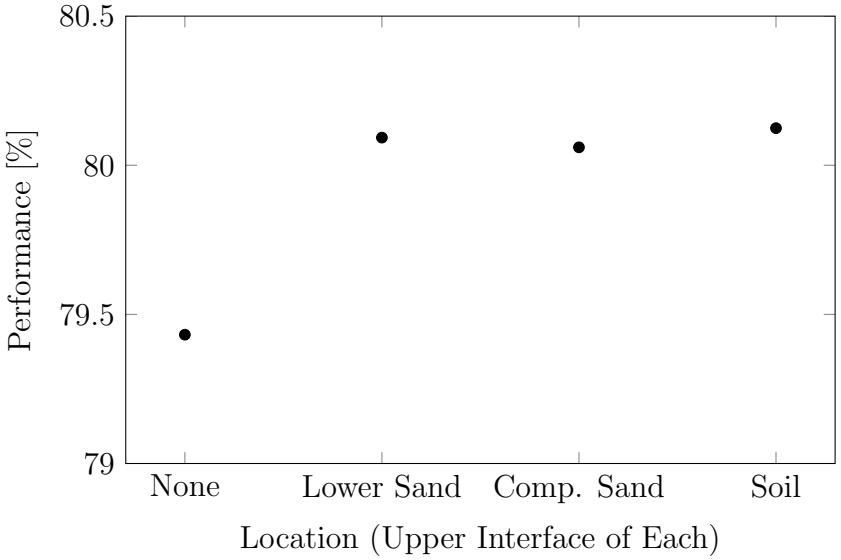

Figure C.35: SPS Results - LowerIns_Layer

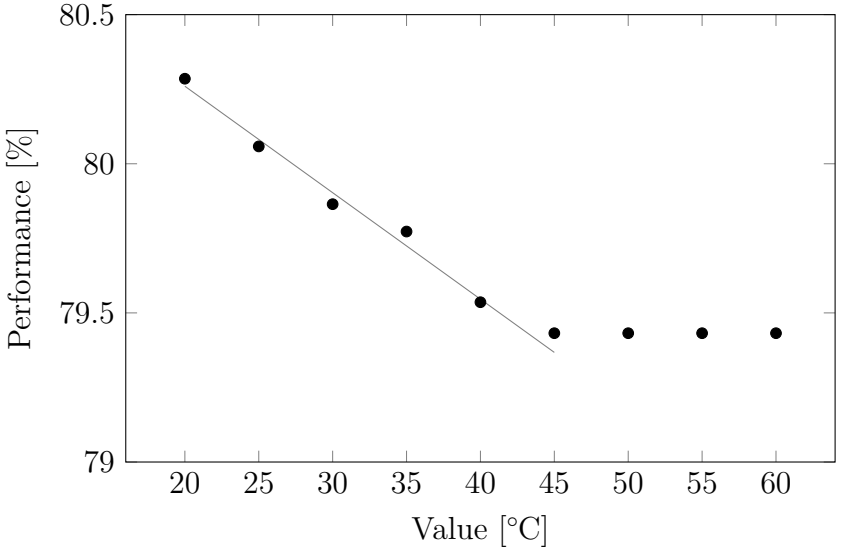

Figure C.36: SPS Results - MaxHeaterTemp

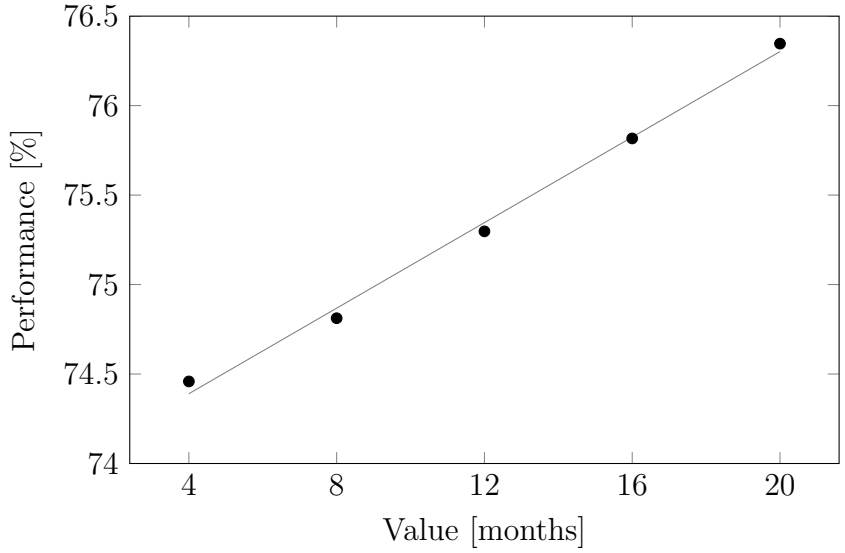

Figure C.37: SPS Results - SimLengthMonths

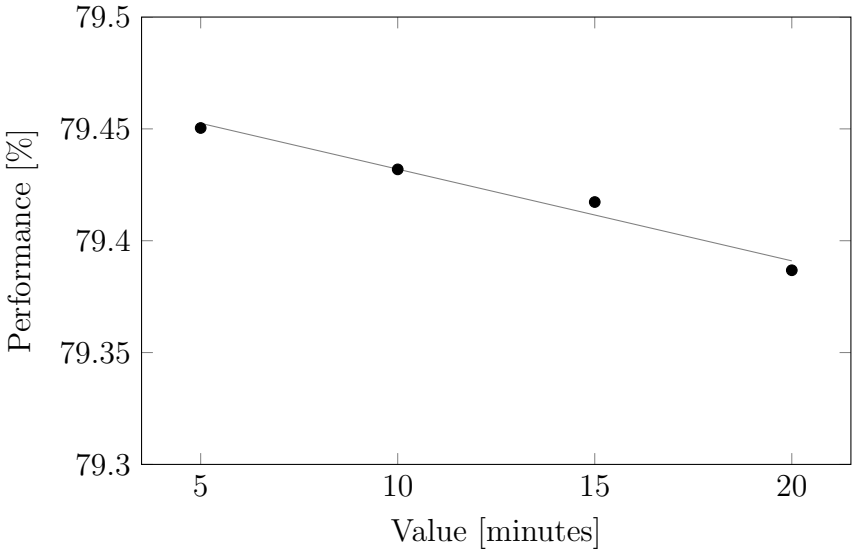

Figure C.38: SPS Results - SimTimeStepMinutes

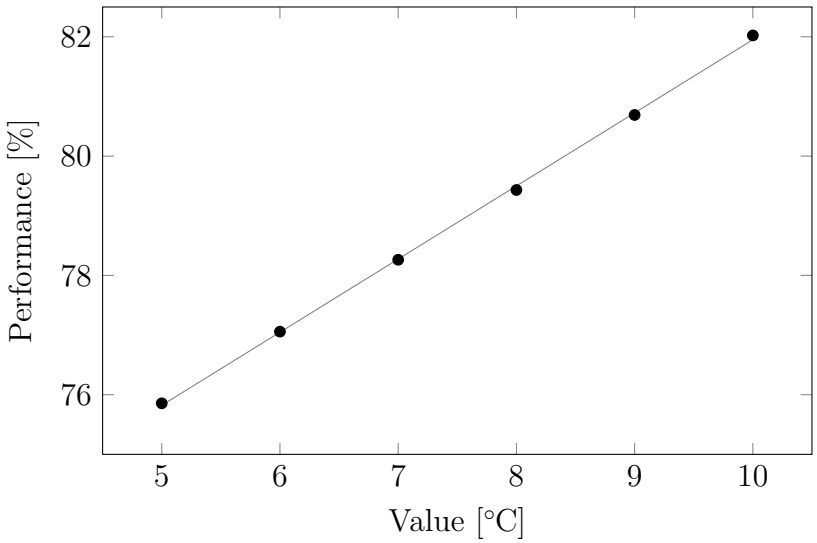

Figure C.39: SPS Results - Soil_Temp_Full_Depth

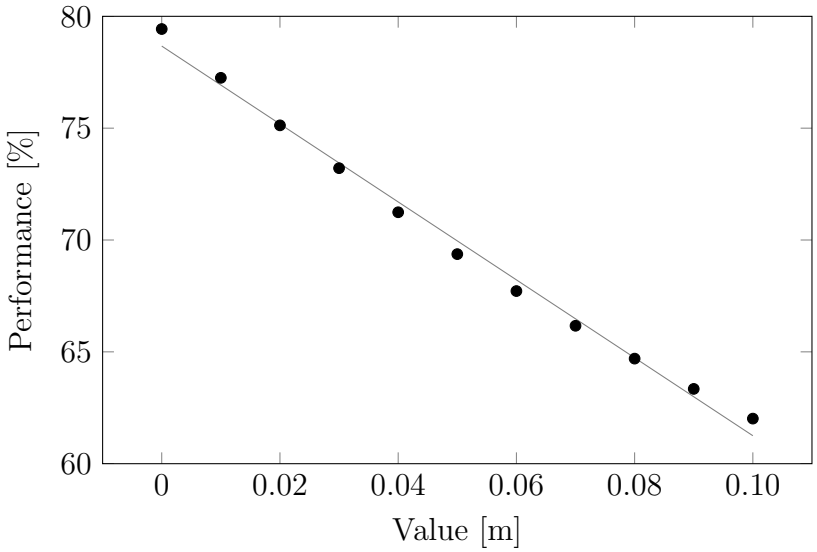

Figure C.40: SPS Results - UpperInsulationThickness

Appendix D

Radiation Model Validation

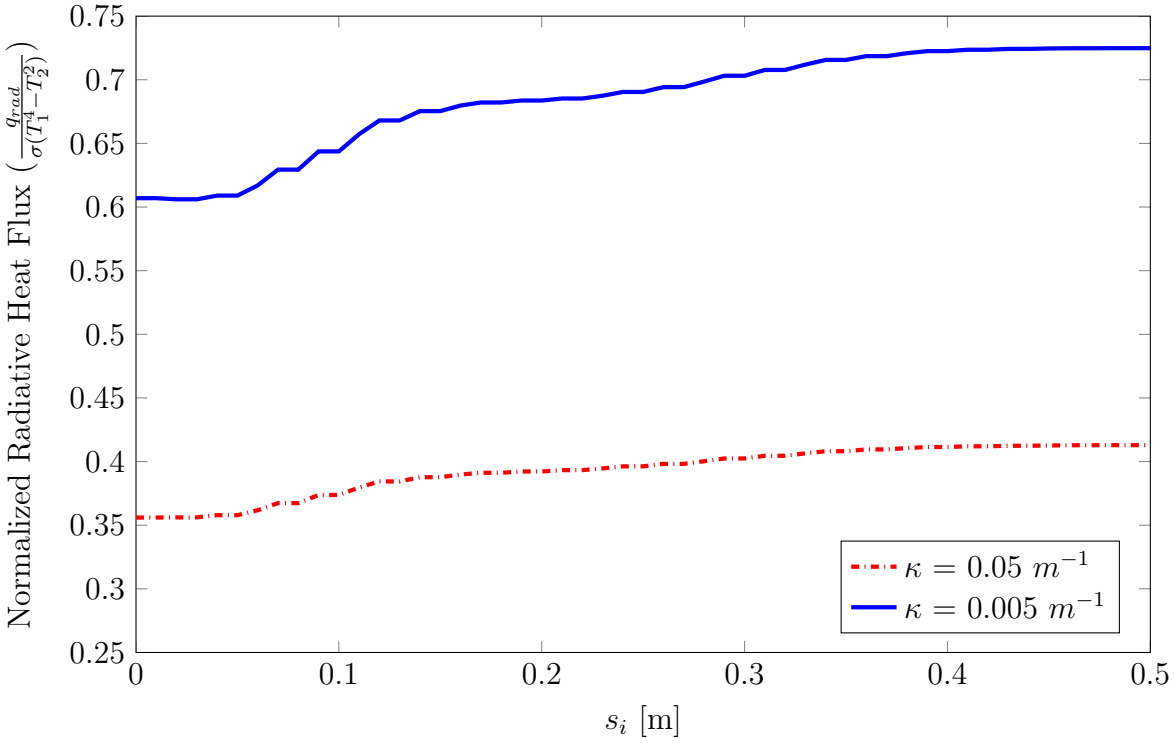

Figure D.1: Effect of Absorption Coefficient (σ)

Variable	**Value**	
	Run #1	Run #2
$\boldsymbol{\kappa\ (m^{-1})}$	**0.05**	**0.005**
T_1 (K, relative to T_{ref})	64.8	64.8
T_{ref} & T_2 (K)	273	273
L_n	32	32
κd	1	1

Table D.1: Data for Effect of Absorption Coefficient (κ) Study

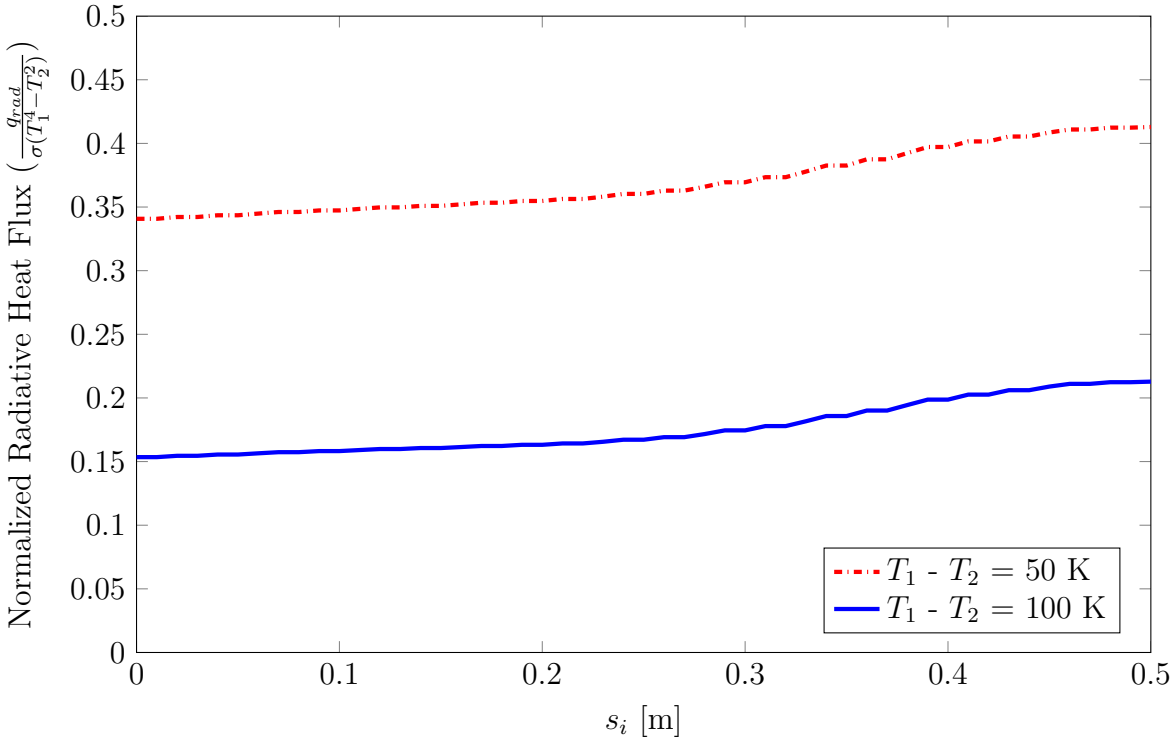

Figure D.2: Effect of T_1 - T_2

Variable	**Value**	
	Run #1	Run #2
κ (m^{-1})	0.1	0.1
T_1 **(K, relative to** $\boldsymbol{T_{ref}}$**)**	**50**	**100**
T_{ref} & T_2 (K)	100	100
L_n	8	8
κd	2	2

Table D.2: Data for Effect of T_1 - T_2 Study

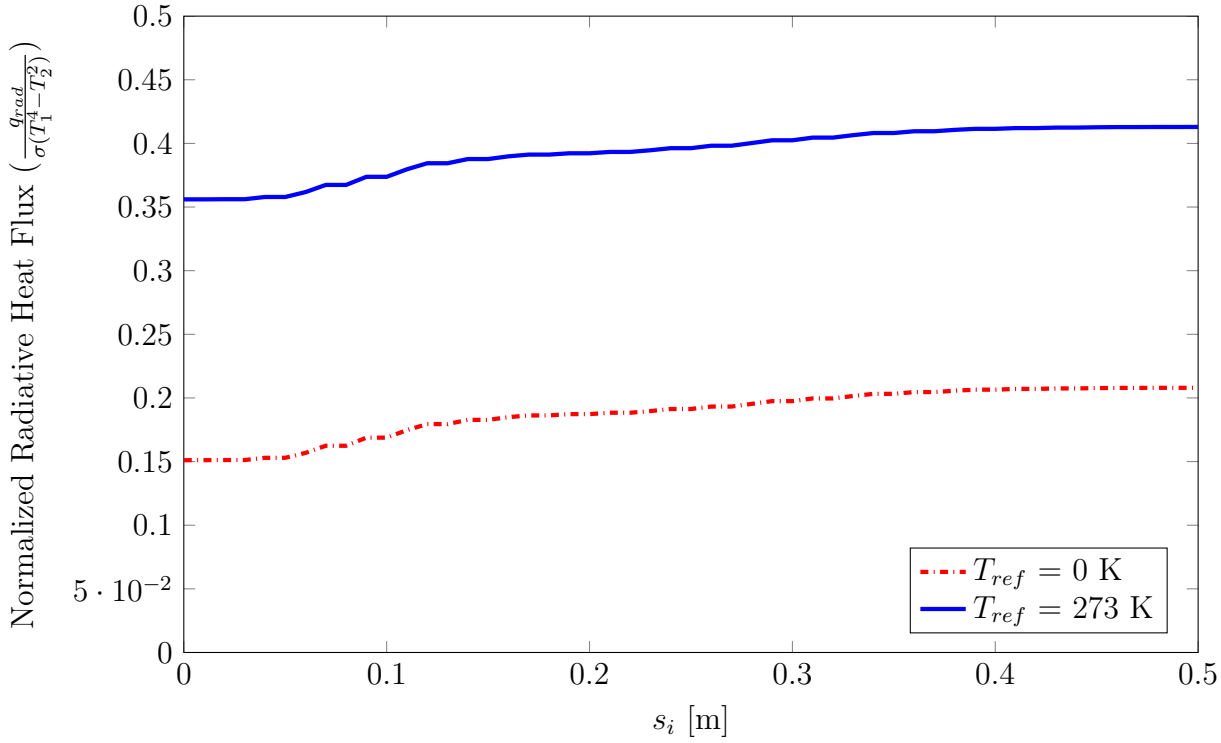

Figure D.3: Effect of Reference Temperature (T_{ref})

Variable	**Value**	
	Run #1	Run #2
κ (m^{-1})	0.05	0.05
T_1 (K, relative to T_{ref})	64.8	64.8
$\boldsymbol{T_{ref}}$ **&** $\boldsymbol{T_2}$ **(K)**	**0**	**273**
L_n	32	32
κd	1	1

Table D.3: Data for Effect of Reference Temperature (T_{ref}) Study

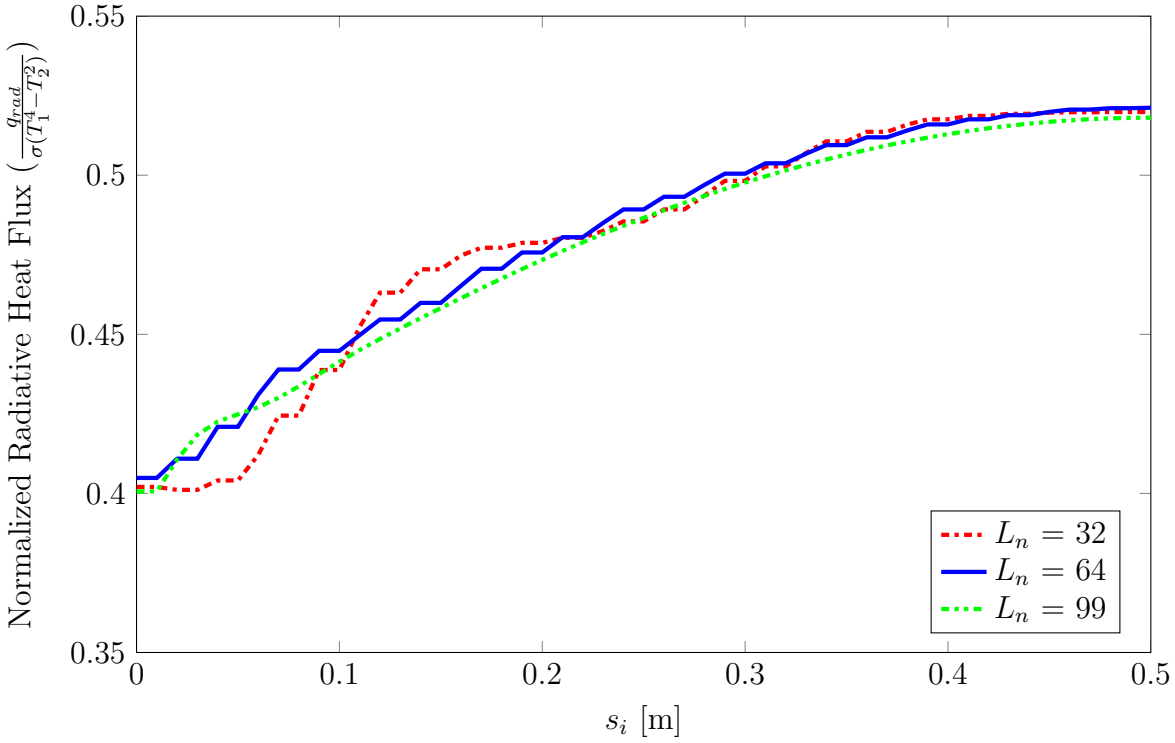

Figure D.4: Effect of Number of Solid Angles (L_n)

Variable	**Value**		
	Run #1	Run #2	Run #3
κ (m^{-1})	0.005	0.005	0.005
T_1 (K, relative to T_{ref})	64.8	64.8	64.8
T_{ref} & T_2 (K)	0	0	0
$\boldsymbol{L_n}$	**32**	**64**	**99**
κd	0.1	0.1	0.1

Table D.4: Data for Effect of Number of Solid Angles (L_n) Study

Appendix E

EXN/Aero Simulations

E.1 Foundation Perimeter Parameters

While not used in this research, the Table E.1 provides the suggested specifications for an ESS-heated building's foundation perimeter. This may be beneficial for future studies regarding ThermaRay's ESS. For details on each layer of the TES region, please refer to Table A.1 on page 199.

Layer	**Thickness**	**Thermal Conductivity (W/mK)**
TES Layers	See Table A.1	See Table A.1
XPS Insulation	5 cm [4]	0.029 W/mK [91]
Concrete	300 mm [101]	0.75 [102]

Table E.1: Foundation Perimeter Specifications (From Inside Outwards)

E.2 Boundary Conditions

BC Location	BC Type	Variable	Value
Room Ceiling	Wall	Insulation Value	R30 (RSI 5.3) [12]
		Exterior Temperature	−9.8 °C* [103]
		Ceiling Height	10 m [2]
Room/Concrete Slab Interface	Wall	Automatic	–
Vertical Walls	Symmetry	–	–
Block Interfaces	BC Connectivity	Pure Conduction	–
Undisturbed Soil Lower Limit	Wall	Wall Temperature	8°C [3]

Table E.2: EXN/Aero Simulations: Boundary Conditions

* Average air temperature in January over the last five years in Ottawa, ON (the location for which soil temperatures are available) [103].

E.3 Simulation Meshes

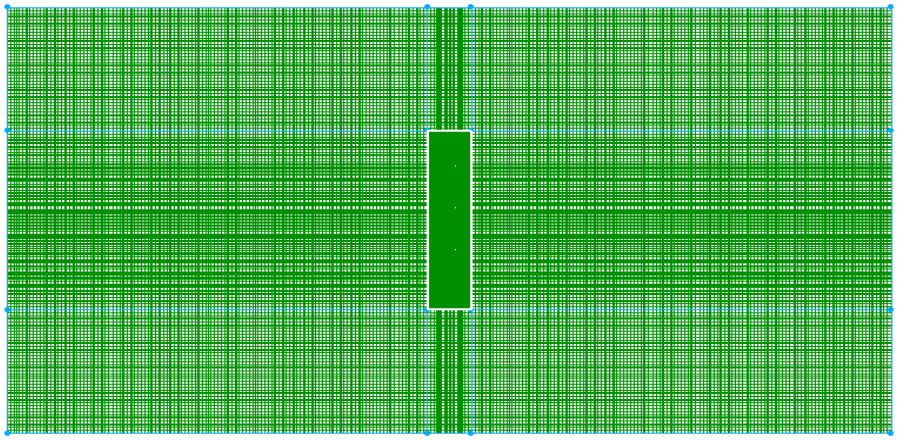

Figure E.1: Full Scale EXN/Aero Mesh: Top View

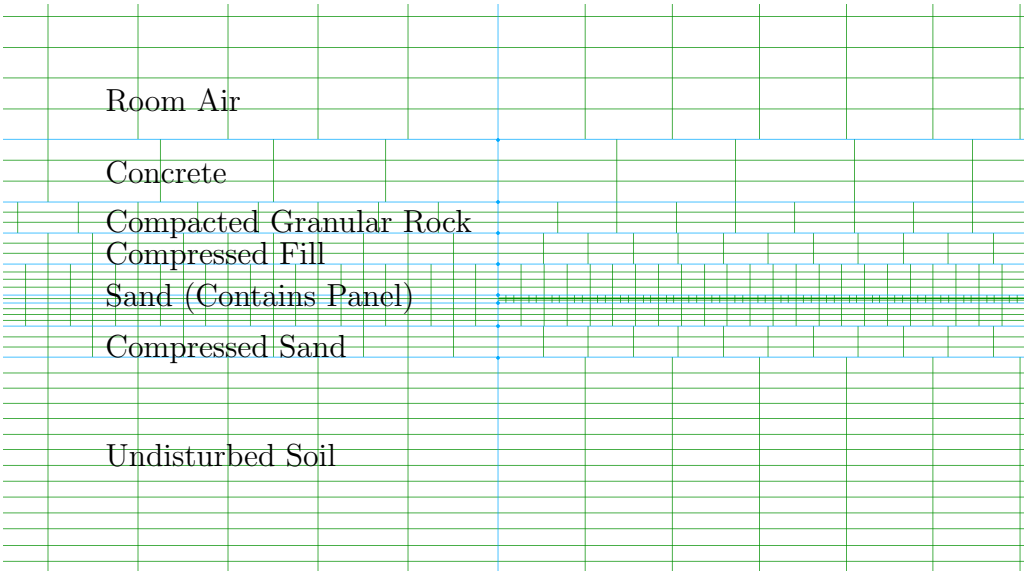

Figure E.2: Full Scale EXN/Aero Mesh:
Side View Close-Up of Heating Panel Region

Curriculum Vitae

Candidate's Full Name: Eric Labrecque

Universities Attended:

(1) Carleton University

Bachelor of Engineering in Sustainable and Renewable Energy

Specialization: Efficient Energy Conservation & Generation

Graduation Date: June 2015

Master of Applied Science in Sustainable Energy

Specialization: Hydrokinetic Turbine Debris Avoidance

Graduation Date: N/A (transferred to UNB)

(2) University of New Brunswick

Master of Science in Mechanical Engineering

Expected Graduation Date: January 2020

Publications: None.

Conference Publications: None.